THE JOURNAL OF THE AMERICAN CERAMIC SOCIETY, SEPTEMBER 1, 1943

THE JOURNAL

OF THE

AMERICAN CERAMIC SOCIETY

OCTOBER 1, 1943

MONTHLY PUBLICATION DEVOTED TO THE ARTS AND SCIENCES RELATED TO THE SILICATE INDUSTRIES

TABLE OF CONTENTS

Vol. 26 October 1, 1943 No. 10

THE JOURNAL

The Compound Merwinite ($3CaO \cdot MgO \cdot 2SiO_2$) and Its Stability Relations Within the System $CaO–MgO–SiO_2$ (Preliminary Report) 321–32
By E. F. Osborn

Physical Chemistry of Firing Steatite Ceramics 333–36
By R. L. Stone

Physical Testing of Talc for High-Frequency Ceramics 336–38
By Sidney Speil

Spherical Furnace Calorimeter for Direct Measurement of Specific Heat and Thermal Conductivity 339–49
By John R. Winckler

Measurement of the Thermal Conductivity of Fire-Clay Refractories 350–58
By T. C. Patton and C. L. Norton, Jr.

Mechanics of Enamel Adherence: XV, Influence of Cobalt and Nickel Oxides on Metal Precipitation at the Ground Coat-Iron Interface 358–60
By R. M. King

Publication Office: 20th & Northampton Sts., Easton, Pa.
Editorial Office: 2525 N. High St., Columbus 2, Ohio
Committee on Publications: J. D. SULLIVAN, *Chairman;* H. H. BLAU, R. L. STONE, J. J. CANFIELD, H. THIEMECKE, AND R. C. PURDY, *ex officio.*
Entered as second-class matter at the post office at Easton, Pa., under the act of March 3, 1879. Published monthly.
Subscription fifteen dollars ($15.00) a year. Single numbers $1.50
(Foreign and Canadian postage, 50¢ additional on subscriptions)
(Copyright 1943, American Ceramic Society, Inc.)

THE JOURNAL

OF

THE AMERICAN CERAMIC SOCIETY

Vol. 26 October 1, 1943 No. 10

THE COMPOUND MERWINITE ($3CaO \cdot MgO \cdot 2SiO_2$) AND ITS STABILITY RELATIONS WITHIN THE SYSTEM CaO–MgO–SiO_2 (PRELIMINARY REPORT)*

By E. F. Osborn

Abstract

Preliminary investigations on compositions between Ca_2SiO_4 and akermanite ($Ca_2MgSi_2O_7$), between merwinite ($Ca_3Mg(SiO_4)_2$) and akermanite, and between merwinite and monticellite ($CaMgSiO_4$) indicate that a field of merwinite appears on the liquidus surface of the system CaO–MgO–SiO_2 and that merwinite melts incongruently at 1575°C. to Ca_2SiO_4, MgO, and liquid.

I. Introduction

The crystallization processes of many igneous rocks and the mode of formation of certain metamorphic rocks could be more readily interpreted if the phase relations in a system containing as components SiO_2, Al_2O_3, iron oxides, MgO, and CaO were known. Investigations of portions of this complex system are a part of the silicate program at the Geophysical Laboratory on the fundamental chemistry of igneous rocks and minerals. Unary, binary, and ternary systems of these oxides have been reported on from time to time. Recently a study of three quaternary systems involving combinations of four of the five oxides, SiO_2, Al_2O_3, FeO, CaO, and MgO, has been in progress. Preliminary data for the system CaO–FeO–Al_2O_3–SiO_2 have been presented,[1] and the manuscript of a preliminary report on part of one join in the system CaO–FeO–MgO–SiO_2 is in preparation.[2] On portions of the third system, CaO–MgO–Al_2O_3–SiO_2, considerable data have been obtained. During the past two years data for one ternary system and one triangular system which is nearly ternary have been published.[3]

As a part of the recent studies of this quaternary system at the Geophysical Laboratory, various binary systems and invariant points appearing within the two limiting ternary systems CaO–Al_2O_3–SiO_2 and CaO–MgO–SiO_2 were reinvestigated. In most cases the results have been in excellent agreement with the earlier work, but in a few cases discrepancies were found. Two binary systems have been corrected by Schairer and Bowen.[4] Another discrepancy appeared during a check on compositions between $2CaO \cdot MgO \cdot 2SiO_2$ and $2CaO \cdot SiO_2$. This join is not binary as formerly supposed, and the peculiar phase relations exhibited along this join could be explained only on the assumption that crystals appearing in equilibrium with liquid in several of the mixtures were merwinite ($3CaO \cdot MgO \cdot 2SiO_2$) rather than $2CaO \cdot SiO_2$. Inasmuch as a field for merwinite was not shown on the original diagram of the system CaO–MgO–SiO_2,[5] a series of compositions was studied to outline the field of this compound. This study is not completed and the investigation has been temporarily interrupted. It seemed desirable to present at this time the preliminary data which have been obtained so that the results might be available to the ceramist and metallurgist.

Data discussed in the following pages show that merwinite has a field on the liquidus surface in the ternary system CaO–MgO–SiO_2 and that this compound melts incongruently at 1575° ± 5°C. to MgO, $2CaO \cdot SiO_2$ (or a solid solution of this compound and merwinite), and liquid of the composition CaO 43.0, MgO 18.2, SiO_2 38.8. These findings are in fairly good

* Presented at the Forty-Fourth Annual Meeting, The American Ceramic Society, April 22, 1942, Cincinnati, Ohio (Refractories Division). Received July 15, 1943.

[1] J. F. Schairer, "System CaO–FeO–Al_2O_3–SiO_2: I, Results of Quenching Experiments on Five Joins," *Jour. Amer. Ceram. Soc.*, 25 [June, No. 10] 241–74 (1942).

[2] J. F. Schairer and E. F. Osborn, "System CaO–MgO–FeO–SiO_2: I, Preliminary Data on the Join $CaSiO_3$–MgO–FeO." Paper presented at the Forty-Fourth Annual Meeting, The American Ceramic Society, April 22, 1942, Cincinnati, Ohio (Refractories Division).

[3] (*a*) E. F. Osborn and J. F. Schairer, "Ternary System Pseudowollastonite–Akermanite–Gehlenite," *Amer. Jour. Sci.*, 239, 715–63 (1941); *Ceram. Abs.*, 21 [2] 50 (1942).

(*b*) E. F. Osborn, "System $CaSiO_3$–Diopside–Anorthite," *Amer. Jour. Sci.*, 240, 751–88 (1942); *Ceram. Abs.*, 22 [3] 63 (1943).

[4] J. F. Schairer and N. L. Bowen, "Binary System $CaSiO_3$–Diopside and Relations Between $CaSiO_3$ and Akermanite," *Amer. Jour. Sci.*, 240, 725–42 (1942); *Ceram. Abs.*, 22 [3] 58 (1943).

[5] J. B. Ferguson and H. E. Merwin, "Ternary System CaO–MgO–SiO_2, *Amer. Jour. Sci.*, 48, p. 93 (1919).

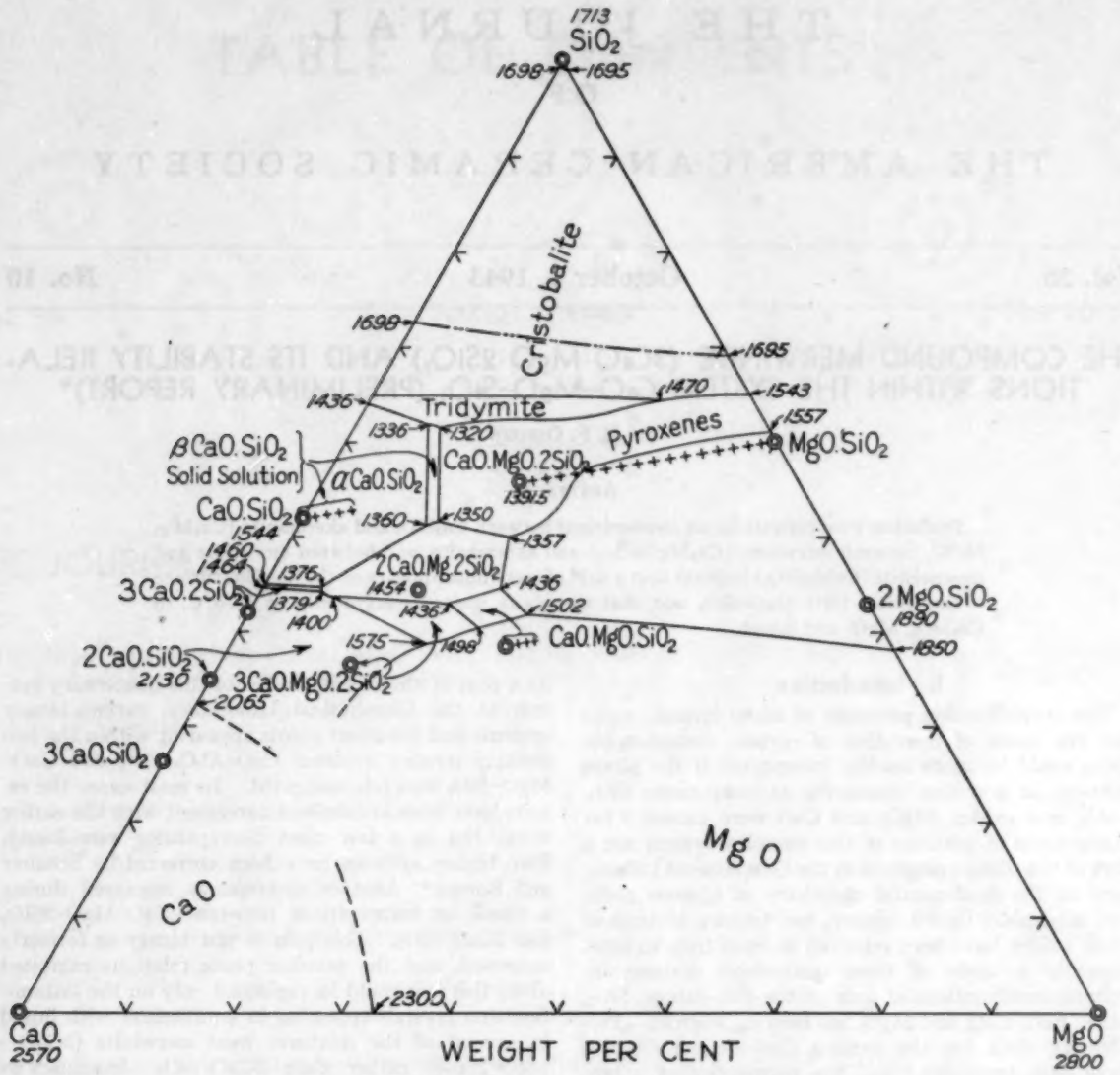

FIG. 1.—Equilibrium diagram of the system CaO–MgO–SiO_2.

agreement with the recent investigations of Lee* and of Phemister, Nurse, and Bannister.[6] Lee found that a field of merwinite was present in the system CaO–MgO–SiO_2, and his data indicated that this compound melts incongruently at about 1600°C. to $2CaO \cdot SiO_2$ and liquid. Phemister, Nurse, and Bannister found that merwinite decomposes at 1590°C. to liquid and a phase resembling $2CaO \cdot SiO_2$.

II. Method of Investigation

The laboratory technique used is similar to that employed in many previous investigations pursued at the Geophysical Laboratory and discussed at length elsewhere.[7] A charge of about 10 mg. of finely crystalline material of known chemical composition is wrapped in platinum foil and held at a constant temperature in a platinum resistance furnace until equilibrium, or a close approach to equilibrium, is attained. The charge is then quenched and the phases are identified, usually by examining the crushed charge with the petrographic microscope. Because of the close resemblance of crystals of $2CaO \cdot SiO_2$ and $3CaO \cdot MgO \cdot 2SiO_2$ when they are embedded in glass or a mesostasis of devitrification products, no attempt was made in the preliminary work to differentiate these two phases. Their fields were separated by indirect methods such as the use of conjugation lines and slopes of liquidus curves.

Most of the compositions used in this investigation were found to be very difficult to quench satisfactorily.

* H. C. Lee, personal communication, 1940.

[6] James Phemister, R. W. Nurse, and F. A. Bannister, "Merwinite as an Artificial Mineral," *Mineralog. Mag.*, 26, 225–30 (1942).

[7] See, for example, Osborn and Schairer, p. 716 of reference 3(*a*).

TABLE I

DATA FOR MIXTURES LYING ALONG THE $2CaO \cdot SiO_2$–$2CaO \cdot MgO \cdot 2SiO_2$ JOIN

Composition (wt. %)					Temp. (°C.)	Time (hr.)	Phases present in quenched product*
$2CaO \cdot SiO_2$	$2CaO \cdot MgO \cdot 2SiO_2$	CaO	MgO	SiO_2			
5	95	42.34	14.05	43.61	1454	1/2	Gl only
					1452	1/2	$2CaO \cdot MgO \cdot 2SiO_2$ and gl
					1450	1	Orthosil, $2CaO \cdot MgO \cdot 2SiO_2$, and rare gl
10	90	43.54	13.31	43.15	1459	1/2	Gl only
					1454	1/2	Orthosil and gl
					1450	1	Orthosil, $2CaO \cdot MgO \cdot 2SiO_2$, and rare gl
15	85	44.74	12.57	42.69	1475	1	Gl only
					1470	1	Orthosil and gl
					1450	1	Orthosil and gl
					1445	1	Orthosil, $2CaO \cdot MgO \cdot 2SiO_2$, and gl
20	80	45.94	11.83	42.23	1495	1/2	Gl only
					1490	1/2	Orthosil and gl
					1450	1	Orthosil and gl
					1445	1	Orthosil, rare $2CaO \cdot MgO \cdot 2SiO_2$, and gl
					1441	1	Orthosil, $2CaO \cdot MgO \cdot 2SiO_2$, and gl
25	75	47.14	11.09	41.77	1535	1	Gl only
					1530	1	Rare orthosil, and gl
					1441	1	Orthosil and gl
					1437	1	Orthosil, $2CaO \cdot MgO \cdot 2SiO_2$, and gl
30	70	48.34	10.35	41.31	1600	1/4	Gl only
					1590	1/4	Rare orthosil, and gl
					1437	1	Orthosil and gl
					1430	2	Orthosil, rare $2CaO \cdot MgO \cdot 2SiO_2$, and gl
35	65	49.53	9.62	40.85	1670	1/4	Gl only
					1660	1/4	Rare orthosil, and gl
					1410	1	Orthosil and gl
					1400	1	Orthosil, $2CaO \cdot MgO \cdot 2SiO_2$, and gl
					1395	1	Orthosil and $2CaO \cdot MgO \cdot 2SiO_2$
40	60	50.73	8.88	40.39	1710	1/4	Gl only
					1400	2	Orthosil and gl
					1395	2	Orthosil and $2CaO \cdot MgO \cdot 2SiO_2$

* In this and succeeding tables, the following abbreviations are used: Orthosil = crystals of either or both $2CaO \cdot SiO_2$ or $3CaO \cdot MgO \cdot 2SiO_2$ in mixtures in which these two orthosilicates were not differentiated. Gl = glass or devitrified glass.

Instead of a clear glass being obtained, a devitrification product was commonly present in the quenched charge. This necessitated the exercise of extreme care in distinguishing primary crystals, or those in equilibrium with liquid at the temperature of the run, from secondary crystals formed during quenching.

III. Discussion of Data

(1) General Statement

The equilibrium diagram of the ternary system CaO–MgO–SiO_2, modified on the basis of data given herein, is presented in Fig. 1. The field of $3CaO \cdot MgO \cdot 2SiO$ is shown, and other changes in the original diagram, which have been discussed elsewhere,[3,4] are incorporated.

Figure 2 is an enlargement of that part of the ternary diagram which includes the field of $3CaO \cdot MgO \cdot 2SiO_2$. The dots represent the compositions of the mixtures which have been investigated to give the data summarized in Tables I to IV, inclusive. The positions of and temperatures at the four invariant points at the corners of the field of $CaO \cdot MgO \cdot SiO_2$ are taken from the work of Ferguson and Merwin.[5] Redetermined values for the composition and temperature of each of the four invariant points at the corners of the field of $3CaO \cdot 2SiO_2$ and data for the two invariant points at 1400° and 1575° are listed in Table IV.

Two joins, along which series of dots are shown in Fig. 2, are of particular interest. These are the joins $2CaO \cdot SiO_2$–$2CaO \cdot MgO \cdot 2SiO_2$ (Fig. 3) and $3CaO \cdot MgO \cdot 2SiO_2$–$2CaO \cdot MgO \cdot 2SiO_2$ (Fig. 4). In each of these diagrams (Figs. 3 and 4), open circles represent points for which data are given in Tables I and II, heavy lines depict binary equilibrium relations, light lines illustrate relations within the ternary system and therefore lying outside the plane of the diagram, and dashed lines represent conjectured rather than established equilibrium relations.

(2) Join $2CaO \cdot SiO_2$–$2CaO \cdot MgO \cdot 2SiO_2$

The join $2CaO \cdot SiO_2$–$2CaO \cdot MgO \cdot 2SiO_2$ (Fig. 3) was originally shown as a binary system on the basis of the limited data obtained by Ferguson and Merwin.[5] It is not binary, however, because it crosses the field of $3CaO \cdot MgO \cdot 2SiO_2$. The relations shown in Fig. 3, as well as those in Fig. 4, were derived without differentiating the two orthosilicates, $2CaO \cdot SiO_2$ and $3CaO \cdot MgO \cdot 2SiO_2$, and in the tables the term "orthosilicate" refers to either or both of these compounds. But when the data are plotted (Fig. 3), it is clear that merwinite is a phase occurring within certain areas. The reasoning behind this statement may be summarized as follows: Pure $2CaO \cdot SiO_2$ cannot be the crystalline phase in equilibrium with liquid along the line AB because the line AC is not horizontal. This crystalline phase must then be either an orthosilicate solid solution or a compound such as merwinite. To decide between these alternatives, conjugation lines were con-

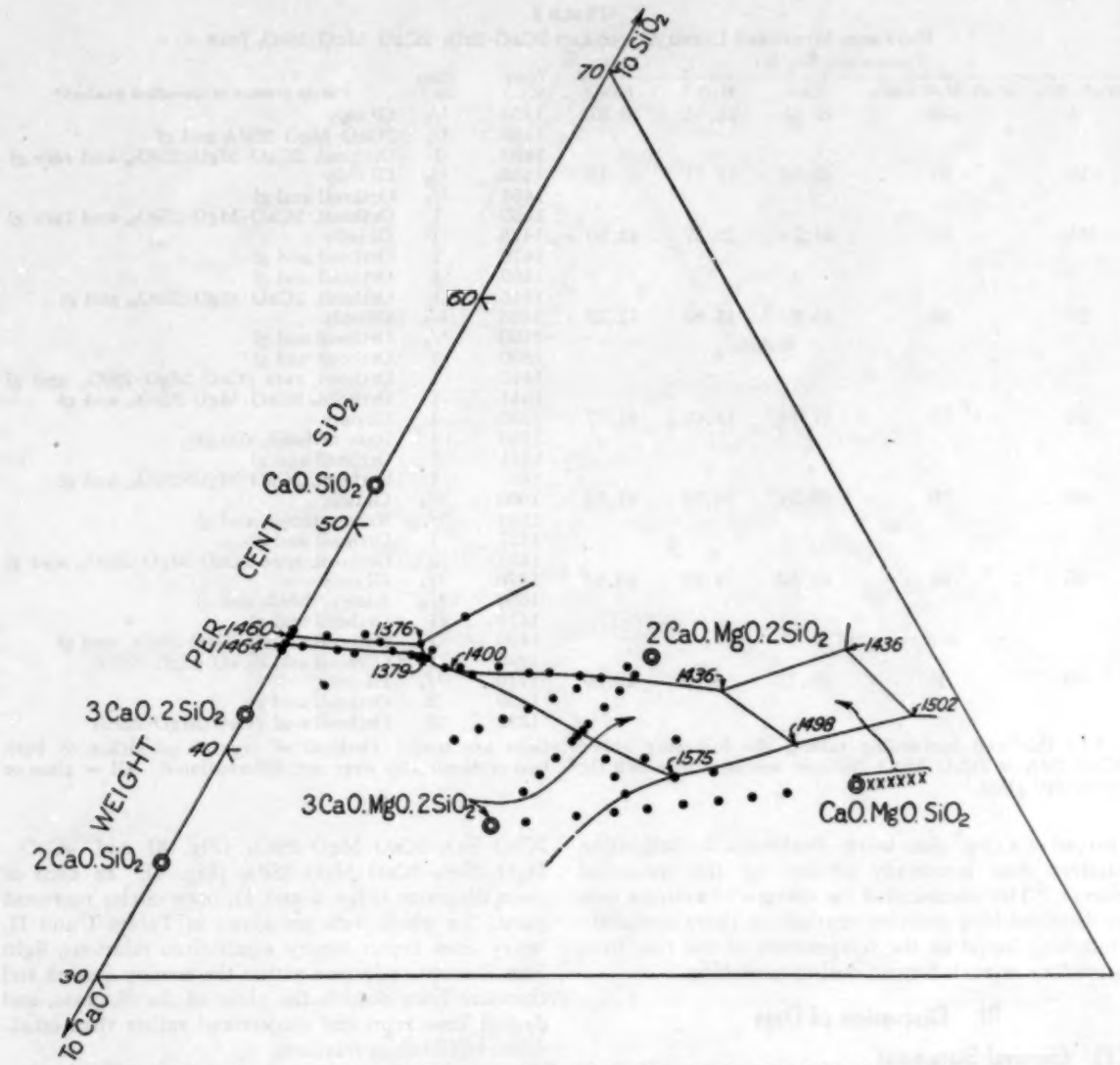

FIG. 2.—Equilibrium diagram of part of the system CaO–MgO–SiO_2 showing the field of merwinite; dots represent compositions of mixtures studied.

structed. The fulcrum of each conjugation line is a point on the ternary diagram representing the composition of one of the mixtures which furnished points along the line *AC*. The liquid end of each line is fixed because it must lie on the ternary diagram at the junction of the akermanite–orthosilicate boundary curve and the isotherm for the point. When these conjugation lines are constructed, they converge on merwinite within the limits of error of the experimental method. The temperature of the point *C* (1400° ± 5°C.) is that of a ternary invariant point (point 3, Fig. 5) at which $2CaO \cdot SiO_2$, $3CaO \cdot MgO \cdot 2SiO_2$, $2CaO \cdot MgO \cdot 2SiO_2$, and liquid CaO 49.5, MgO 6.8, SiO_2 43.7 are in equilibrium.

(3) Join $3CaO \cdot MgO \cdot 2SiO_2$–$2CaO \cdot MgO \cdot 2SiO_2$

If there is a field of merwinite in the ternary diagram, then the join merwinite–akermanite should be at least partly binary. Data obtained from mixtures lying along this join are summarized in Table II and are plotted in Fig. 4. It is apparent from a study of Fig. 4 that the join is binary at all temperatures below that of the point *D* (1548° ± 2°C., $3CaO \cdot MgO \cdot 2SiO_2$ 45, $2CaO \cdot MgO \cdot 2SiO_2$ 55). A eutectic occurs at *E*, at the composition $3CaO \cdot MgO \cdot 2SiO_2$ 13, $2CaO \cdot MgO \cdot 2SiO_2$ 87, and at 1450° ± 2°C. Phase relations above 1548°C. are ternary because of the incongruent melting of $3CaO \cdot MgO \cdot 2SiO_2$. In mixtures along this join, as well as those along the join $2CaO \cdot SiO_2$–$2CaO \cdot MgO \cdot 2SiO_2$, it was not necessary to differentiate $2CaO \cdot SiO_2$ from $3CaO \cdot MgO \cdot 2SiO_2$. The discontinuity in the slope of the liquidus curve at *D* must lie on the ternary boundary curve separating the fields of these two compounds; and because liquid disappears in all mixtures at a temperature immediately below that of *E* (1450°C.), $3CaO \cdot MgO \cdot 2SiO_2$ must be the

TABLE II

DATA FOR MIXTURES LYING ALONG THE $3CaO \cdot MgO \cdot 2SiO_2$–$2CaO \cdot MgO \cdot 2SiO_2$ JOIN

Composition (wt. %)					Temp. (°C.)	Time (hr.)	Phases present in quenched product
$3CaO \cdot MgO \cdot 2SiO_2$	$2CaO \cdot MgO \cdot 2SiO_2$	CaO	MgO	SiO_2			
10	90	42.15	14.54	43.31	1452	1	Gl only
					1450	1	$2CaO \cdot MgO \cdot 2SiO_2$, orthosil, and gl
					1448	1	Completely crystalline
20	80	43.15	14.29	42.56	1485	1/2	Gl only
					1480	1/2	Rare orthosil, and gl
					1452	1	Orthosil and gl
					1450	1	$2CaO \cdot MgO \cdot 2SiO_2$, orthosil, and gl
					1448	1	Completely crystalline
30	70	44.16	14.03	41.81	1520	1/2	Gl only
					1515	1/2	Rare orthosil, and gl
					1452	1	Orthosil and gl
					1448	1	Completely crystalline
40	60	45.16	13.78	41.06	1545	1/2	Gl only
					1540	1/2	Rare orthosil, and gl
					1452	1	Orthosil and gl
					1448	1	Completely crystalline
43	57	45.46	13.71	40.83	1550	1/2	Gl only
					1545	1/2	Rare orthosil, and gl
47	53	45.86	13.61	40.53	1565	1/2	Rare orthosil, and gl
					1560	1/2	Orthosil and gl
50	50	46.17	13.53	40.30	1600	1/4	Gl only
					1590	1/4	Rare orthosil, and gl
					1452	1	Orthosil and gl
					1448	1	Completely crystalline
60	40	47.17	13.28	39.55	1650	1/4	Gl only
					1640	1/4	Rare orthosil, and gl
					1452	1	Orthosil and gl
					1448	1	Completely crystalline
70	30	48.17	13.03	38.80	1700	1/4	Gl only
					1690	1/4	Rare orthosil, and gl
					1452	1	Orthosil and gl
					1448	1	Completely crystalline
80	20	49.18	12.77	38.05	1720	1/4	Orthosil and gl
					1452	1	Orthosil and gl
					1448	1	Completely crystalline
100	0	51.19	12.27	36.54	1580	1/2	Orthosil, MgO, and gl
					1570	1/2	$3CaO \cdot MgO \cdot 2SiO_2$

crystalline phase in equilibrium with liquid along the curve *DE*.

(4) Ternary Invariant Points

Four invariant points (numbered 3, 4, 5, and 6, Fig. 5) at which merwinite is one of the phases appear in the ternary system. At point 4, $3CaO \cdot MgO \cdot 2SiO_2$, $2CaO \cdot MgO \cdot 2SiO_2$, $CaO \cdot MgO \cdot SiO_2$, and liquid are in equilibrium, and at point 5, $3CaO \cdot MgO \cdot 2SiO_2$, $CaO \cdot MgO \cdot SiO_2$, MgO, and liquid are in equilibrium. The temperatures of these two points and the composition of the two liquids were obtained by Ferguson and Merwin.[5] The manner in which points 3 and 6 were obtained will be briefly discussed.

The temperature of point 3 was obtained from Fig. 3, its temperature being the same as that of point *C* in Fig. 3; that is, the temperature (1400° ± 5°C.) at which liquid disappears on cooling a mixture lying along the join $2CaO \cdot SiO_2$–$2CaO \cdot MgO \cdot 2SiO_2$ is the temperature of point 3 (Fig. 5). The location of point 3 is then given by the intersection of the 1400° isotherm with the $2CaO \cdot MgO \cdot 2SiO_2$–orthosilicate boundary curve. The approximate position of this point may also be obtained by the use of conjugation lines emanating from $3CaO \cdot MgO \cdot 2SiO_2$ and terminating along the $2CaO \cdot MgO \cdot 2SiO_2$–orthosilicate boundary curve. The data listed in Table I and plotted in Fig. 3 show that the composition of the liquid in the mixture $2CaO \cdot SiO_2$ 35, $2CaO \cdot MgO \cdot 2SiO_2$ 65 crosses the field of $3CaO \cdot MgO \cdot 2SiO_2$ during crystallization, whereas the liquid in the mixture $2CaO \cdot SiO_2$ 40, $2CaO \cdot MgO \cdot 2SiO_2$ 60 does not enter this field. The invariant point must therefore lie on the boundary curve between the two points, (*a*) the junction of the boundary curve and a conjugation line passing through the point $2CaO \cdot SiO_2$ 35, $2CaO \cdot MgO \cdot 2SiO_2$ 65 and (*b*) the junction of the boundary curve and the extension of a line passing from $3CaO \cdot MgO \cdot 2SiO_2$ through the point $2CaO \cdot SiO_2$ 40, $2CaO \cdot MgO \cdot 2SiO_2$ 60.

The temperature of point 6 (1575° ± 5°C.) was established by the following three methods, all in close agreement: (1) A mixture made to have the composition $3CaO \cdot MgO \cdot 2SiO_2$ (CaO 51.19, MgO 12.27, SiO_2 36.54) when quenched from 1570° was composed entirely of an orthosilicate. When quenched from 1580°, a small amount of glass, rare crystals of MgO, and crystals of an orthosilicate were present. (2) A profile along the boundary curve separating the field of MgO from the fields of $2CaO \cdot SiO_2$ and $3CaO \cdot MgO \cdot 2SiO_2$ was constructed from data found in Table III. A discontinuity in the slope of this boundary curve appears at 1575° ± 5°C. (3) The location and tem-

TABLE III

DATA FOR MIXTURES IN TERNARY SYSTEM CaO–MgO–SiO_2 NOT LISTED IN TABLES I AND II

Composition (wt. %)			Temp. (°C.)	Time (hr.)	Phases present in quenched product
CaO	MgO	SiO_2			
55.52	0	44.48	1540	1	Rare $2CaO \cdot SiO_2$, and gl
			1565	1	$2CaO \cdot SiO_2$ and gl
			1462	1	$3CaO \cdot 2SiO_2$ and gl
			1460	1	$3CaO \cdot 2SiO_2$, $CaO \cdot SiO_2$, and gl
55.35	0	44.65	1465	1	$2CaO \cdot SiO_2$ and gl
			1460	1	$3CaO \cdot 2SiO$ and gl
			1456	1	$3CaO \cdot 2SiO_2$, $CaO \cdot SiO_2$, and gl
55.02	0	44.98	1462	1	Gl only
			1460	1	$3CaO \cdot 2SiO_2$, $CaO \cdot SiO_2$, and gl
54.68	0	45.32	1474	1	Gl only
			1469	1	Rare $CaO \cdot SiO_2$
			1460	1	$CaO \cdot SiO_2$, $3CaO \cdot 2SiO_2$, and gl
54.66	0.74	44.60	1476	1	Gl only
			1458	1	$2CaO \cdot SiO_2$ and gl
			1448	1	$3CaO \cdot 2SiO_2$, and gl
			1440	1	$3CaO \cdot 2SiO_2$, $CaO \cdot SiO_2$, and gl
53.46	1.48	45.06	1450	1	Gl only
			1445	1	$CaO \cdot SiO_2$ and gl
			1435	1	$CaO \cdot SiO_2$ and gl
			1430	1	$CaO \cdot SiO_2$, $3CaO \cdot 2SiO_2$, and gl
53.27	2.22	44.51	1455	1	Gl only
			1447	1	$2CaO \cdot SiO_2$ and gl
			1435	1	$2CaO \cdot SiO_2$ and gl
			1430	2	$3CaO \cdot 2SiO_2$ and gl
			1425	1	$3CaO \cdot 2SiO_2$ and gl
			1420	1	$3CaO \cdot 2SiO_2$, $CaO \cdot SiO_2$, and gl
54.65	2.51	42.84	1640	1/4	Rare $2CaO \cdot SiO_2$, and gl
			1435	1	$2CaO \cdot SiO_2$ and gl
			1430	1	$2CaO \cdot SiO_2$, $3CaO \cdot 2SiO_2$, and gl
52.75	2.96	44.29	1450	1	Gl only
			1445	1	$2CaO \cdot SiO_2$ and gl
			1425	1	$2CaO \cdot SiO_2$ and gl
			1420	2	$3CaO \cdot 2SiO_2$ and gl
51.90	2.96	45.14	1430	1	Gl only
			1425	1	$CaO \cdot SiO_2$ and gl
			1415	1	$CaO \cdot SiO_2$ and gl
			1410	1	$CaO \cdot SiO_2$, $3CaO \cdot 2SiO_2$, and gl
51.55	3.70	44.75	1410	1	Gl only
			1405	1	$CaO \cdot SiO_2$, $3CaO \cdot 2SiO_2$, and gl
51.19	4.44	44.37	1405	1	Gl only
			1400	1	Rare $3CaO \cdot 2SiO_2$, and gl
			1390	1	$3CaO \cdot 2SiO_2$ and gl
			1385	1	$3CaO \cdot 2SiO_2$, $CaO \cdot SiO_2$, and gl
50.43	5.32	44.25	1400	2	Gl only
			1395	1	$2CaO \cdot SiO_2$ and gl
			1390	2	$3CaO \cdot 2SiO_2$ and gl
49.85	5.47	44.68	1378	2	Gl only
			1375	1	$CaO \cdot SiO_2$, $3CaO \cdot 2SiO_2$, $2CaO \cdot MgO \cdot 2SiO_2$, and rare gl
50.28	5.62	44.10	1395	1	Gl only
			1390	1	$2CaO \cdot SiO_2$ and gl
			1385	1	$2CaO \cdot SiO_2$ and gl
			1380	1	$2CaO \cdot SiO_2$, $3CaO \cdot 2SiO_2$, and gl
			1378	2	$3CaO \cdot 2SiO_2$, $2CaO \cdot MgO \cdot 2SiO_2$, and gl
49.64	5.91	44.45	1385	1	Gl only
			1380	2	$2CaO \cdot MgO \cdot 2SiO_2$ and gl
			1378	2	$2CaO \cdot MgO \cdot 2SiO_2$ and gl
			1375	2	$2CaO \cdot MgO \cdot 2SiO_2$, $CaO \cdot SiO_2$, and $3CaO \cdot 2SiO_2$
49.97	5.92	44.11	1400	2	Rare $2CaO \cdot SiO_2$, and gl
			1390	2	$2CaO \cdot SiO_2$ and gl
			1385	2	$2CaO \cdot SiO_2$, $2CaO \cdot MgO \cdot 2SiO_2$, and gl
			1378	2	$3CaO \cdot 2SiO_2$, $2CaO \cdot MgO \cdot 2SiO_2$, and gl
47.59	6.66	45.75	1395	1	Gl only
			1390	1	$CaO \cdot SiO_2$, $2CaO \cdot MgO \cdot 2SiO_2$, and gl
49.54	6.81	43.65	1430	2	Gl only
			1425	2 1/2	Rare orthosil, and gl
			1410	1	Orthosil and gl
			1405	6	Orthosil, rare $2CaO \cdot MgO \cdot 2SiO_2$, and gl
48.92	7.40	43.68	1410	2	Rare $2CaO \cdot MgO \cdot 2SiO_2$, and gl
			1405	4	$2CaO \cdot MgO \cdot 2SiO_2$, orthosil, and gl
48.57	8.13	43.30	1435	1	Gl only
			1430	1	Orthosil and gl
			1420	1	Orthosil and gl
			1415	1	Orthosil, $2CaO \cdot MgO \cdot 2SiO_2$, and gl

TABLE III (*concluded*)

Composition (wt. %)			Temp. (°C.)	Time (hr.)	Phases present in quenched product
CaO	MgO	SiO_2			
47.37	8.87	43.76	1430	1	Gl only
			1425	1	$2CaO \cdot MgO \cdot 2SiO_2$ and gl
			1415	2	$2CaO \cdot MgO \cdot 2SiO_2$ and gl
			1410	1½	$2CaO \cdot MgO \cdot 2SiO_2$, rare orthosil, and gl
46.32	10.35	43.33	1455	1½	Gl only
			1450	1	Rare orthosil, and gl
			1440	1	Orthosil and gl
			1435	1	Orthosil, $2CaO \cdot MgO \cdot 2SiO_2$, and gl
45.45	11.10	43.45	1450	1¼	Gl only
			1448	1	Rare $2CaO \cdot MgO \cdot 2SiO_2$, and gl
			1445	2	$2CaO \cdot MgO \cdot 2SiO_2$ and gl
			1440	2½	$2CaO \cdot MgO \cdot 2SiO_2$, orthosil, and gl
44.37	12.28	43.35	1450	1	Gl only
			1447	1	$2CaO \cdot MgO \cdot 2SiO_2$, orthosil, and gl
45.20	15.20	39.60	1610	¼	Gl only
			1600	¼	Orthosil and gl
45.20	16.00	38.80	1630	¼	Gl only
			1620	¼	Orthosil and gl
43.60	16.80	39.60	1560	¼	Gl only
			1550	¼	Orthosil and gl
45.20	16.80	38.00	1640	¼	Gl only
			1630	¼	Orthosil, MgO, and gl
42.00	17.60	40.40	1540	¼	Gl only
			1535	¼	Rare orthosil, and gl
42.80	18.40	38.80	1580	¼	Rare MgO, and gl
			1570	¼	MgO, orthosil, and gl
41.20	19.80	39.00	1620	¼	Gl only
			1610	¼	Rare MgO, and gl
			1565	¼	MgO and gl
			1555	¼	MgO, orthosil, and gl
49.60	13.66	36.74	1720	¼	Orthosil and gl
			1695	¼	Orthosil and gl
			1685	¼	Orthosil, MgO, and gl
47.55	15.46	36.99	1720	¼	Gl only
			1710	¼	Orthosil and gl
			1700	¼	Orthosil and gl
			1690	¼	Orthosil, MgO, and gl
46.09	16.75	37.16	1710	¼	Gl only
			1695	¼	MgO and gl
44.62	18.04	37.34	1720	¼	Very rare MgO, and gl
			1640	¼	MgO, very rare orthosil, and gl
			1630	¼	MgO, orthosil, and gl
43.16	19.33	37.51	1720	¼	MgO and gl
			1620	¼	MgO and gl
			1610	¼	MgO, rare orthosil, and gl
41.70	20.62	37.68	1580	½	MgO and gl
			1570	½	MgO, orthosil, and gl
40.24	21.90	37.86	1560	½	MgO and gl
			1555	¼	MgO, orthosil, and gl
38.77	23.19	38.04	1540	¼	MgO and gl
			1530	¼	MgO, orthosil, and gl

perature of each of four points lying on the boundary curve separating the fields of $2CaO \cdot SiO_2$ and $3CaO \cdot MgO \cdot 2SiO_2$ have been obtained. These were (*a*) point 3, Fig. 5, (*b*) point *B*, Fig. 3, (*c*) point *D*, Fig. 4, and (*d*), a discontinuity occurring in the slope of a liquidus profile across the boundary curve at a point between *D* (Fig. 4) and 6 (Fig. 5). A line passing through these four points gives a profile of the $2CaO \cdot SiO_2$–$3CaO \cdot MgO \cdot 2SiO_2$ boundary curve, which, if extrapolated to the MgO–orthosilicate boundary curve, joins the latter at 1575° ± 5°C. The location of point 6 is that of the discontinuity in the slope of the MgO–orthosilicate boundary curve. A check on this location is given by the fact that, if the $2CaO \cdot SiO_2$–$3CaO \cdot MgO \cdot 2SiO_2$ boundary curve, shown by the four known points on the curve, as given in (*a*) to (*d*), is extended to the MgO–orthosilicate boundary curve, it joins the latter at the point 6.

(5) Evidence of Solid Solution

Insufficient data were obtained to prove that there is solid solution between $2CaO \cdot SiO_2$ and $3CaO \cdot MgO \cdot 2SiO_2$, but data for the mixture CaO 54.65, MgO 2.51, SiO_2 42.84 suggest that a limited series of solid solutions extends from $2CaO \cdot SiO_2$ toward $3CaO \cdot MgO \cdot 2SiO_2$. In this mixture, if pure $2CaO \cdot SiO_2$ were the primary phase, then the secondary phase ($3CaO \cdot 2SiO_2$) should appear at 1423°C. This becomes apparent when data contained in Table III are plotted. But in this mixture, the phase $3CaO \cdot 2SiO_2$ appears at 1433°C. This points to the conclusion that the orthosilicate in this mixture in equilibrium with liquid at 1433° is a

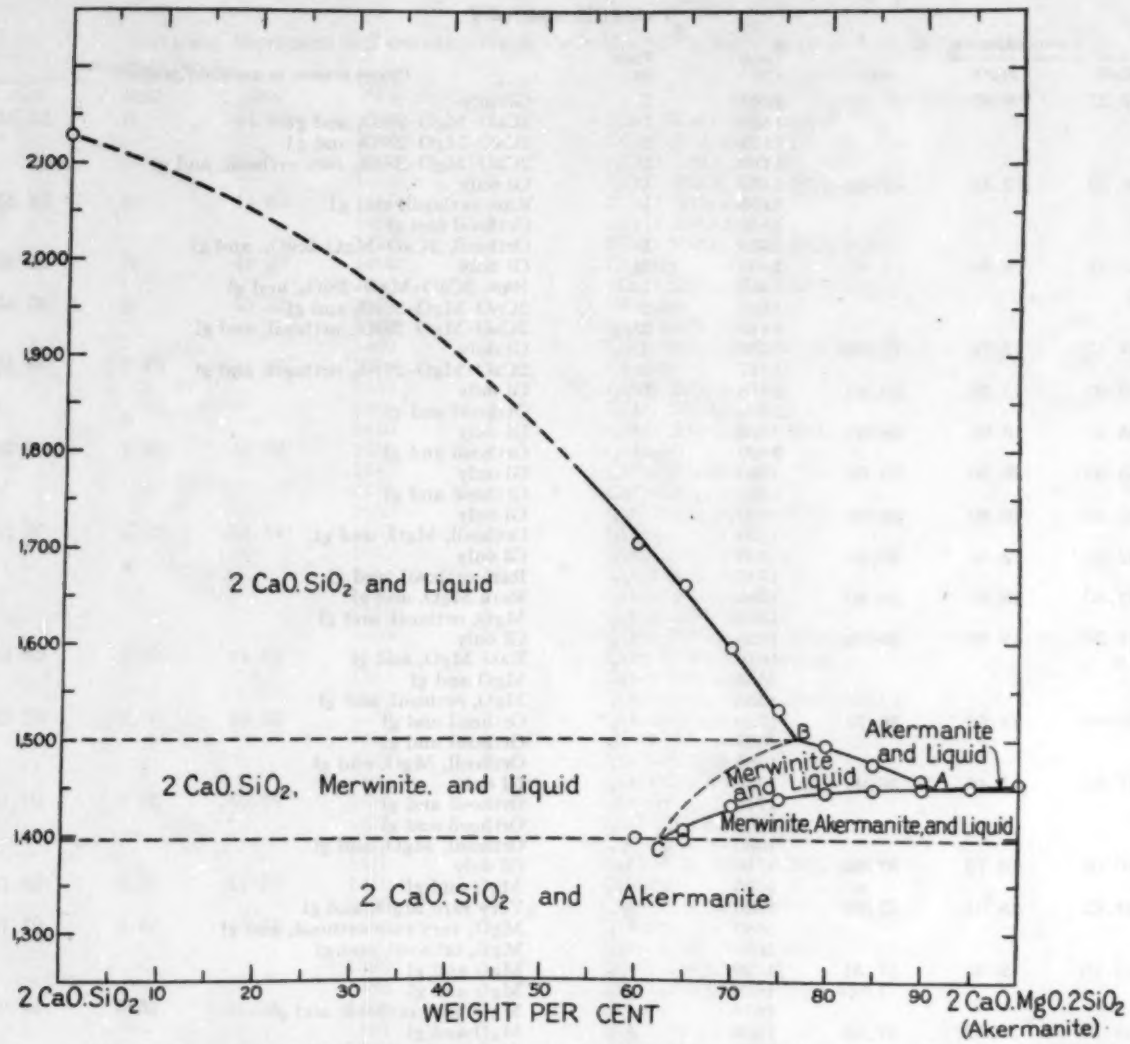

FIG. 3.—Equilibrium diagram of the join $2CaO \cdot SiO_2$–$2CaO \cdot MgO \cdot 2SiO_2$; heavy lines represent binary equilibrium relations; light lines illustrate relations lying outside the plane of this diagram.

solid solution whose composition, expressed in terms of the percentage of weight of the two compounds, is approximately $2CaO \cdot SiO_2$ 70, $3CaO \cdot MgO \cdot 2SiO_2$ 30. This evidence for solid solution is not conclusive and should be checked by further data.

The evidence on hand indicates that there is no appreciable solid solution extending from the compound $3CaO \cdot MgO \cdot 2SiO_2$ in either direction along the orthosilicate line.

(6) Courses of Crystallization

Courses of crystallization of compositions within that part of the ternary system CaO–MgO–SiO_2 which is being considered are of interest because of the varied assemblage of compounds that may appear in a mixture with varying conditions of crystallization. This variation in the number and type of compounds to which a given composition may crystallize results from the fact that three of the compounds ($3CaO \cdot 2SiO_2$, $3CaO \cdot MgO \cdot 2SiO_2$, and $CaO \cdot MgO \cdot SiO_2$) melt incongruently. Consequently, along two of the boundary curves marked with arrows in Fig. 5, a crystalline phase decreases in amount as the liquid moves down the boundary curve.* Along the curve 8–2, $3CaO \cdot 2SiO_2$ crystallizes while $2CaO \cdot SiO_2$ dissolves, and along 6–3, $2CaO \cdot SiO_2$ dissolves and $3CaO \cdot MgO \cdot 2SiO_2$ crystallizes. Along the boundary curve 6–5, however, MgO bears essentially a neutral relation to the liquid, that is, no appreciable amount of MgO either crystallizes or dissolves as the liquid moves along 6–5. The data obtained are not sufficient to prove that MgO either dissolves or crystallizes, but they suggest that the tangent to the upper end of the curve (near 6) passes above the point $3CaO \cdot MgO \cdot 2SiO_2$ and that tangents to the

* This is also true of the $CaO \cdot MgO \cdot SiO_2$ boundary curve along which MgO dissolves as $CaO \cdot MgO \cdot SiO_2$ solid solutions crystallize; this boundary curve is discussed by Ferguson and Merwin on p. 116 of reference 5.

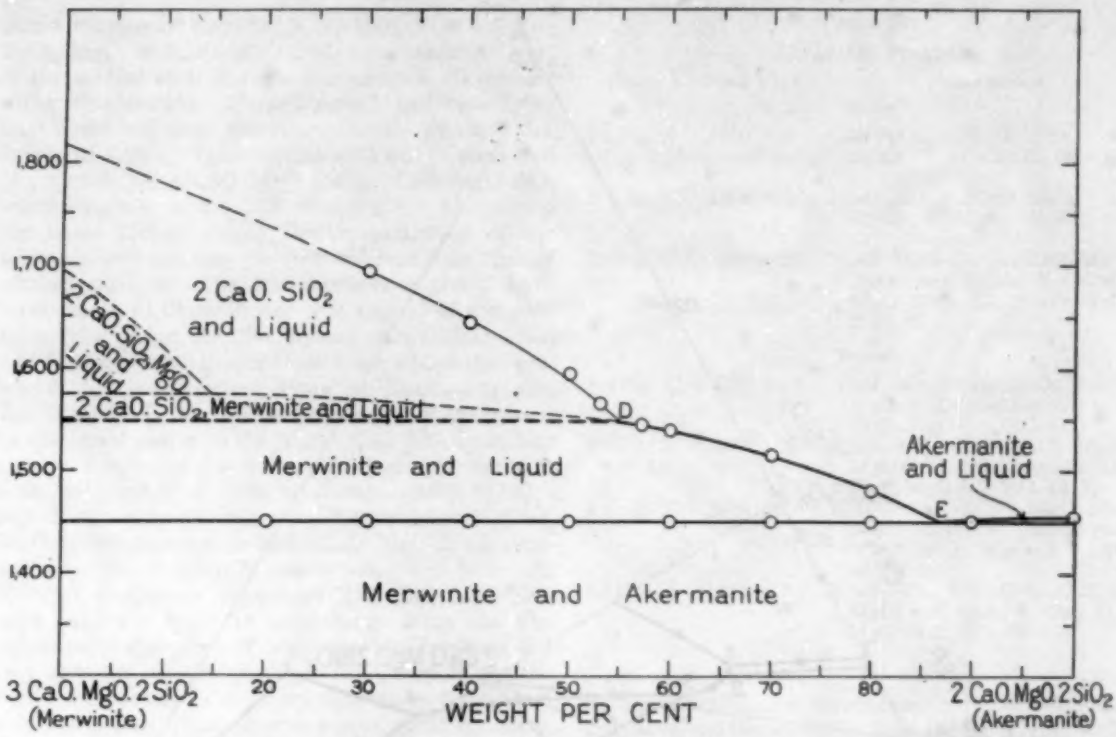

FIG. 4.—Equilibrium diagram of the join $3CaO \cdot MgO \cdot 2SiO_2$–$2CaO \cdot MgO \cdot 2SiO_2$; heavy lines represent binary equilibrium relations; light lines illustrate relations lying outside the plane of this diagram.

middle and lower parts of this curve pass below this point or, in other words, MgO at first dissolves and then crystallizes.

In Fig. 5, six triangles have been constructed by using, as the apices of each, the three crystalline phases which appear in equilibrium at one of the six ternary invariant points lettered from 1 to 6. The crystallization of compositions within each of the triangles will be briefly discussed. It is assumed that no solid solution exists except that established by Ferguson and Merwin[5] between monticellite and forsterite. Mention is made earlier of the possibility of limited solid solution extending from $2CaO \cdot SiO_2$ toward merwinite. If such exists, the crystallization of some compositions would be slightly different from that discussed below.

If a melt has a composition which places it within the $2CaO \cdot SiO_2$–$3CaO \cdot MgO \cdot 2SiO_2$–MgO triangle, the first phase to crystallize is either MgO or $2CaO \cdot SiO_2$. In each case, as crystallization proceeds, the composition of the liquid changes along a straight line directed away from the composition of the crystallizing compound. As the liquid reaches the MgO–$2CaO \cdot SiO_2$ boundary curve, the other crystalline phase ($2CaO \cdot SiO_2$ or MgO) appears, and with continued falling temperature the liquid moves down the boundary curve to 6 as both MgO and $2CaO \cdot SiO_2$ crystallize. If equilibrium is maintained, the composition of the liquid remains that of point 6 and the temperature remains constant at 1575° until the liquid disappears. Both $2CaO \cdot SiO_2$ and MgO react with the liquid and partially disappear as $3CaO \cdot MgO \cdot 2SiO_2$ crystallizes. If, however, equilibrium is not maintained between the crystals and liquid, that is, if the crystals of MgO and $2CaO \cdot SiO_2$ fail to react with the liquid, the liquid will move from 6 to 5† as $3CaO \cdot MgO \cdot 2SiO_2$ crystallizes and from 5 to 4 as $CaO \cdot MgO \cdot SiO_2$ solid solutions and $3CaO \cdot MgO \cdot 2SiO_2$ simultaneously crystallize. At 4, $2CaO \cdot MgO \cdot 2SiO_2$ appears and the liquid disappears.‡ Thus, if equilibrium conditions are maintained during crystallization, the melt will crystallize to an aggregate of $2CaO \cdot SiO_2$, $3CaO \cdot MgO \cdot 2SiO_2$, and MgO, and the final liquid will have the composition of 6 and will disappear at 1575°. If no reaction occurs between crystals and liquid, the final product will be composed of the five compounds $2CaO \cdot SiO_2$, $3CaO \cdot MgO \cdot 2SiO_2$, MgO, $CaO \cdot MgO \cdot SiO_2$ solid solutions, and 2CaO··

† The liquid will move along 6–5 to 5 provided a straight line passing through $3CaO \cdot MgO \cdot 2SiO_2$ and 6 passes through or below 5, that is, does not intersect the boundary curve 5–4. Otherwise the liquid will leave 6–5 and cross the field of $3CaO \cdot MgO \cdot 2SiO_2$ to the 5–4 boundary curve. From the data obtained, it is impossible to determine on which side of 5 this line lies. The location of both 6 and 5 is not known with sufficient accuracy. In the discussion, it is assumed that the line does not intersect the boundary curve 5–4.

‡ The liquid disappears completely at 4 instead of moving to the invariant point at which the fields of 2CaO··$MgO \cdot 2SiO_2$, $CaO \cdot MgO \cdot SiO_2$ and $2MgO \cdot SiO_2$ join because of the limited solid solution as established by Ferguson and Merwin (see reference 5) between $CaO \cdot MgO \cdot SiO_2$ and $2MgO \cdot SiO_2$.

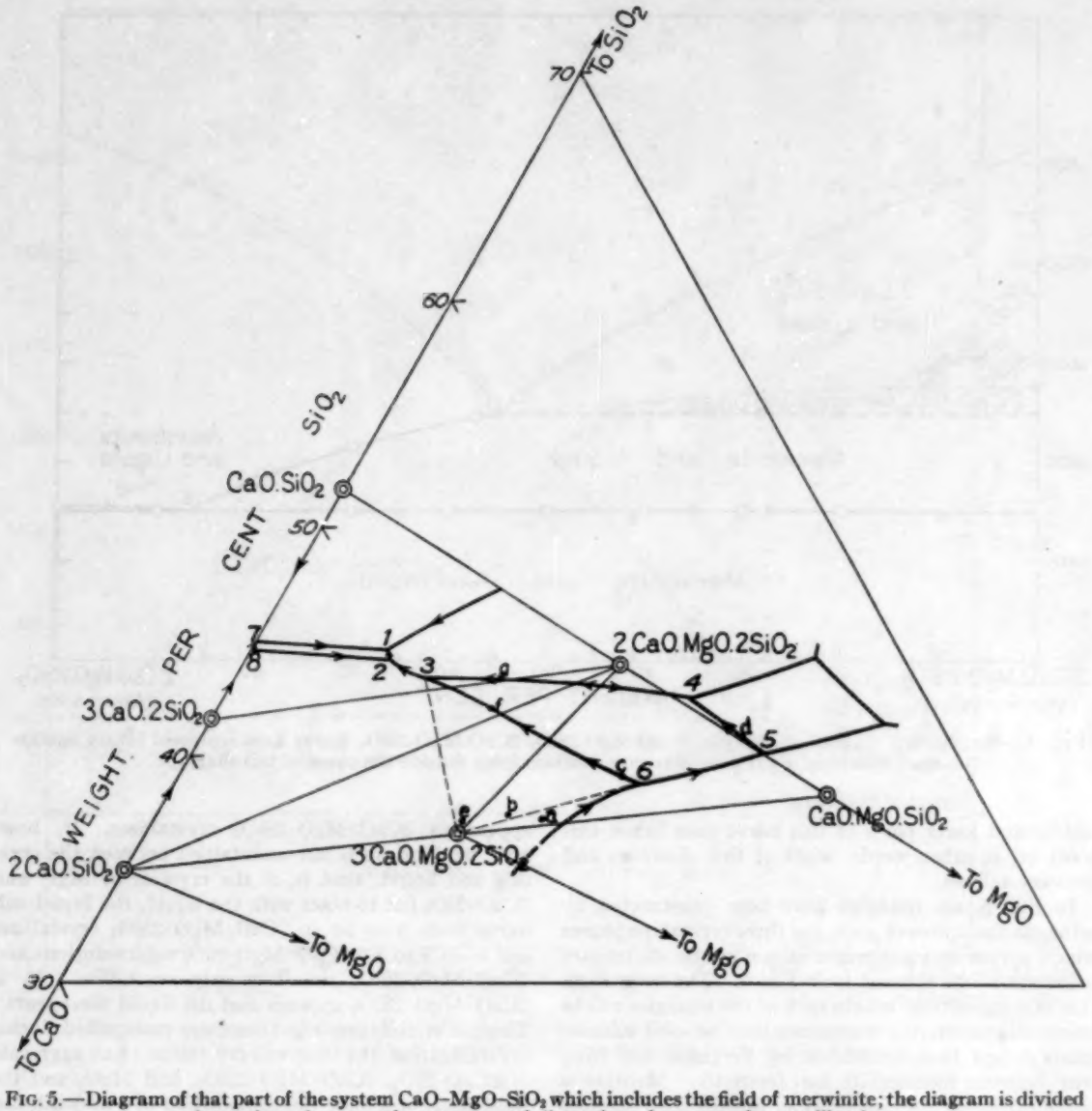

FIG. 5.—Diagram of that part of the system CaO–MgO–SiO_2 which includes the field of merwinite; the diagram is divided into triangular areas for purposes of discussion of courses of crystallization.

$MgO \cdot 2SiO_2$; the final liquid will have the composition of 4; and this liquid will disappear at 1436°.

The next triangle to be considered is that whose apices are $3CaO \cdot MgO \cdot 2SiO_2$, $CaO \cdot MgO \cdot SiO_2$, and MgO. As in the previous example, parts of the primary phase fields of both $2CaO \cdot SiO_2$ and MgO lie within the triangle. If the mixture lies within the field of $2CaO \cdot SiO_2$, this compound first crystallizes, causing the composition of the liquid to follow a straight line to the MgO–$2CaO \cdot SiO_2$ boundary curve. The liquid then moves along the boundary curve to 6 as MgO and $2CaO \cdot SiO_2$ simultaneously crystallize. If equilibrium is maintained, the crystals of MgO react with liquid 6 and partly disappear, $3CaO \cdot MgO \cdot 2SiO_2$ begins to crystallize, and the crystals of $2CaO \cdot SiO_2$ completely disappear as the temperature drops below that of point 6 (1575°). The liquid then moves along 6–5 to 5 as $3CaO \cdot MgO \cdot 2SiO_2$ continues to crystallize. At 5 (1498°), crystals of MgO react with the liquid and partly disappear as $CaO \cdot MgO \cdot SiO_2$ solid-solution crystals appear. The final liquid has the composition 5 and disappears at 1498°. If MgO is the primary phase and equilibrium is maintained, courses of crystallization will be similar except that the second phase to appear will be either $2CaO \cdot SiO_2$ or $3CaO \cdot MgO \cdot 2SiO_2$, depending on whether the liquid reaches the boundary curve above 6 or below 6. If equilibrium conditions are not maintained and $2CaO \cdot SiO_2$ and MgO fail to react with the liquid, the liquid will move to 4 as in the previous example.

If a composition lies within the $3CaO \cdot MgO \cdot 2SiO_2$–$CaO \cdot MgO \cdot SiO_2$–$2CaO \cdot MgO \cdot 2SiO_2$ triangle, the first

phase to appear may be $2CaO \cdot SiO_2$, $3CaO \cdot MgO \cdot 2SiO_2$, MgO, or $2CaO \cdot MgO \cdot 2SiO_2$, inasmuch as a part of the field of each of these four compounds appears within this triangle. If equilibrium is maintained, the final liquid will have the composition 4. and will disappear at 1436°. The resulting solid will be composed of crystals of $3CaO \cdot MgO \cdot 2SiO_2$, $CaO \cdot MgO \cdot SiO_2$ solid solutions, and $2CaO \cdot MgO \cdot 2SiO_2$. The course the liquid follows during the crystallization of one mixture, however, may be very different from that of another mixture. The two mixtures *a* and *b* have been chosen as illustrations; *a* is typical of compositions lying below the line joining $3CaO \cdot MgO \cdot 2SiO_2$ and 6, and *b* is typical of those lying above this line, where MgO is the second crystalline phase to appear. The compound $2CaO \cdot SiO_2$ first crystallizes from *a* as the liquid moves to the MgO–$2CaO \cdot SiO_2$ boundary curve. The liquid then follows the boundary curve to 6 as MgO and $2CaO \cdot SiO_2$ crystallize. At 6, $2CaO \cdot SiO_2$ disappears completely if equilibrium is maintained, MgO partly disappears, and $3CaO \cdot MgO \cdot 2SiO_2$ crystallizes. The liquid then moves along 6–5 to 5. At 5, MgO completely disappears and $CaO \cdot MgO \cdot SiO_2$ solid solutions begin to crystallize. With the disappearance of crystals of MgO, the liquid follows 5–4 to 4, at which point $2CaO \cdot MgO \cdot 2SiO_2$ appears and the liquid disappears. The liquid of mixture *b* follows a course similar to that of *a* as far as point 6. Here, however, if equilibrium is maintained, MgO completely disappears rather than $2CaO \cdot SiO_2$, and the liquid moves down along the boundary curve 6–3.* As the liquid moves along 6–3, $2CaO \cdot SiO_2$ dissolves as $3CaO \cdot MgO \cdot 2SiO_2$ crystallizes. The compound $2CaO \cdot SiO_2$ completely disappears at *c*. The liquid, therefore, leaves the boundary curve following a straight line across the field of $3CaO \cdot MgO \cdot 2SiO_2$ to *d*. The liquid then follows the boundary curve from *d* to 4 as $3CaO \cdot MgO \cdot 2SiO_2$ and $CaO \cdot MgO \cdot SiO_2$ solid solutions crystallize. At 4, the liquid disappears. If crystals of $2CaO \cdot SiO_2$ and MgO in either *a* or *b* fail to react completely with the liquid and disappear, these two phases will, of course, appear along with the other three phases in the crystalline aggregate.

The first phase to crystallize from a composition within the triangle $2CaO \cdot SiO_2$–$3CaO \cdot MgO \cdot 2SiO_2$–$2CaO \cdot MgO \cdot 2SiO_2$ will be one of these three compounds. If equilibrium is maintained during crystallization, the last liquid will have the composition of the point 3 and will disappear at 1400°. As liquid 3 diminishes in amount, $2CaO \cdot MgO \cdot 2SiO_2$ and $2CaO \cdot SiO_2$ crystallize, while part of the previously crystallized $3CaO \cdot MgO \cdot 2SiO_2$ reacts with the liquid and disappears. If a composition within this triangle lies in the field of $3CaO \cdot MgO \cdot 2SiO_2$ or $2CaO \cdot MgO \cdot 2SiO_2$, the liquid during crystallization moves directly to the 4–3 boundary curve and thence to 3. A composition lying within the field of $2CaO \cdot SiO_2$ will follow the 6–3 boundary curve to 3 only if its particular composition lies to the left of a line joining $3CaO \cdot MgO \cdot 2SiO_2$ and 3. If it lies to the right of this line, the crystals of $2CaO \cdot SiO_2$ will completely disappear before the liquid reaches 3, whereupon the liquid will leave the 6–3 boundary curve, will cross the field of $3CaO \cdot MgO \cdot 2SiO_2$ to the 4–3 boundary curve, and will then follow this to 3. As an illustration of the course a liquid may follow during its crystallization, point *e* may be used as an example. Assuming in the first instance that equilibrium is maintained, the liquid will move along a straight line to the $2CaO \cdot SiO_2$–MgO boundary curve and then along this boundary curve to 6. Crystals of MgO present as the liquid reaches 6 react with the liquid and completely disappear as the liquid leaves 6 and moves down the 6–3 boundary curve. When the liquid reaches *f*, $2CaO \cdot SiO_2$ has completely disappeared. The liquid then moves from *f* to *g* as $3CaO \cdot MgO \cdot 2SiO_2$ continues to crystallize. At *g*, $2CaO \cdot MgO \cdot 2SiO_2$ begins to crystallize and continues to precipitate along with $3CaO \cdot MgO \cdot 2SiO_2$ while the liquid moves to 3. At 3, some of the $3CaO \cdot MgO \cdot 2SiO_2$ disappears as $2CaO \cdot SiO_2$ again crystallizes along with $2CaO \cdot MgO \cdot 2SiO_2$ until the liquid is exhausted. If equilibrium is not maintained, the course of the liquid may be very different. For example, in *e*, if equilibrium is maintained, it is necessary that MgO react with liquid 6 and disappear, and crystals of $2CaO \cdot SiO_2$ must continuously dissolve if the liquid is to move from 6 toward 3. If these reactions fail to occur, the liquid will move to 4 just as would a liquid from a mixture of the composition of 6, and the final aggregate will consist of $2CaO \cdot SiO_2$, MgO, $3CaO \cdot MgO \cdot 2SiO_2$, $CaO \cdot MgO \cdot SiO_2$

TABLE IV

INVARIANT POINTS

Point	Temp. (°C.)	Phases present
		Binary
7 (Fig. 5)	1460 ± 2	$CaO \cdot SiO_2$, $3CaO \cdot 2SiO_2$, and liquid 7 (CaO 55.02, SiO_2 44.98)
8 (Fig. 5)	1464 ± 3	$2CaO \cdot SiO_2$, $3CaO \cdot 2SiO_2$, and liquid 8 (CaO 55.32, SiO_2 44.68)
E (Fig. 4)	1450 ± 2	$3CaO \cdot MgO \cdot 2SiO_2$, $2CaO \cdot MgO \cdot 2SiO_2$, and liquid *E* ($3CaO \cdot MgO \cdot 2SiO_2$ 13, $2CaO \cdot MgO \cdot 2SiO_2$ 87)
		Ternary
1 (Fig. 5)	1376 ± 2	$CaO \cdot SiO_2$, $3CaO \cdot 2SiO_2$, $2CaO \cdot MgO \cdot 2SiO_2$, and liquid 1 (CaO 49.8, MgO 5.6, SiO_2 44.6)
2 (Fig. 5)	1379 ± 2	$2CaO \cdot SiO_2$, $3CaO \cdot 2SiO_2$, $2CaO \cdot MgO \cdot 2SiO_2$, and liquid 2 (CaO 50.0, MgO 5.7, SiO_2 44.3)
3 (Fig. 5)	1400 ± 5	$2CaO \cdot SiO_2$, $3CaO \cdot MgO \cdot 2SiO_2$, $2CaO \cdot MgO \cdot 2SiO_2$, and liquid 3 (CaO 49.5, MgO 6.8, SiO_2 43.7)
6 (Fig. 5)	1575 ± 5	$2CaO \cdot SiO_2$, $3CaO \cdot MgO \cdot 2SiO_2$, MgO, and liquid 6 (CaO 43.0, MgO 18.2, SiO_2 38.8)

* Whether a liquid during equilibrium crystallization moves from 6 toward 3 or toward 5 depends on the total composition of the mixture. If the mixture lies on or below a straight line joining $3CaO \cdot MgO \cdot 2SiO_2$ and 6, the liquid will move to 5 or to a point on the 5–4 boundary curve very close to 5 (see (†) reference, p. 329). If the mixture lies above this line, the liquid will move toward 3; and if the mixture has the composition of $3CaO \cdot MgO \cdot 2SiO_2$, the liquid will disappear at 6.

solid solutions, and $2CaO \cdot MgO \cdot 2SiO_2$. On the other hand, if reactions at 6 and along 6–3 are complete but if $3CaO \cdot MgO \cdot 2SiO_2$ fails to react with liquid 3, then the liquid will move to 2 where crystals of $3CaO \cdot 2SiO_2$ will appear. The liquid will completely crystallize at 2 only if $2CaO \cdot SiO_2$ reacts with liquid 2 and partly disappears. If this reaction fails to occur, the liquid will move to 1 and disappear as $CaO \cdot SiO_2$ crystallizes. The final aggregate in this case will be $2CaO \cdot SiO_2$, $3CaO \cdot MgO \cdot 2SiO_2$, $2CaO \cdot MgO \cdot 2SiO_2$, $3CaO \cdot 2SiO_2$, and $CaO \cdot SiO_2$. If MgO fails to react with liquid 6 but $2CaO \cdot SiO_2$ reacts with the liquid as it moves along 6–3, MgO will also be present along with the other five compounds as the liquid disappears at 1. Thus, if equilibrium is not maintained, various assemblages of compounds may appear from a single composition and the final liquid may have the composition of the point 4, of the point 2, or of the point 1.

The crystallization of compositions lying within the triangle $2CaO \cdot SiO_2$–$2CaO \cdot MgO \cdot 2SiO_2$–$3CaO \cdot 2SiO_2$ is similar to that of compositions lying within the triangle just discussed, except that if equilibrium is maintained the final liquid has the composition of 2. If the liquid passes through 3, all previously crystallized $3CaO \cdot MgO \cdot 2SiO_2$ reacts with liquid 3 and disappears. If the composition lies within the field of $2CaO \cdot SiO_2$, the second phase to crystallize may be $3CaO \cdot MgO \cdot 2SiO_2$, $2CaO \cdot MgO \cdot 2SiO_2$, or $3CaO \cdot 2SiO_2$, depending on the total composition of the selected charge.

During the crystallization of compositions lying within the triangle $3CaO \cdot 2SiO_2$–$2CaO \cdot MgO \cdot 2SiO_2$–$CaO \cdot SiO_2$, the liquid moves to the ternary eutectic 1 and disappears. It is apparent that one or both of $3CaO \cdot MgO \cdot 2SiO_2$ and $2CaO \cdot SiO_2$ will appear as phases during some stage of the crystallization of many compositions lying within this triangle. If equilibrium is maintained, the crystals of $3CaO \cdot MgO \cdot 2SiO_2$ disappear completely at 3 and the crystals of $2CaO \cdot SiO_2$ disappear at 2. To the extent that these reactions are incomplete, these two compounds will appear with $3CaO \cdot 2SiO_2$, $2CaO \cdot MgO \cdot 2SiO_2$, and $CaO \cdot SiO_2$ in the crystalline aggregate. As in the case of the boundary curve 6–3, a liquid will move down the boundary curve 8–2 only as long as crystals of $2CaO \cdot SiO_2$ are dissolving. If $2CaO \cdot SiO_2$ disappears before the liquid reaches 2 or if the $2CaO \cdot SiO_2$ crystals fail to dissolve, the liquid will leave 8–2, crossing the field of $3CaO \cdot 2SiO_2$ either to 7–1 or 2–1, and will then proceed to 1.

IV. Summary

New data have been presented for silicate compositions lying in the region of the orthosilicate join in the ternary system CaO–MgO–SiO_2. Phase equilibrium data obtained on 59 mixtures are summarized in Tables I to IV, inclusive, and are presented and discussed with the aid of five figures. Of chief interest is the delineation of a field for the compound merwinite ($3CaO \cdot MgO \cdot 2SiO_2$) on the liquidus surface in the ternary system. This compound melts incongruently at 1575° ± 5°C. to MgO, $2CaO \cdot SiO_2$, and liquid of the composition CaO 43.0, MgO 18.2, SiO_2 38.8. The data suggest that there is limited solid solution extending from $2CaO \cdot SiO_2$ toward merwinite. A second ternary invariant point established by these data occurs at the composition CaO 49.5, MgO 6.8, SiO_2 43.7, at a temperature of 1400° ± 5°C., and with the solid phases $2CaO \cdot SiO_2$, $3CaO \cdot MgO \cdot 2SiO_2$, and $2CaO \cdot MgO \cdot 2SiO_2$.

The join $2CaO \cdot SiO_2$–$2CaO \cdot MgO \cdot 2SiO_2$ is not binary, as formerly believed. But the join $3CaO \cdot MgO \cdot 2SiO_2$–$2CaO \cdot MgO \cdot 2SiO_2$ was found to be binary in part, with a binary eutectic at 1450° ± 2°C. and at the composition $3CaO \cdot MgO \cdot 2SiO_2$ 13, $2CaO \cdot MgO \cdot 2SiO_2$ 87. In addition to the foregoing data, revised data are presented (summarized in Table IV) for two ternary invariant points in the system CaO–MgO–SiO_2 and for two binary invariant points in the system CaO–SiO_2.

A discussion of courses of crystallization of ternary mixtures is given, and a corrected equilibrium diagram of the ternary system CaO–MgO–SiO_2 is given as Fig. 1.

Acknowledgment

The author wishes to thank J. F. Schairer and N. L. Bowen for critically reading the manuscript.

Geophysical Laboratory
Carnegie Institution of Washington
Washington, D. C.

PHYSICAL CHEMISTRY OF FIRING STEATITE CERAMICS *

By R. L. Stone

Abstract

The composition of normal as well as low-loss steatite bodies is shown on the MgO–Al_2O_3–SiO_2 phase diagram. Clay-talc bodies containing 10% or less of clay have the longest firing range. Bodies near the forsterite corner of the clinoenstatite-forsterite-cordierite triangle have a firing range of about 100°C. but they are too refractory. Auxiliary fluxes, such as CaO and BaO, shorten the firing range appreciably. The alkalis lengthen it but are electrically detrimental. The RO_2 elements, such as SiO_2 and ZrO_2, when added in appreciable quantities, give good firing range but an excessive increase in the refractoriness of the body.

I. Introduction

The most serious objection that whiteware manufacturers offer when they have had occasion to convert to the production of steatite ceramics is that the firing range of the bodies is extremely short, that is, too short for practical use. There are fundamental reasons for this short firing range and for the fact that it cannot be appreciably lengthened.

Petrologists have long recognized that, when a magma is cooled, the ferromagnesian minerals crystallize first and the residuum liquid, high in alkalis and silica, is the last to crystallize. When this liquid is absent, the crystallization temperature interval is quite short.

The physical and chemical effects produced in firing such heterogeneous mixtures as ceramic bodies are not exactly the reverse of those produced in cooling a magma, but the physicochemical principles involved are the same.

II. Decomposition of Steatite Body Materials

According to recent X-ray analyses made in Germany,[1] talc breaks down below 900°C. into MgO + SiO_2 + H_2O. Prolonged heating at 900°C. produces a magnesium metasilicate, $MgSiO_3$, known as mesoenstatite (other names are protoenstatite and metatalc), which does not have the same lattice structure as enstatite. Thilo and Rogge[1] give stability temperatures for enstatite up to 900°C. and for mesoenstatite, from 900° to 1270°C.

Clay minerals, essentially kaolinite, are reported to lose their water at 500° to 600°C. with the resulting formation of Al_2O_3 + SiO_2 + H_2O. Amorphous mullite and cristobalite form at 850° to 1040°C., and the mullite begins to grow into microscopically recognizable crystals at approximately 1350°C.

Clay and talc theoretically should produce tridymite below 1470°C., but X-ray examination has shown that cristobalite is actually the product of decomposition. In phase diagrams with silica as one of the components, cristobalite is shown above 1470°C., and tridymite below 1470°C., but this is true only for melts being cooled. The cristobalite is in an unstable state below 1470°C. and therefore is more active chemically than the tridymite would be.

All of the temperatures referred to are greatly affected by associated constituents and at best are applicable only to specific samples.

When a mixture of pure talc and pure clay grains is fired to 1300°C., the products of thermal decomposition, before any vitrification has taken place, will be (1) clinoenstatite and cristobalite in the talc grains and (2) mullite and cristobalite in the clay grains. The metatalc grains and metakaolin grains, 0.044 mm. or 325-mesh in size, are extremely large compared with their molecular size. The crystals of clinoenstatite, mullite, and cristobalite are extremely small, in the order of 60 a.u. or about 3 unit crystal diameters. The 325-mesh grain size, on this basis, is about 6000 times the diameter of the crystals present.

At the contact interface of the grains in the mixture of talc and clay, therefore, the following pairs of crystals may be touching each other: (1) cristobalite and clinoenstatite, (2) cristobalite and mullite, and (3) mullite and clinoenstatite. There will be 50% by volume (that is, area) of each component at the interface of any pair. The eutectics in these pairs are, respectively, (1) 1545°C., (2) 1543°C., and (3) 1580°C. Reactions in the solid state in (3), however, will form a very thin film of cordierite, and the resulting eutectic will occur at 1362°C. When a third raw material is added, such as $BaCO_3$, three more types of contact interfaces exist. Each of these has its eutectic temperature. The lowest eutectic in the BaO–SiO_2 system occurs at approximately 1370°C., and a ternary eutectic probably exists in the BaO–MgO–SiO_2 system, which has a melting temperature of about 1150°C.

A phase-rule study of high MgO bodies has been made by Kraner and McDowell[2] in which bodies containing lime were considered.

III. Softening Rate of Steatite Compositions

Steatite dielectric compositions lie on the metatalc-metakaolin line near the cristobalite-clinoenstatite

* Presented at the Forty-Fifth Annual Meeting, The American Ceramic Society, Pittsburgh, Pa., April 20, 1943 (Materials and Equipment Division). Received April 20, 1943.

[1] E. Thilo and Gerhard Rogge, "Chemical Investigation of Silicates: VIII, Thermal Transformation on Anthrophyllite, $Mg_7Si_8O_{22}(OH)_2$; Polymorphism of Magnesium Metasilicate and Mechanism of Transformation of Anthrophyllite and Talc upon Heating," *Ber. Deut. Chem. Ges.*, **72B**, 341–62 (1939); *Ceram. Abs.*, **19** [1] 25 (1940).

[2] H. M. Kraner and S. J. McDowell, "Talc as the Principal Body Ingredient in Vitrified Ceramic Bodies," *Jour. Amer. Ceram. Soc.*, **8** [10] 626–35 (1925).

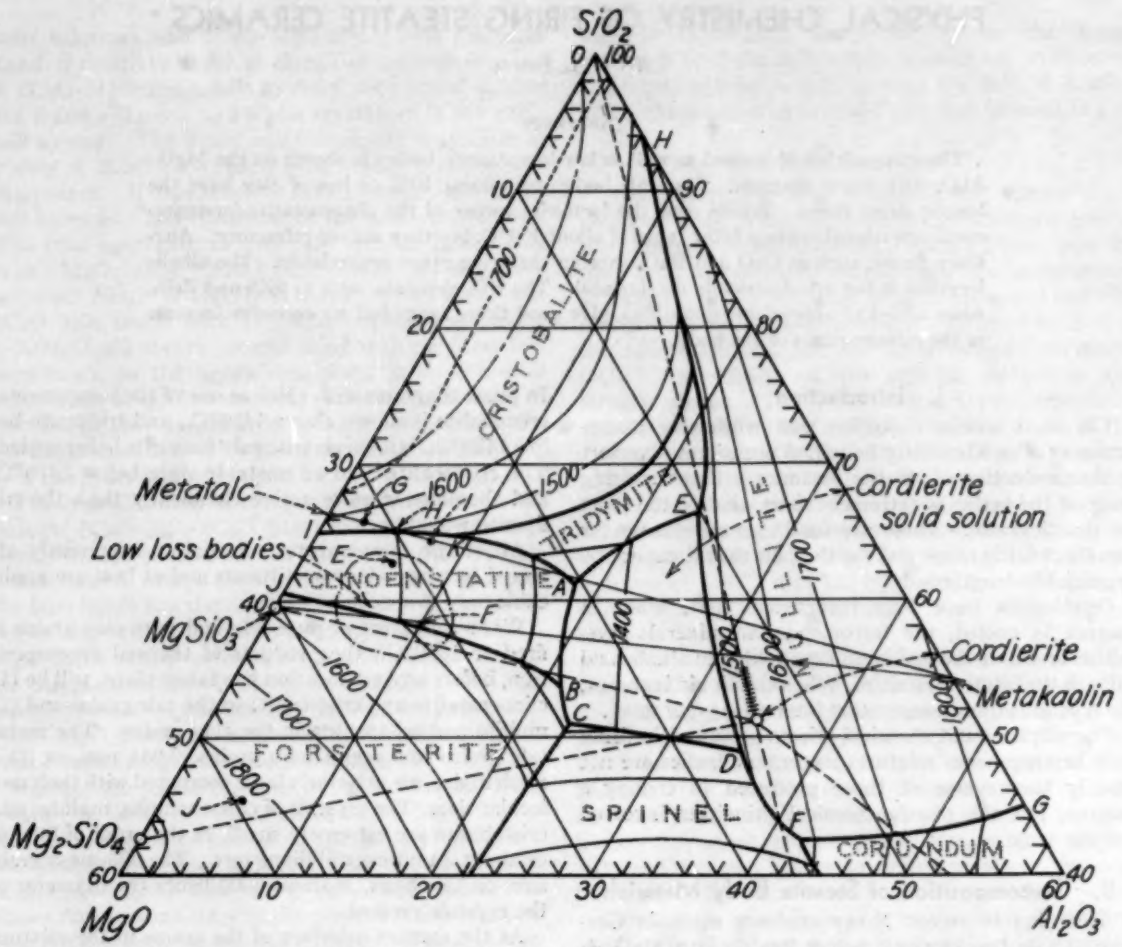

FIG. 1.—Portion of system MgO–Al_2O_3; (*A*) 1347°C., (*B*) 1362°C., (*C*) 1372°C., (*D*) 1463°C., (*E*) 1427°C., (*F*) 1580°C., (*G*) 1830°C., (*H*) 1549°C., (*I*) 1547°C., (*J*) 1562°C., and (*K*) 1470°C.

boundary and low-loss steatite dielectric compositions lie near the forsterite-clinoenstatite boundary, both in the forsterite and clinoenstatite areas. These areas are shown in the phase diagram of the MgO–Al_2O_3–SiO_2 system (Fig. 1).

An analysis of many low-loss steatite body compositions shows that the proportions of talc to magnesium carbonate result in a composition close to that of enstatite. The basic low-loss bodies are therefore essentially mixtures of enstatite and clay. The BaO and CaO and other oxides in these bodies are only modifiers that alter the glass phase and improve the dielectric properties.

Points *G*, *H*, and *I* of Fig. 1 are commercial steatite compositions which contain 5, 10, and 15% of metakaolin (5.2, 10.5, and 17.7% of kaolin), respectively, with no added magnesium carbonate. Figure 2 shows that each of these bodies theoretically begins to liquefy at the eutectic temperature, 1347°C. Body G at 1347°C. has 14.6% of liquid, and body H has 29%. Assuming that 35% of liquid is sufficient to vitrify the mass and that 45% causes distortion, body H becomes vitrified at 1390°C. and is overfired at 1430°C. and body G vitrifies at 1460°C. and is overfired at 1490°C. Bodies E, F, and I are practically overfired at 1347°C.

A body having a composition in the forsterite area, point *J*, has a long firing range, but the temperature necessary to produce vitrification is high. This body becomes vitrified under the foregoing assumption at about 1550°C. and is not overfired until about 1660°C.

A low-loss steatite composition containing approximately one part of clay to four parts of enstatite lies on the 10% Al_2O_3 line in the low-loss body area of Fig. 1 (point *F*), disregarding the presence of any BaO. When a body of this composition is heated, the first liquid is formed at 1347°C., at which temperature about 21% of the mass liquefies. If it is heated to 1355°C., there is about 30% of liquid, and when the temperature reaches 1360°C., 51% of liquid occurs. Under these assumptions of vitrifying and overfiring, body F passes from an underfired to an overfired condition during the 5°C. rise.

Point *I* in Fig. 1 is a steatite composition containing 9.4% of $MgCO_3$. When this composiion is heated under equilibrium conditions the first liquid appears at 1347°C. and amounts to 45% of the weight of the mass.

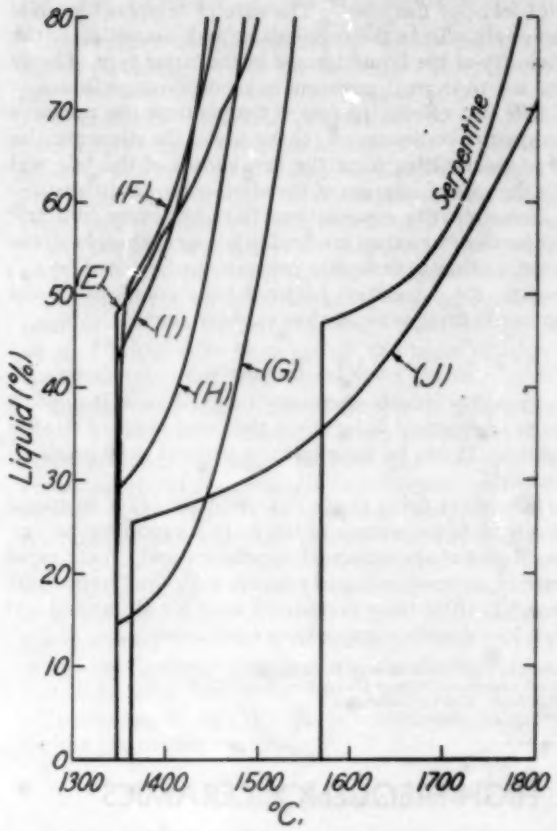

FIG. 2.—Theoretical melting curves of steatite body compositions.

Body (curve)	Talc	Clay	$MgCo_3$
E	72.9	18.7	9.4
F	63.4	21.8	14.7
G	94.8	5.2	
H	89.5	10.5	
I	84.3	15.7	
J	45.2	10.0	44.8

An increase of temperature to 1360°C. increases the liquid content only to about 50%, but the 45% of liquid is sufficient to cause severe distortion.

Specimens having the composition I will be porous and opaque at *x* temperature, just below the proper firing temperature, but with an increase of 5°C. they will be beautifully translucent. The shrinkage is high during this 5° rise, and the liquid formed is very fluid, allowing the specimen to slump. Compositions E and F have even shorter firing range.

The effect of the very large talc and clay grains is to raise the temperature of the first liquid formation and thereby to shorten the firing range. The traces of alkalis and alkaline earths as impurities conversely lowers the temperature of first liquid formation and thereby helps to lengthen the firing range.

IV. Effect of Composition Modifiers

Any of the substances that can be added to the steatite bodies to alter the firing behavior may be called "modifiers." Among these modifiers are the elements

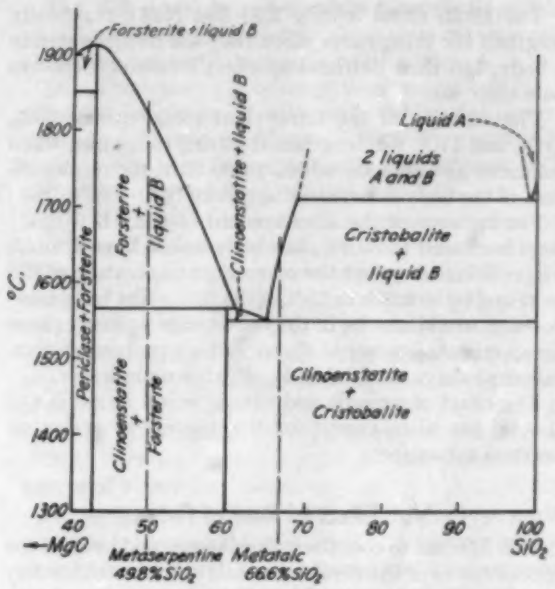

FIG. 3.—System $MgO–SiO_2$.

of (1) alkaline earths, (2) alkalis, and (3) tetravalent metals. Magnesia and BaO, added as carbonates, are the most popular modifiers. Figure 3 shows that talc (metatalc) has a short softening or melting interval. Pure talc becomes 97% liquid at the eutectic temperature, 1545°C., and is completely molten at approximately 1630°C.

An addition of 1.5% of MgO to the talc produces the eutectic composition, which melts congruently. If a sufficient amount of MgO is added to take the composition well into the forsterite region, for example, a composition containing 53% of MgO, the firing range is materially lengthened but the maturing temperature would be about 1600°C.

The addition of MgO to the body by chemically precipitated $MgCO_3$ or by serpentine, however, causes an even higher firing shrinkage than occurs when only talc is used. Forsterite and periclase may also be used as a source of MgO, but they are extremely abrasive and cause excessive die wear during forming.

The other alkaline earth oxides, CaO and BaO, do not have the same effect as MgO. Bowen and Schairer[3] and many others, in studying the relation of CaO to the crystallization phenomenon of ferromagnesia melts, have shown that lime has the characteristic of lowering the melting temperatures rapidly. The behavior of barium is similar to that of calcium in this respect as shown by an examination of the $BaO–SiO_2$ system.

Additions of BaO or CaO to the body will therefore lower and shorten the firing range. They enter into the glass phase when they are added in amounts of 10 to 12% of RO. When larger amounts are used, crystalline $RSiO_3$ appears because the composition is taken into an area where it exists at the maturing temperature of the body.

[3] N. L. Bowen and J. F. Schairer, "System MgO–FeO–SiO_2," *Amer. Jour. Sci.*, **29** [2] 151–217 (1935); *Ceram. Abs.*, **15** [9] 288 (1936).

The alkali metal oxides, K_2O and Na_2O, materially lengthen the firing range when they are incorporated in a body, but their detrimental effect on dielectric losses bars their use.

The addition of the tetravalent metal oxides, SiO_2, ZrO_2, and TiO_2, will lengthen the firing range but, when sufficient amounts are added to do that, the refractoriness of the body is increased appreciably.

For instance, if the silica content of body E (Fig. 1) were increased to 80.0%, the body would have a much longer firing range but the maturing temperature would be raised by as much as 75°C. (135°F.). The body composition would also be in the cristobalite primary phase area; cristobalite would therefore be a prominent crystalline phase in the fired body, which is undesirable.

The effect of zirconia and titania would be similar to that of the silica except for the deleterious action on thermal expansion.

V. Effect of Rate of Firing

It is difficult to cool the orthosilicates and most of the metasilicates of the divalent metals at a rate sufficiently rapid to prevent crystal formation; conversely, when a mixture of components is heated to produce meta- and ortho-silicates, it will attain equilibrium very rapidly. Steatite body compositions attain equilibrium much more rapidly during firing than do the common clay-flint-feldspar mixtures. The rate of temperature rise definitely affects the compositon and, accordingly, the viscosity of the liquid formed in the latter type of body but not to so great an extent in steatite compositions.

The only effects the rate of temperature rise can have on steatite bodies are on (1) the size of the clinoenstatite crystals resulting from the breakdown of the talc and (2) the rate of solution of the aluminous constituents.

Some steatite compositions have optimum dielectric properties when they are fired in 6 hours, whereas others reach optimum dielectric properties when fired in $1^1/_2$ hours. No correlation between body composition and optimum firing schedule has yet been found.

VI. Summary

From the silicate chemistry point of view, it appears to be impractical to lengthen the firing range of steatite bodies. It can be done but not without deleterious effects.

The short firing range is a result of (1) a comparatively large percentage of the body composition becoming liquid at the eutectic temperature and (2) the rapid rate of increase in liquid content with the temperature rise. Both of these conditions exist for all normal and low-loss steatite compositions used today.

Department of Ceramic Engineering
University of North Carolina, Raleigh Unit,
Raleigh, North Carolina

PHYSICAL TESTING OF TALC FOR HIGH-FREQUENCY CERAMICS*

By Sidney Speil†

Abstract

The preparation of test specimens is described as well as methods employed in testing approximately seventy different talcs, including materials for commercial use and samples from new sources. Correlations are noted between chemical analysis and the measured physical properties, if they are present to any degree.

I. Introduction

The expansion of the steatite industry in the past few years has been caused to a large extent by increased demands of the military service for high-frequency insulators. Before the war, much talc was imported, and a large portion of the pure domestic talc was produced by one California mine. Although no shortage of general ceramic- or filler-grade talc has occurred, there has been some anxiety concerning a possible scarcity of high-grade talc suitable for high-frequency insulator manufacture. The Bureau of Mines, therefore, was asked by the Joint Steatite Committee of the Army and Navy Munitions Board to investigate new sources of high-grade talc.

(1) Chemical Specifications

Specifications for talc have been established by different manufacturers, based mainly on the talc or talcs that have proved satisfactory in their steatite production. The maximum lime content ranges from 0.6 to 1.0%, and the ferric oxide maximum ranges from 0.1 to 1.5%. The stringent limitations on lime may be due to the fact that high-lime talcs have shown considerable variation in the lime content of successive shipments and the greater abrasive action of the tremolitic talcs shortens the life of dies and molds. The usual specification for steatite talc is designed actually to eliminate only the definitely inferior talcs. Experience indicates the lack of complete coordination between chemical oxide analysis and production or service requirements. Any talc that satisfies chemical specifications is qualified only for a practical ceramic and electrical test in the production line.

---

* Presented at the Forty-Fifth Annual Meeting, The American Ceramic Society, Pittsburgh, Pa., April 20, 1943 (Materials and Equipment Division). Received May 24, 1943.

Published by permission of the Director, Bureau of Mines, U. S. Department of the Interior; the work has been done in cooperation with the Tennessee Valley Authority.

† Associate Nonmetals Engineer, Electrotechnical Laboratory, Bureau of Mines, U. S. Department of the Interior, Norris, Tenn.

(2) Physical Properties

Iron oxide is the principal cause of color changes, and higher percentages lower the dielectric efficiency. Lime has been shown by some investigators to improve the high-frequency dielectric characteristics.[1] High-lime talcs containing appreciable amounts of tremolite are abrasive and have proved undesirable except as blends. High-lime talcs usually have a shorter vitrification range and sometimes a high shrinkage. The amount of shrinkage also depends on the fineness of grinding and on the green-pressed density. One manufacturer reports that the volume-shrinkage versus green-density relation is a practical working criterion for new talcs. Those talcs that satisfy the same relation as the production talc usually are good substitutes.

Actually each manufacturer prepares a body composition which, after firing to a given temperature on a given schedule, produces definite physical properties including shrinkage, strength, absorption, and power factor. Any variation in shrinkage would scrap the manufacturer's stock of steel dies. Variations in other properties might not be so harmful, but they would necessitate changes in plant operation. The final test of a new talc, therefore, is its direct substitution for the talc being used and a comparison of the properties of the new body with those of the standard production body. In some cases, a talc can be used as a blend constituent even though it is not a satisfactory substitute for the production material.

II. Steatite Body Testing

In the Bureau of Mines physical tests, all talcs were substituted directly for White Mountain Mine No. 3 talc from the Sierra Talc Company in a cone-14 test body consisting of talc 90, Edgar Florida kaolin 5, and Minpro 69–31 feldspar 5%. The body was wet-milled for 30 minutes, dried, and crushed to 14-mesh. A solution of 2% of gum arabic in 15% of water, both based on the weight of the talc body, was incorporated thoroughly.

Part of the material was dried and then reincorporated to give the final 16- to 100-mesh press powder containing $1^1/_2$% of moisture. The material was pressed at 4000 lb. per sq. in. to give 4-in. diameter by $^3/_{16}$-in. thick round tile and 6-in. square by $^1/_4$-in. thick tile for more accurate dielectric measurements by the Naval Research Laboratory. Round transverse strength bars, 1 by 6 in., were made by plastic extrusion in a small vacuum auger machine. The specimens were placed on a bedding of Ottawa sand and fired to cone 14^5 to 14^d in 24 hours, including a 5-hour soaking period in an electric Globar-fired kiln of 20- by 28- by 30-in. inside dimensions. The maximum temperature was approximately 1370°C. under these conditions. Standard Sierra talc body samples were placed in each firing and tested for uniformity of firing not only for different parts of the kiln but for the successive firings.

The test methods and specifications for acceptable talcs are summarized briefly. Six specimens were used unless the original talc sample was insufficient.

(*A*) *Absorption:* Specimens were evacuated for 20 minutes and saturated with water while still under a vacuum of 20 mm. of mercury. They were soaked for at least one hour before releasing the vacuum. The maximum acceptable absorption was 0.1%.

(*B*) *Shrinkage:* Two diameter measurements, normal to each other, were made with micrometer calipers. The acceptable shrinkage range was 6 to 10%. The standard body had a shrinkage of 7.4% with a maximum variation of ±0.8%.

(*C*) *Mechanical Properties:* The modulus of rupture was determined on a machine using lead shot at the end of an 8-to-1 lever arm.[2] The American Standards Association specification for high-frequency insulators of 3000 lb. per sq. in. was used. All acceptable bodies were well above this value.

Impact tests were made with a pendulum-type impact machine graduated in foot-pounds.[3] A 5-ounce hammer struck the center of the 4-in. round tile, which was supported at three points, until the specimen cracked. The first impact was 0.05 ft.-lb., and successive impacts were increased by 0.01 ft.-lb. increments. This rough determination gave comparable values. The standard body had an average impact resistance of 0.15 ft.-lb. with an average variation of ±0.02. A value of 0.12 was acceptable.

(*D*) *Dielectric Measurements:* The measurements were made with a Q meter, a commercial instrument measuring power factor and capacity at frequencies from 50 kilocycles to 50 megacycles. The theory of measurement with this instrument has been described by Thurnauer and Badger.[4] The samples were prepared and calculations were made according to specifications of the American Society for Testing Materials, using the simple capacitor circuit without shield or guard rings.[5] The *Q* value, or ratio of reactance to resistance, increases with improvement of the high-frequency electrical characteristics. The *Q* value of an acceptable talc body either was greater than or equaled that of the standard body within the experimental error of ±10%. The standard cone 14 test body had a *Q* value of 270 and was in class L–3 of the recent American Standards Association high-frequency insulator classification.[6]

---

[1] Hans Thurnauer, "Review of Ceramic Materials for High-Frequency Insulation," *Jour. Amer. Ceram. Soc.*, **20** [11] 368–72 (1937).

[2] American Ceramic Society, Standards Report, "A-15, Elasticity and Transverse Strength Apparatus," *Jour. Amer. Ceram. Soc.*, **11** [6] 514–19 (1928).

[3] Improved model of Bureau of Standards chinaware impact testing machine described by G. W. Wray and C. M. Brand, "Comparative Tests of Chinaware Using Two Forms of Testing Machines," *ibid.*, **12** [11] 716–24 (1929).

[4] Hans Thurnauer and A. E. Badger, "Dielectric Loss of Glass at High Frequencies," *ibid.*, **23** [1] 9–12 (1940).

[5] American Society for Testing Materials, Tentative Methods of Test for Power Factor and Dielectric Constant of Electrical Insulating Materials, Specification D150–41T.

[6] American Standards Association, Proposed American War Standard for Ceramic Radio Insulating Materials, Class L, Specification C75/93.

III. Cone 12 Bodies

A cone 12 body, using alkaline earth fluxes and no feldspar and with a Q value of approximately 1000, was also used to make certain that the test results were not specific and applicable only to the particular cone 14 test body used. The composition used was talc 78.5, Edgar Florida kaolin 5.0, barium carbonate 14.5, and calcium carbonate 2.0%. Talcs that were acceptable in one body were usually satisfactory in the other.

IV. Results

Tests were made on 64 samples, 19 of which were beneficiated by flotation at the Southern Experiment Station of the Bureau of Mines; 31 proved to be satisfactory substitutes for the standard talc, 27 were suitable as blend materials, and six appeared to be entirely unsuitable for use in high-grade steatite manufacture. It should be noted that most of these talcs were given ceramic tests only after passing preliminary chemical tests in which a large percentage of the original number was rejected.

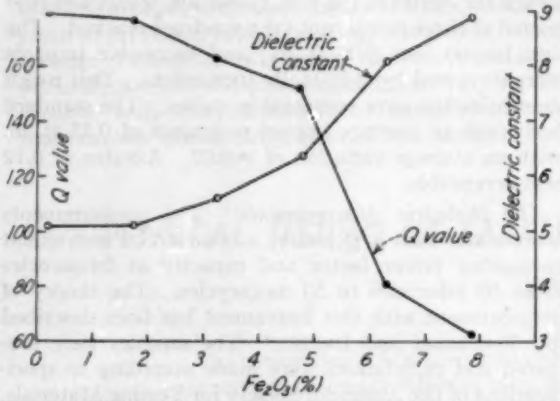

FIG. 1.—Effect of Fe_2O_3 content on properties of a cone 14 steatite body.

Attempts were made to correlate the physical properties with the chemical analyses. The statement that high-lime talcs have excessive shrinkage cannot be verified by the data of this investigation. The two talcs showing highest shrinkages (approximately 10%), for example, contained 0.03 and 0.05 of CaO. Extremely fine particle size accompanied by development of plasticity may have been the cause of high shrinkage in one case. Two other talcs containing 5.4 and 6.2% of lime had a linear shrinkage of 8%, which was almost equal to the standard Sierra talc with 0.6% of CaO. There are several factors entering into the problem of shrinkage, notably particle sizing, which controls the behavior of the steatite body in pressing. Results obtained in a different investigation showed that micronizing could increase the shrinkage by 4% and decrease the firing temperature by 15°C.

The same complex situation occurs in the firing temperatures. A New York talc containing 6.0% of CaO, presumably as tremolite, was porous, although another New York talc with 7.9% of lime was overfired when it was substituted into the same standard body and fired under the same conditions. In the case of California talcs, one containing 5.4% was vitrified at cone 14, whereas others containing 5.5 and 6.2% were overfired. The lime content therefore does not definitely indicate vitrification characteristics. High-lime talcs, however, were more often overfired than refractory when substituted for low-lime talc.

Iron oxide in talc has been avoided by steatite manufacturers inasmuch as it is a colorant. The restrictions on color have been decreased recently by the armed services. A maximum of 2% of iron oxide showed no definite correlation with dielectric properties. A decrease in Q value with increase of iron oxide, however, was noted above 2%. A series of test bodies was made using a low-iron New York talc and a Maryland talc containing 8% of Fe_2O_3. All bodies were vitrified at cone 14 with an absorption of less than 0.05%. The results given in Fig. 1 showed that as the iron oxide increased above 2% the Q value decreased and the dielectric constant increased.

Shrinkage also varied regularly with the percentage of each talc in the mixture. A blend of two or more talcs is commonly used in the manufacture of steatite insulators, and, by varying the percentage of the talcs, it is possible to compensate for slight changes between different shipments of talc.

The specifications of some manufacturers appear to be arbitrary because a talc that is satisfactory to one company may be rejected by another. The stringent chemical limitations are applied as a protective measure because the manufacturer knows that such high-purity talcs are more likely to be satisfactory in his process. It is entirely possible that high-lime, nonabrasive talcs would be acceptable in steatite manufacture if uniformity from shipment to shipment were better, but considerable research work by the manufacturer might be required.

New sources of high-grade talc which have been recently developed have greatly relieved the talc situation. There seems to be no necessity at the present time of using the high-lime talcs except to safeguard the future and to provide the eastern section of the country with a large quantity of talc at a more convenient location for ready shipments and lower freight rates. In testing new talcs for steatite production, chemical oxide analysis is helpful for preliminary classification, but the only test which the steatite manufacturer considers conclusive is the successful substitution in his own production body.

ELECTROTECHNICAL LABORATORY
BUREAU OF MINES
NORRIS, TENNESSEE

SPHERICAL FURNACE CALORIMETER FOR DIRECT MEASUREMENT OF SPECIFIC HEAT AND THERMAL CONDUCTIVITY*

By John R. Winckler†

Abstract

A spherical calorimeter was constructed for measuring true specific heat and thermal conductivity. It was formed of two concentric spherical platinum shells, and a spherical sample was fitted into the inner shell. Electric heat was supplied at the center of the sample, and the calorimeter was housed in a spherical electric furnace.

Thermal conductivity was measured by determining the inner and outer sample temperatures at steady heat flow using the equation of heat conduction in a sphere; specific heat was measured by noting the temperature rise of the sample with a known heat input while maintaining the calorimeter shells near the adiabatic condition; and a correction for heat leakage was made by using the conductivity determination to calculate this factor.

Specific heat and thermal conductivity measurements were made on quartz sand, chrome refractory cement, four types of insulating firebrick, and 85% magnesia insulation over a total temperature range of 100° to 2200°F. The estimated accuracy of specific heat measurement of 3 to 5% is consistent with engineering requirements. No estimate of accuracy can be given as yet for thermal conductivity results.

I. Introduction

The apparatus described here was developed as the result of an investigation during which various types of equipment for measuring the specific heats of refractory and insulating materials over a wide temperature range were examined. The equipment is advantageous because it can be used for measuring thermal conductivity as well as specific heat. Both of these measurements are usually desirable on the materials to which this apparatus is applicable.

Careful measurements of the specific heat and thermal conductivity of refractory and thermal insulations seem more nearly justified now because of the development of methods of exact calculation of temperatures and heat flow for design purposes.[1] Average values of specific heat and thermal conductivity were formerly sufficient for the approximate graphical or numerical methods available, but full advantage may now be taken of a knowledge of these thermal properties and their dependence on temperature. The spherical furnace calorimeter described here provides a convenient means of determining directly the thermal properties which effect the flow of heat, with an accuracy consistent with engineering requirements.

II. Historical Survey

The most widely used calorimetric apparatus for determining specific heats at high temperatures makes use of the method of mixtures in which the amount of heat given out by the sample under measurement when cooling from temperature t to room temperature is measured by transferring the sample from a furnace to the calorimeter. The resultant temperature rise of the calorimeter, whether it be of the fluid or of the aneroid or copper block type, gives a measure of the heat carried from the furnace by the sample. The technique of constructing and operating this type of calorimeter is well developed. A bibliography on this subject compiled by Seil, Heck, and Heiligman[2] has proved helpful in this investigation.

A method of measuring the specific heat, used less frequently, consists of supplying a measured amount of heat to the sample and determining the resultant temperature rise. The specific heat may then be calculated from these observations plus the sample weight. This method is useful for low-temperature calculations. The method is generally known as furnace calorimetry because the calorimeter itself is contained in the furnace which is used to obtain the high temperatures. The heat gained by the sample may be supplied electrically or by transfer from the furnace walls. Thermal electrons were used in one case to heat the sample by bombardment.[3] White,[4] Perrier and Roux,[5] Cohn,[6] Carpenter and Harle,[7] and Moser[8] have investigated or

* Presented at the Forty-Fifth Annual Meeting, The American Ceramic Society, Pittsburgh, Pa., April 20, 1943 (Refractories Division). Received March 31, 1943.

† Formerly assistant physicist, Johns-Manville Research Laboratory, Manville, N. J.

[1] V. Paschkis and H. D. Baker, "Method of Determining Unsteady-State Heat Transfer by Means of Electrical Analogy," *Trans. Amer. Soc. Mech. Eng.*, **64** [2] 105–12 (1942).

[2] G. E. Seil, F. G. Heck, and H. A. Heiligman, "Specific Heats of Chrome and Magnesia Refractories," *Jour. Amer. Ceram. Soc.*, **24** [6] 204–12 (1941).

[3] H. Klinkhardt, "Measurement of True Specific Heats at High Temperature by Heating with Thermionic Electrons," *Ann. Physik*, **84**, 167–200 (1927).

[4] W. P. White, "Calorimetry in Furnaces," *Jour. Phys. Chem.*, **34** [6] 1121–36 (1930); *Ceram. Abs.*, **9** [8] 657 (1930).

[5] A. Perrier and H. Roux, *Mem. Soc. Vaudoise Sci. Nat.*, pp. 109–36 (1923); abstracted in *Arch. Sci. Phys. Nat.*, **5** [5] 310–12 (1923).

[6] W. M. Cohn, "Determination of Specific Heats and Heat Tone from Temperature-Time Curves," *Z. Angew. Chem.*, **40**, 1557–59 (1927).

[7] G. L. Carpenter and T. F. Harle, "A Vacuum Calorimeter for High Temperatures," *Proc. Phys. Soc.* [London], **44**, 383 (1932).

[8] H. Moser, "Measurement of True Specific Heats of Silver, Nickel, β-Brass, Quartz, and Vitreous Silica Between 50° and 700°C. by a Refined Method," *Physik. Z.*, **37**, 737–53 (1936).

used furnace calorimeters. Moser's method, which makes use of an evacuated silver calorimeter developed from the method of Perrier and Roux, is apparently the most successful of the direct methods encountered so far, with an accuracy of the order of 0.5%. The temperature range, however, is limited.

Thermal conductivity at all temperatures is usually determined by measuring the temperatures and heat flow in the test sample in the form of a flat slab so that the problem reduces to a one-dimensional, steady-state heat flow calculation, which, in theory at least, is very simple.[9] Cylindrical sections of the sample with the source of heat along the axis have also been used, especially for determining the heat conductivity of pipe insulation.[10] A spherical sample with the source of heat at the center of the sphere has also been used by several observers.[11]

Each of these types of thermal apparatus has its merits and disadvantages. The fluid and aneroid calorimeters are capable of great precision, but they do not yield the specific heat directly; the total heat in the sample is obtained instead as a function of temperature. The true specific heat is the first derivative of the total heat function and can be calculated only with a considerable loss of accuracy. This effect is exaggerated if a change of form or transition point occurs in the sample under measurement, with a corresponding discontinuity in the specific heat (e.g., quartz, see Fig. 8). The furnace calorimeter, however, will yield direct true specific heat measurements over small-temperature increments, but it contains features, especially at high temperatures, which lower the precision of measurement.

A spherically shaped furnace calorimeter, theoretically, is the most desirable because a sphere presents the least surface for heat leakage for a given volume of material and because of its symmetry.

The flat-slab thermal conductivity apparatus has the advantage that the test sample is easy to prepare and install. Extensive guarding heaters and careful balancing, however, are required to eliminate edge effects and to make the heat flow truly linear. The cylinder requires guarding only at the ends, but shaping a cylindrical section for test is often more difficult than preparing a flat slab. The sphere requires no guarding because all of the heat which is generated at its center flows directly through the test sample. The sphere, however, probably is the most difficult shape to prepare for test.

The present apparatus is a calorimeter of the furnace type, which is arranged to accommodate a spherical sample so that both thermal conductivity and specific heat measurements may be obtained.

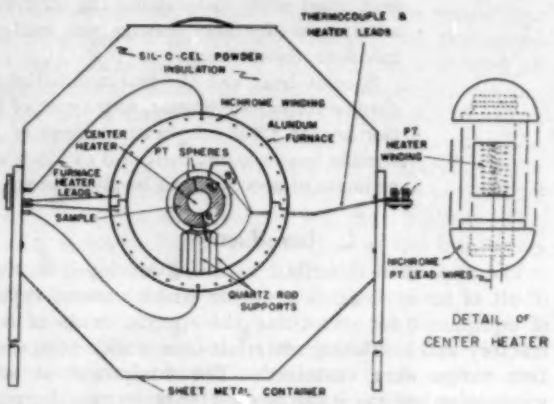

FIG. 1.—Cross section of calorimeter and furnace.

III. Plan of Procedure and Apparatus

The most important parts of the apparatus are the calorimeter and the furnace (see cross section, Fig. 1). The calorimeter consists of two concentric spheres of 0.012-in. thick platinum with radii of 1.38 in. and 1.77 in., respectively. Each sphere is constructed in two hemispheres, which fit together in a friction-tight lap joint. The inner sphere is supported within the outer one by a tripod of porcelain tubes and Alundum cement. The outer sphere rests on the rounded tips of three $^1/_2$-in. quartz rods which are set in the bottom of the furnace. The furnace is constructed of Alundum cement and is in the form of a sphere of 8-in. inside diameter with walls 1 in. thick. The furnace is heated by a uniform winding of Nichrome wire and is also made in two hemispheres that fit together with a lap joint. This furnace is contained in a metal can (see Fig. 2) and is insulated in all directions and supported in place by 6 in. of insulating firebrick dust. The sample to be measured is cut from the brick or block of material with the hardened steel cutters (Fig. 3) and is also in the shape of two hemispheres, which join to form a hollow sphere, 1.38-in. outside and 0.590-in. inside radii. The cutters are arranged for use in a drill press. The sample fits inside the inner platinum sphere and supports the center heater in the hollow at the center. This heater is a 0.590-in. radius ball of Nichrome V, which is hollowed out to contain a heater winding of No. 34 B & S platinum alloy wire, cemented in with fine Alundum (see detail, Fig. 1).

[9] (*a*) M. S. Van Dusen, "Thermal Conductivity of Heat Insulators," *Jour. Amer. Soc. Heating Ventilating Engrs.*, **26** [7] 625–56 (1920).
(*b*) C. E. Weinland, "Method of Measuring Thermal Conductivity at Furnace Temperatures," *Jour. Amer. Ceram. Soc.*, **17** [7] 194–202 (1934).
(*c*) C. E. Weinland, "Celite-Type High Temperature Thermal Conductivity Apparatus," *Proc. Amer. Soc. Testing Materials*, **37** [Part II] 269–76 (1937); *Ceram. Abs.*, **17** [4] 149 (1938).

[10] (*a*) C. Dinger, A. Kind, W. Shütz, and A. Dietzel, "New Method for Determination of Thermal Conductivity at High Temperatures," *Ber. Deut. Keram. Ges.*, **20** [8] 347–62 (1939); *Ceram. Abs.*, **20** [4] 95 (1941).
(*b*) L. B. McMillan, "Heat Transfer Through Insulation in Moderate and High-Temperature Fields: Statement of Existing Data," *Trans. Amer. Soc. Mech. Eng.*, **48**, 1269–1317 (Appendix No. 7) (1939).

[11] (*a*) L. Beuken, "Measurement of Thermal Conductivity of Insulating Brick," *Wärme- & Kälte-Tech.*, **40** [11] 161–63 (1938); *Ceram. Abs.*, **20** [8] 195 (1941).
(*b*) S. E. Green, "Spherical Shell Method of Determining the Thermal Conductivity of a Thermal Insulator," *Proc. Phys. Soc.*, [London], **44**, 295–313 (1932).
(*c*) R. Glazebrook, Dictionary of Applied Physics, Vol. I, p. 431. Macmillan & Co., 1922.

FIG. 2.—Assembled calorimeter in furnace.

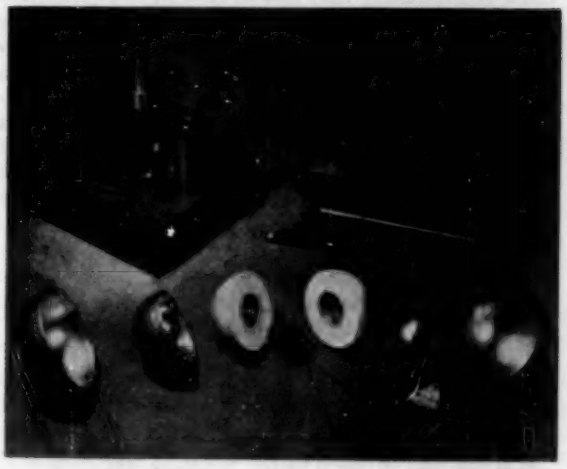

FIG. 3.—Center heater, sample, and calorimeter spheres ready to be assembled; sample cutters in background.

The calorimeter and the furnace, consisting of the center heater, the sample, the inner and outer calorimeter spheres, the furnace, the insulation, and the metal can, are thus composed of six spheres, one within the other. This arrangement provides for temperature symmetry in the apparatus. Each sphere constitutes a nearly equithermal surface, which is a necessary condition for correct operation.

The temperatures are measured by 28-gauge platinum to 90% platinum–10% rhodium thermocouples that have previously been calibrated against a Bureau of Standards certificate thermocouple accurate to within 2°F. The inner surface temperature, θ_1, is read by a thermocouple forced into a small hole on the surface of the center heater; the outer surface temperature, θ_2, by a thermocouple with its head flattened and

FIG. 4.—Complete apparatus; furnace at right, photoelectric temperature controller under bench at right.

spot welded to the smaller platinum sphere; and θ_3, by a thermocouple similarly attached to the larger sphere. The inside thermocouples and center-heater leads are brought out through the calorimeter spheres in small holes insulated with 1-mm. outside diameter porcelain tubes. Current and potential leads are welded to the center-heater leads between the inside furnace wall and the calorimeter and, together with the thermocouple leads, are brought to a terminal board outside the container through larger-sized porcelain tubes. The furnace-power leads are brought to a second terminal board on the opposite side of the container.

The additional apparatus used for the measurements consists of a photoelectric temperature control for maintaining the furnace at the desired temperature, a Transtat, switches and fuses for controlling the power to the furnace, an accurate potentiometer (a Leeds and Northrup type K-2) for measuring θ_1, θ_2, and θ_3, a voltmeter and ammeter of the thermocouple type, a multiple-junction iced thermocouple, and an auxiliary slide-wire potentiometer of low range (Fig. 4). The power for the center heater is obtained from a Variac connected to a 60-cycle controlled voltage alternating current source.[12]

IV. Test Methods

(1) Thermal Conductivity Test Method

After the apparatus has been assembled (Fig. 2), the furnace temperature controller is set at the desired point and the furnace power is switched on. An amount of power sufficient to give a convenient temperature drop across the sample is also supplied to the center heater. After a number of hours, depending on the temperature of the test and the nature of the test material, the steady state is attained. Under this condition, all of the heat generated in the center heater flows directly through the sample to the inner calorimeter sphere, then to the outer sphere, and to the furnace wall by radiation. All temperatures remain constant.

[12] C. E. Weinland, "Thyratron Voltage Regulator for Alternator," *Rev. Sci. Instruments.* **3** [1] 9–19 (1932).

θ_1 being higher than θ_2, which in turn slightly exceeds θ_3 and the furnace-wall temperature. The thermocouple readings, $E\theta_1$, $E\theta_2$, and $E\theta_3$, and the voltage and current are recorded. This condition is shown in the interval, *A–B*, of Fig. 5.

An expression for the conductivity in terms of the dimensions of the sample, the temperature drop across it, and the rate of heat flow through it may be derived from the general equation of heat conduction in a sphere; the final form is shown by equation (1).

$$k = \frac{r_2 - r_1}{4\pi r_1 r_2(\theta_1 - \theta_2)} \frac{dq}{dt} \qquad (1)$$

r_2 = outside radius of sample.
r_1 = inside radius of sample.
θ_1 = inner surface temperature.
θ_2 = outer surface temperature.
$\frac{dq}{dt}$ = time-rate of heat flow through sample.

The sample dimensions and the necessary conversion factors may be lumped into a constant for any one sample. This procedure gives equation (2) for conductivity.

$$k = A \cdot \frac{W_c}{\Delta\theta} \cdot \frac{\text{B.t.u.·in.}}{\text{hr.·ft.}^2\text{·°F.}} \qquad (2)$$

$A = 39.2 \frac{r_2 - r_1}{r_1 r_2}$.
W_c = corrected watts to center heater.
$\Delta\theta$ = temperature drop $(\theta_1 - \theta_2)$ (°F.).
r_1, r_2 = inside and outside radii of sample (in.).

W_c differs from the total watts, $W = E \times I$, as read by the meters because of (1) the power dissipated by the voltmeter, given by E^2/R_1, where E is the voltage read by the meter and R_1 its resistance, and (2) the power dissipated in the heater leads between the sample and the poirt where the potential is measured. This power is given by I^2R_2, where I is the current read by the ammeter and R_2 the lead wire resistance. Because R_2 changes with temperature, a curve was drawn from equation (3) given for platinum by the International Critical Tables.[13]

$$\frac{R_t}{R_{t'}} = 1 + {}^{5}/_{9}A(t - t')10^{-3} + ({}^{5}/_{9})^2 B(t - t')^2 10^{-6} \qquad (3)$$

R_t = resistance at t°F.
$R_{t'}$ = resistance at 32°F. (t').
$A = 3.981$.
$B = 0.585$.

$R_{t'}$ was measured directly for the 28-gauge platinum lead wire in an ice bath so that R_t could be determined easily from the curve. The average temperature of the wire is assumed to be θ_2.

The corrected power is then given by equation (4).

$$W_c = W - \left(\frac{E^2}{R_1} + I^2R_2\right) \qquad (4)$$

The temperature drop across the sample, $\Delta\theta$, is obtained by multiplying the corrected thermocouple

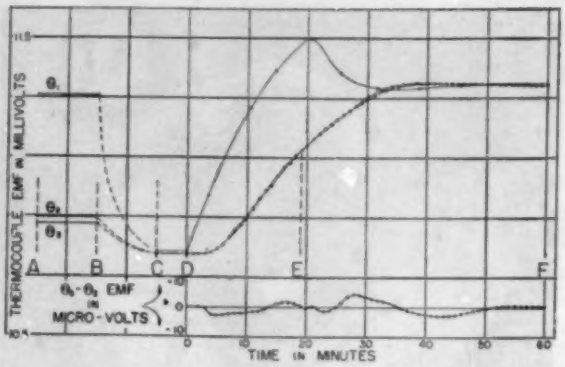

FIG. 5.—Temperature behavior during a thermal conductivity and specific heat determination.

electromotive-force difference across the sample in microvolts $(E\theta_1 - E\theta_2)$, by the degrees per microvolt given by the International Critical Tables for platinum to 90% platinum–10% rhodium thermocouples at the mean temperature, $\theta_m = {}^{1}/_{2}(\theta_1 + \theta_2)$. The actual e.m.f. difference $(E\theta_1 - E\theta_2)$ associated with a flow of heat, W_c, through the sample must be corrected because this quantity may not be zero when equilibrium is reached at $W_c = 0$ as a result of small differences in the thermocouples or slight asymmetry of the furnace temperatures. This correction is determined as a part of the specific heat measurement to be described.

The following data were taken to obtain the highest temperature conductivity point on curve *F*, Fig. 11. These conditions are also shown in *A–B* of Fig. 5.

$E\theta_1$ = 11.3059 mv. I = 0.2645 amp.
$E\theta_2$ = 10.8955 mv. E = 16.20 volts.
$E\theta_3$ = 10.8758 mv. R_1 = 3750 ohms.

Platinum wire resistance at 32°F. = 0.0122 ohms/cm
Heater lead length = 20.1 cm.
Avg. r_1 = 0.604 in.
Avg. r_2 = 1.374 in.

The calculations were as follows:

Calibration correction to $E\theta_1$ = 0.0210 mv
Calibration correction to $E\theta_2$ = 0.0218 mv.
Corrected $E\theta_1$ = 11.2859 mv. = 2096°F.
Corrected $E\theta_2$ = 10.8737 mv. = 2033°F.
θ mean = 2065°F.
$R_{t'}$ = 0.246 ohm.
$\frac{R_t}{R_{t'}}$ at 2033°F. = 4.71.
R_2 = 1.160 ohms.

$$W_c = (0.2645 \times 16.20) - \left[(0.2645)^2 \times 1.16 + \frac{(16.20)^2}{3750}\right] = 4.139 \text{ watts}$$

$(E\theta_1 - E\theta_2)$ = 0.4122 mv.
Correction (from "initial equilibrium" of specific heat measurement) = −0.0062 mv.
Corrected $(E\theta_1 - E\theta_2)$ = 0.4060 mv.
Temperature conversion factor at 2065°F. = 0.1529°F./μ volt.
$\Delta\theta$ = 62.2°F.

$$k = 39.2 \times \frac{1.374 - 0.604}{1.374 \times 0.604} \times \frac{4.139}{62.2} = 2.41 \frac{\text{B.t.u.·in.}}{\text{hr.·ft.}^2\text{·°F.}}$$

at mean temp. of 2065°F.

[13] International Critical Tables, Vol. VI, 136 (1927).

(2) Specific Heat Test Method

Starting with the apparatus in the steady flow condition for obtaining a conductivity value, the first step in making a specific heat measurement is to remove the power from the center heater. The sample and calorimeter then cool until their temperature becomes equal to the furnace temperature, which is held constant by the photoelectric control. This action is represented by the interval *B–C* in Fig. 5. W now equals zero and closely uniform temperature conditions exist throughout the furnace. A small difference will exist in most cases between $E\theta_1$ and $E\theta_2$ at this time. This is the correction to be applied to the $\Delta E\theta$ of the conductivity test mentioned previously. The potentiometer is now connected to read $(E\theta_3 - E\theta_2)$ by connecting θ_2 and θ_3 in series differential; $(E\theta_3 - E\theta_2)$ is also seldom equal to zero but has a value representing the adiabatic point of the calorimeter walls. $E\theta_1$, $E\theta_2$, and $(E\theta_3 - E\theta_2)$ are read at intervals for ten to fifteen minutes to make sure that constant temperature conditions have been reached. This is the "initial equilibrium" condition preceding a specific heat measurement (interval $C–D$, Fig. 5). The adiabatic reading $(E\theta_3 - E\theta_2)$ may be adjusted to any desired point on the potentiometer scale by inserting the small variable slide wire (range 0 to 40 μ volts) in series. It is customarily adjusted to 30 μ volts.

At a measured initial time, the power is again applied to the center heater; θ_1 and, shortly afterward, θ_2 begin to increase as shown in the interval *D–E* (Fig. 5). An effort is made to keep the calorimeter walls at the adiabatic point given by the initial $(E\theta_3 - E\theta_2)$ reading by removing the furnace temperature controller and controlling the furnace temperature by manual operation of the Transtat, which supplies the power to the furnace windings. The overshoot and undershoot of this controlling action result in the $(E\theta_3 - E\theta_2)$ controlling curve shown in Fig. 5. An area under the axis represents heat lost by the calorimeter and an area above shows a gain of heat. The potentiometer readings are recorded each minute. The supplied power and the time of application are adjusted so that the heat is sufficient to make $\Delta\theta$ of a convenient value. The power is again cut off at point *E* (Fig. 5). The temperature gradient established in the sample soon flattens out, $E\theta_1$ and $E\theta_2$ arrive at a new value during the interval *E–F* (Fig. 5), and $E\theta_1$ and $E\theta_2$ finally become constant at the "final equilibrium" condition and their values are recorded. The total increases ($\Delta E\theta_1$ and $\Delta E\theta_2$) in $E\theta_1$ and $E\theta_2$ from the initial equilibrium condition are nearly the same and are averaged to obtain $\Delta E\theta$; $\Delta\theta$ is obtained from $\Delta E\theta$ as in the conductivity measurement. This process may be repeated in steps over the desired temperature range, or points may be taken at separated intervals of temperature.

At temperatures above about 1500°F., where the ceramic parts of the apparatus become more electrically conductive, difficulties are encountered with leakage between thermocouple and power circuits. A difference of potential appears between the two calorimeter shells when the center heater is turned on, and the differential reading $(E\theta_3 - E\theta_2)$ is disturbed. This effect is greatly accentuated if direct current is used on this heater instead of alternating current. It has been found necessary to plot $E\theta_2$ and $E\theta_3$ separately during measurements above 1500°F. because the thermocouple readings taken individually are not appreciably affected by the leakage.

The voltmeter and ammeter are read at intervals during the heating period and are averaged to compute the total power, W. This power is corrected to W_c by the same method used in the conductivity test.

The $(E\theta_3 - E\theta_2)$ adiabatic control, in general, is not sufficiently precise so that the area under the axis is exactly equal to that above. These areas may be subtracted graphically with a planimeter, and the resultant area figure may be converted to heat units if the heat flow rate, represented by a given value of $(E\theta_3 - E\theta_2)$, is known. This value is determined from the measurement of $E\theta_3$ and $E\theta_2$ made under steady state conditions of the conductivity test. This factor varies greatly with the temperature and must be known for the approximate temperature of the test. A typical curve of rate of heat flow through the calorimeter walls per unit of thermocouple e.m.f. difference at various temperatures is shown in Fig. 6, and this curve was closely duplicated on each test run.

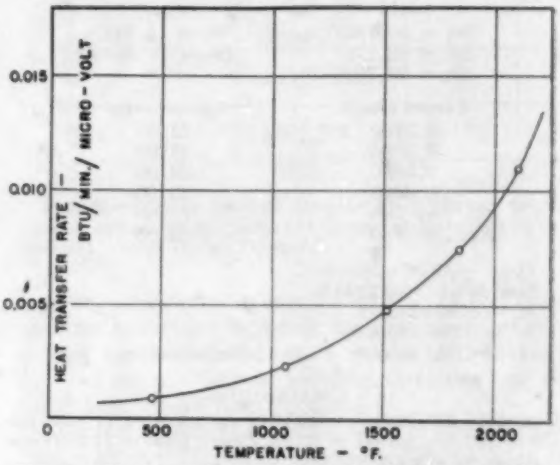

FIG. 6.—Heat transfer rate through calorimeter walls.

The heat leakage is then given by equation (5).

$$Q = KA \tag{5}$$

Q = B.t.u. gained or lost during test through calorimeter walls.
K = heat-transfer factor for avg. temp. determined in B.t.u./min./μ volt.
A = area of $(E\theta_3 - E\theta_2)$ curve in μ volt-minutes.

The heat capacity is calculated from equation (6).

$$H_1 = \frac{Q'}{\Delta\theta} \tag{6}$$

Q' = total supplied energy (B.t.u.).
$\Delta\theta$ = sample temp. rise (°F.).

This heat capacity consists of the sample heat capacity, H, and the heat capacity of the center heater and inner platinum sphere of the calorimeter, H_2. It

is thus necessary to know the value of H_2 in order to calculate H and the sample specific heat.

To determine H_2, the apparatus was assembled exactly as described for a specific-heat measurement but with no sample in the calorimeter. The center heater was supported at the center of the inner calorimeter sphere by a small light tripod of ceramic tubes and Alundum cement. Blank heat-capacity measurements of the calorimeter were then made by the method just described. The heat capacity of the tripod, used only for calibration purposes, was plotted as a function of temperature from values obtained for alumina from tables, and correction was made accordingly. The curve of H against temperature is shown in Fig. 7.

After enough values of H_1 have been obtained to draw a curve of total heat capacity against temperature, the specific heat is determined by subtracting the calorimeter heat capacity at any desired temperature and dividing by the sample weight.

A sample calculation of H_1 uses the values obtained for one of the highest temperature points, curve G, Fig. 7. This determination is also the same as that whose temperature behavior is shown in Fig. 5.

DATA

Equilibrium (mv.)

Initial	Final
$E\theta_1 = 10.7857$	$E\theta_1 = 11.3447$
$E\theta_2 = 10.7787$	$E\theta_2 = 11.3440$
$E\theta_3 = 10.7849$	

Current (amp.)	Voltage (volts)
0.3700	23.90
0.3680	23.90
0.3680	23.90
0.3680	23.90
Avg. 0.3685	23.90

Time = 19.00 minutes
Sample wt. = 0.2290 lb.
R_1 = 3750 ohms.
R_t' = 0.246 ohm.
($E\theta_3 - E\theta_2$) area = +103.4 μ volt-minutes.

CALCULATIONS

Corrected $E\theta_1$, initial = 10.7642 mv.; final = 11.3238 mv.
Corrected $E\theta_3$, initial = 10.7571 mv.; final = 11.3231 mv.
Mean θ_2 = 2058°F.

Ratio $\frac{R_t}{R_t'}$ = 4.77 and $\frac{R_t}{R_t}$ = 1.172 ohms.

$$W_r = (0.3685 \times 23.90) - \left[(0.3685)^2 \times 1.172 + \frac{(23.90)^2}{3750}\right] = 8.494 \text{ watts}$$

Total energy supplied electrically = 8.494 × 0.05692 × 19.00 = 9.17 B.t.u.
Factor K at 2058°F. = 0.0124 B.t.u./min./μ volt.
Heat leakage = 0.0124 × 103.4 = +1.28 B.t.u.
Total heat input = 9.17 + 1.28 = 10.45 B.t.u.
Avg. $E\theta$ = 0.5628 mv.
Temp. conversion factor at 2058°F. = 0.1519°F./μ volt.
$\Delta\theta$ = 0.5628 × 0.1519 = 85.5°F.

$$H_1 = \frac{10.45}{85.5} = 0.1222 \text{ B.t.u./°F.}$$

The heat leakage and the difference between $\Delta E\theta_1$ and $\Delta E\theta_2$ are larger than usual in the foregoing example. Both of these factors depend largely on the skill of the operator in controlling the furnace temperature and on the temperature of the test. The heat leakage varies randomly from test to test.

The sample weight was determined after testing.

One of the requirements of the spherical apparatus is that the temperature at all times must be a function of the radius only and must not vary with the angular position about the calorimeter or furnace. Large errors may occur if this condition is not maintained, especially in measurements of specific heat; for example, the adiabatic condition of the calorimeter walls as measured by thermocouples θ_2 and θ_3 might be true only at that portion of the calorimeter where the thermocouples are placed while at another point unknown amounts of heat might flow in or out of the sample during a test.

To determine whether temperature symmetry exists in the apparatus, ten Chromel-Alumel thermocouples were carefully located around the inside of the furnace, and temperature measurements were taken at various times in the cycle of operation of the apparatus.

θ is the angular position of the thermocouple down from the top of the furnace and φ, the angular position around the furnace from a central vertical plane.

Furnace-wall temperatures (°F.)

φ =	0	180	0	90	270
θ =	180	150	150	90	90
	223	222	222	219	222
	307	308	309	308	308
	1052	1051	1051	1050	1051
φ =	180	0	90	270	0
=	90	90	60	60	0
	220	220	219	220	219
	308	307	307	309	308
	1049	1051	1048	1050	1049

Inasmuch as all ten of these temperatures cannot be measured quickly enough to determine the symmetry under changing furnace conditions, the top and bottom center couples were measured at various times during a cycle of operation with the following results:

	Center temp. (°F.)	
Part of cycle	Top	Bottom
Initial	755	754
Final	818	818
Initial	1181	1181
Initial	1527	1527
Final	1545	1545
Initial	2036	2036
Final	2081	2080

Because the outside platinum sphere is in equilibrium with the furnace wall chiefly by radiation and because the platinum is a good heat conductor, the calorimeter was assumed, on the basis of these measurements, to have fulfilled the necessary conditions of temperature.

V. Test Results

Specific heat measurements were made on quartz, chrome refractory cement, four types of insulating firebrick, and 85% magnesia insulation. Thermal

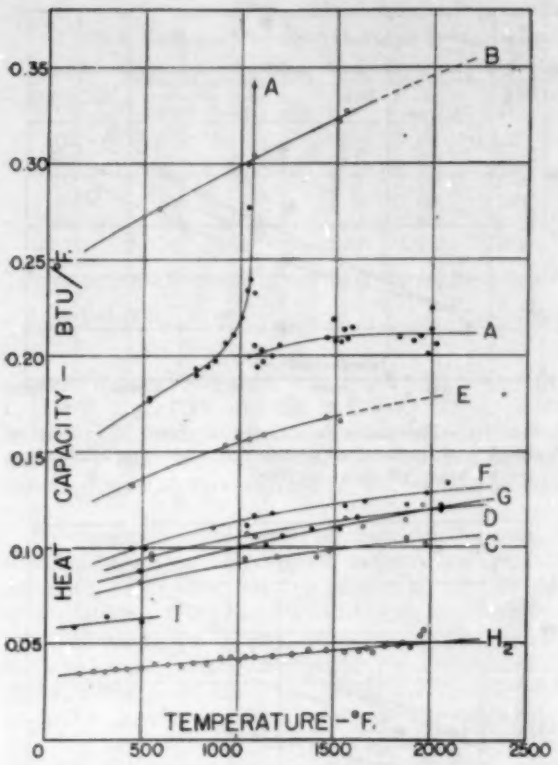

FIG. 7.—Heat capacity curves showing experimental points. *A*, quartz; *B*, chrome cement; *C*, group 20 insulating firebrick; *D*, group 23 insulating firebrick; *E*, group 23 insulating firebrick; *F*, group 26 insulating firebrick; *G*, diatomaceous earth brick; H_2, calorimeter heat capacity; *I*, 85% magnesia.

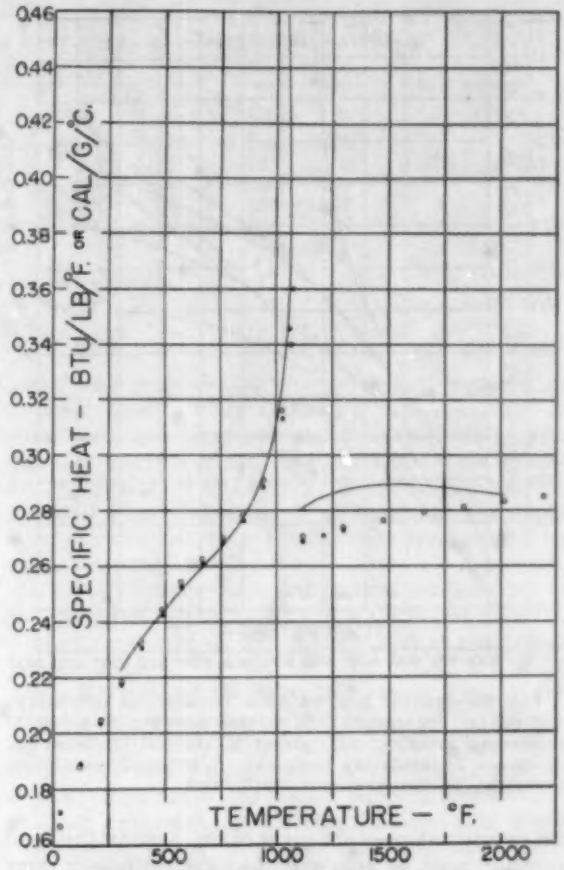

FIG. 8.—Specific heat of quartz. Solid curves, present results; open circles, Sosman[14] (from results of White and Wetzel); solid circles, Moser.[8]

conductivity measurements were made on all materials except the quartz. All of the heat capacity curves and the experimental points are shown in Fig. 7. The resultant specific heat curves are shown in Figs. 8 and 9.

The quartz was in the form of sand with a particle distribution centered approximately at 0.15 mm. Chemical analysis showed the sand to be 99.23% SiO_2. The index of refraction, which was determined by comparison with standard oils under a microscope, was between 1.54 and 1.55. The spherical sample was cut from a brick made with gulac binder, and this binder was burned out after the apparatus was assembled.

The temperature of the transition point from α to β quartz was obtained by plotting a curve of θ_1 as the sample was heated or cooled from the outside. This was found to be 1062.5 ± 2°F. (572.5 ± 1°C.) for either heating or cooling by noting the temperature of the discontinuity in the temperature-time curves caused by the release or absorption of the heat of transformation. Sosman[14] gives the inversion temperature at 573° ± 1°C. for rising temperatures and about 1°C. less for falling temperatures. A heat capacity measurement over an 8.42°F. (4.7°C.) temperature increment, including the inversion point, gives a limit for the latent heat of transformation of 2.45 cal. per gram. Various previous estimates[15] of this value have ranged from 1.7 to 4.3.

Figure 8 shows the specific heat of quartz versus temperature. The curve represents the results of the present investigation; the open circles are from Sosman,[16] based on the investigations of White and Wetzel, and the solid circles represent the data of Moser.[8] The Sosman values are also the same as those given in the International Critical Tables.[17]

The agreement between these three sets of values is exceedingly close for values below the inversion point. Above the inversion point, the values of Sosman and Moser agree very well, but those of the present paper are generally higher. Because of this disagreement, a second quartz sample was prepared and tested at temperatures above the inversion point. These tests confirmed the results obtained on the first sample. Inasmuch as the specific heat of quartz is not expected to decrease with increasing temperature above 1500°F.,

[14] R. B. Sosman, Properties of Silica, p. 114. Chemical Catalogue Co., New York, 1927. 836 pp.; *Ceram. Abs.*, 7 [7] 505 (1928).

[15] *Ibid.*, pp. 312 and 322.

[16] *Ibid.*, p. 314.

[17] International Critical Tables, Vol. V, 105 (1926).

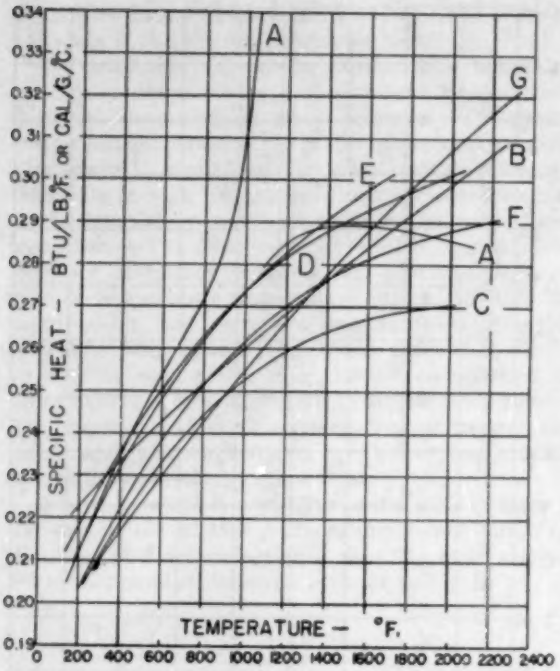

FIG. 9.—Specific heat of some commercial insulations and quartz. *A*, quartz; *B*, chrome cement; *C*, group 20 insulating firebrick; *D*, group 23 insulating firebrick; *E*, group 23 insulating firebrick; *F*, group 26 insulating firebrick; *G*, diatomaceous earth brick.

the negative slope of the curve of Fig. 8 above this temperature must be attributed to some systematic error in the measurement at the highest temperatures.

The chrome refractory cement (curve *B*, Fig. 9) was composed of equal quantities of chromite and dead-burned magnesite, with a small amount of calcium aluminate cement added. The two hemispheres of the spherical sample were first molded to shape and then dried and fired at 2600°F. as the fired cement could not be cut with the steel cutters. Satisfactory results were not obtained on this material above about 1500°F. because of the effect of electrical leakage to the thermocouples. The technique of plotting $E\theta_2$ and $E\theta_3$ separately to avoid this difficulty had not been used when the chrome cement was tested.

Inasmuch as the composition of chrome and magnesite refractories varies widely, no suitable comparative results are available for this material. Seil, Heck, and Heiligman[2] measured the mean specific heats of specially prepared chrome and magnesite ores and found values of 0.226 and 0.283, respectively, between 25° and 850°C. (77° and 1562°F.) A calculation of mean specific heat from the present measurements gives a value of 0.251 for the mean specific heat over the same range.

Curves *C*, *D*, and *F*, of Fig. 9 represent insulating firebrick designed for use at 2000°, 2300°, and 2600°F., respectively. These brick are not of a type now in commercial production. Curve *E* represents a sample of the 2300°F. brick prepared by grinding and rebonding a standard brick at a higher density to ascertain whether results could be repeated with different masses of the same material; curves *D* and *E* agree to about 1%. The check tests could not be carried above 1500°F. because of shrinkage of the rebonded sample which separated the two halves of the sphere. The comparison of curves *D* and *E* also provides an indirect check on the accuracy of the blank calorimeter heat capacity curve.

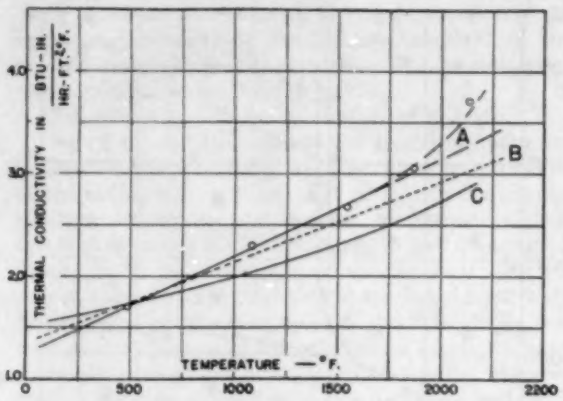

FIG. 10.—Thermal conductivity of group 26 insulating firebrick. *A*, present apparatus; *B*, slab-type apparatus; *C*, temperature gradient method.

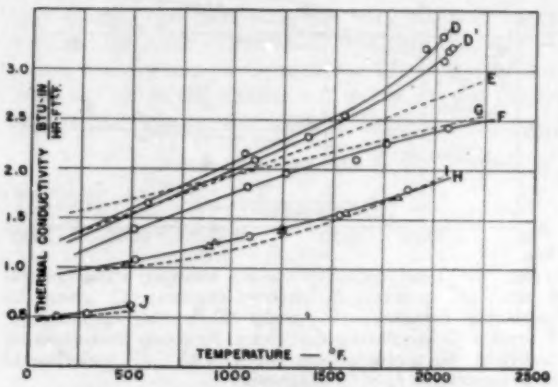

FIG. 11.—Thermal conductivity of some commercial insulating materials. *D*, *D'*, and *E*, group 23 insulating firebrick; *F* and *G*, diatomaceous earth brick; *H* and *I*, group 20 insulating firebrick; *J*, 85% magnesia.

The composition of these brick, based on analyses of the raw materials and the known chemical reactions on firing, are approximately as follows:

2000°F. brick (%)	2300°F. brick (%)
60.2 $Al_2O_3 \cdot 2SiO_2$	74.5 $Al_2O_3 \cdot 2SiO_2$
39.8 SiO_2 and CaO probably as $CaO \cdot SiO_2$	25.5 free SiO_2

2600°F. brick (%)
29.2 $3Al_2O_3 \cdot 2SiO_2$
56.6 $Al_2O_3 \cdot 2SiO_2$
14.2 free SiO_2

Curve *G* represents a molded diatomaceous earth brick calcined at approximately 2400°F.; its chemical

TABLE I

THERMAL CONDUCTIVITY AND SPECIFIC HEAT OF REFRACTORY AND INSULATING MATERIALS*

Temp. (°F.)	Chrome cement		Insulating brick 2600°F.		Insulating brick 2300°F.		Insulating brick 2000°F.		Diatomaceous earth brick		85% magnesia	
	C_p†	k‡	C_p	k	C_p	k	C_p	k	C_p	k	C_p	k
300	0.228		0.213	1.55	0.227	1.40	0.211	0.98	0.210	1.22		
500	.238		.231	1.73	.243	1.56	.226	1.07	.223	1.38	0.325	0.620
1000	.260		.262	2.18	.274	1.99	.253	1.24	.255	1.76		
1500	.280		.279	2.69	.290	2.48	.266	1.54	.283	2.10		
2000	.299	10.3	.288	3.39	.301	3.08	.271	1.90	.307	2.39		
2200			.290	3.77	.305	3.38			.316	2.49		

* No estimate of accuracy can be given yet for thermal conductivity results.

† C_p, Cal./gm./°C. or $\frac{\text{B.t.u.}}{\text{lb.} \cdot {}^\circ\text{F.}}$ ‡ k, $\frac{\text{B.t.u.} \cdot \text{in.}}{\text{hr.} \cdot \text{ft.}^2 \cdot {}^\circ\text{F.}}$

analysis is SiO_2 90.3, Al_2O_3 4.28, Fe_2O_3 0.90, TiO_2 0.24, CaO 2.65, MgO 0.79, and K_2O and Na_2O 1.09%. This brick is composed principally of amorphous silica, and its specific heat does not appear to approach a limiting value within the temperature of test as do the clay brick.

The magnesia is the basic carbonate, the formula of which commonly accepted by the industry is $4MgCO_3 \cdot Mg(OH)_2 \cdot 5H_2O$ with not less than 10% of asbestos fiber content. Wilkes and Wood[18] made mean specific heat measurements on 85% magnesia and calculated the true specific heat. They obtain a value of 0.295 at 500°F. as compared with 0.325 obtained on the spherical apparatus herein described. Because the mass, and thus the heat capacity, of 85% magnesia is low, the experimental uncertainties are greater than with heavier materials. Fewer determinations were made, morever, than on the other materials reported here. It is believed that the variations of these results from those of Wilkes and Wood are within the uncertainties of both tests. A high specific heat would be expected for this material because of the presence of water of crystallization.

The results of the thermal conductivity measurements are shown in Figs. 10 and 11; curves *A*, *B*, and *C* (Fig. 10) show the results of measurements of the 2600°F. insulating firebrick by three methods: Curve *A*, by the present spherical apparatus; *B*, by an apparatus of the flat slab type (Weinand's apparatus[9(b)]; and *C*, by an indirect method to be described later. The shape of the upper part of curve *A* is somewhat uncertain as indicated by the dashed lines.

Curves *D*, *D'*, and *E* in Fig. 11 are the 2300°F. brick; curves *H* and *I*, the 2000°F. brick; curves *F* and *G*, the diatomaceous earth brick; and curve *J*, the 85% magnesia. Curve *H* is drawn through points obtained in two tests on different samples of the 2000°F. brick. The dotted curves in each case were obtained with the slab-type apparatus; curve *I* was taken from a unit smaller than that used for *B*, *E*, and *G* but similar in construction to it. Curves *A*, *B*, and *C* and curves *D*, *D'*, and *E*, respectively, were obtained from brick of the same lot; the *D'* spherical sample was cut from the actual brick used in obtaining *E* on the slab apparatus. Curves *F* and *G* and curves *H* and *I* were from similar type brick but produced at different times. Curves *D* and *D'* and also curve *H* show good agreement between measurements on two different samples of the same material on the spherical apparatus. With curve *J*, on the 85% magnesia, is shown a curve obtained on a Bureau of Standards type guarded hot plate conductivity apparatus[9(c)] on the same material.

Values of specific heat and thermal conductivity of the materials tested have been collected in Table I. These figures were read from the curves at convenient temperatures.

It will be noticed that except for curves *F* and *G* the spherical apparatus gives higher results on the insulating firebrick. The results from the spherical apparatus on the two higher-temperature firebrick show a rapid upward curvature at the highest temperatures whereas the slab apparatus gives a straight line. The lower temperature points of the spherical apparatus determine a straight line in these two cases.

Inasmuch as electrical leakage is troublesome at high temperatures, a test was made of its effect in the spherical apparatus. The apparatus was assembled exactly as for a test with the sample in place but without the center heater. The current and potential leads were fastened instead to two dummy leads, which ran in through the sample but were not connected at the center. Any power being measured but wasted in the insulation or between leads in the sample should thus appear. The effect was zero at 1800°F., but it increased to about 1% of the total power input at 2200°F.

The effect of the heat conduction of the heater and thermocouple leads which extend radially through the sample was calculated to contribute not more than 0.3% of the total heat flow of the lowest thermal conductivity material tested. Inasmuch as the effect of air films between the spherical sample and the platinum shell which surrounds it would be to lower the apparent thermal conductivity at low temperature but to have little effect at higher temperatures, this possible source of error is not consistent with the fact that general agreement is obtained between the two types of equipment at low but not at high temperatures. The most likely source of error in the slab type of apparatus is in the measurement of heat flow, which is accomplished with the aid of a heat-flow meter. This meter, however, was carefully calibrated before use.

[18] G. B. Wilkes and C. V. Wood, "Specific Heat of Thermal Insulating Materials," *Heating, Piping, Air Conditioning*, **14** [6] 370–74 (1942).

To provide an independent means of checking both types of apparatus, a method was devised for determining the shape of the thermal conductivity-temperature curve which would not be dependent on heat-flow measurements. Nine 22 B & S gauge Chromel-Alumel thermocouples were carefully threaded through tight-fitting transverse holes in a 9- by $4^1/_2$- by $2^1/_2$-in. brick of the 2600°F. variety so that the temperature could be measured in a line along the long central axis of the brick. This brick was set on end and surrounded by other brick fastened to it with a thin coat of cement. In four of these other brick, located at 90-degree intervals about the center, balance thermocouples were placed at three levels to detect lateral heat flow. The entire stack was made roughly circular, 9 in. high and 18 in. in diameter. Balancing heater windings were wound around the outside edge at three levels. This assembly was placed in the 18-in. slab apparatus between a Globar furnace and a cooling plate. After steady state heat flow had been established, with the lateral flow reduced to a minimum as indicated by the balance couples, temperatures were measured in the center brick. The brick were then taken apart, and the positions of the thermocouples were accurately measured. The resultant curve of temperature plotted against distance through the brick is shown in Fig. 12, curve *A*. The curvature depends on the manner in which the thermal conductivity varies with temperature; curve *A* would be a straight line if the conductivity remained constant.

In such a temperature distribution, the temperature drop across any section of the brick is inversely proportional to the average thermal conductivity of that section. A curve of the ratio of the conductivity of any section at a given mean temperature to the conductivity of any other section at some other mean temperature may therefore be easily constructed. If the value of the conductivity at one temperature is known, the complete curve is determined. Curve *C*, Fig. 10, is such a curve, matched to curves *A* and *B* at 500°F., where their agreement is good. This curve shows a curvature similar to that of the spherical apparatus but tends to agree better with values given by the slab-type apparatus.

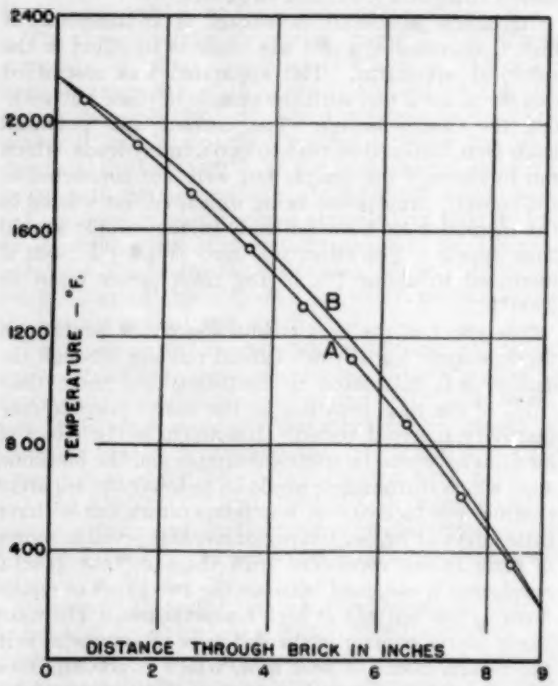

FIG. 12.—Temperature distribution curves. *A*, measured; *B*, calculated.

Curve *B*, Fig. 12, is a temperature-distribution curve derived from the conductivity curve determined by the spherical apparatus. Curves *A* and *B* differ by a maximum of 38°F., an amount not covered by the estimated error in either.

The measurements of the spherical apparatus are consistent among themselves in that the large-pored, denser brick (2600° and 2300°F. brick) show higher thermal conductivities and a rapid increase at high temperatures where radiation across the pores would be effective in increasing the heat conduction. The 2000°F. brick, which is lighter and fine pored, exhibits this effect to a much lower degree; and the diatomaceous earth brick, in which the pores are microscopic in size, actually shows a slight decrease in the slope of the conductivity curve at high temperatures.

The densities of materials tested in different types of apparatus were nearly the same in all cases, but the radial thickness of the spherical sample is 0.77 in. as compared with 2.5 in. for the linear thickness of the slab apparatus.

It should be noted that the temperature gradient in the test sample of the slab apparatus is a constant throughout the sample as given by equation (7).

$$\frac{d\theta}{dx} = \frac{\theta_1 - \theta_2}{d} = \text{constant (neglecting change of } k \text{ with temp.)} \quad (7)$$

θ_1 and θ_2 = surface temperatures.
d = sample thickness.

The gradient in the sphere, however, is given by equation (8).

$$\frac{d\theta}{dr} = \frac{-r_1 r_2(\theta_1 - \theta_2)}{r^2(r_2 - r_1)} \quad (8)$$

r_1 and r_2 = inside and outside radii of sample.
θ_1 and θ_2 = corresponding temperatures.
r = variable point in sample at which temperature gradient, $d\theta/dr$, is determined.

The gradient in the sphere thus varies with the radius, r. For an actual case, temperature gradients in the two types of apparatus might be as follows:

$$\text{At } r = r_1, \frac{d\theta}{dr} = 147°\text{F./in.}$$

$$\text{At } r = r_2, \frac{d\theta}{dr} = 29°\text{F./in.}$$

$$\text{For the slab, } \frac{d\theta}{dx} = 80°\text{F./in.}$$

If the thermal conductivity increased with the temperature drop used for measuring it, then the effect might give a higher conductivity figure when the sphere is

used because of the larger gradient near the inner surface and the larger average gradient through the sample. Measurements, however, on a sample of 2300°F. brick showed the effect to be small, as follows:

θ mean °F.	$(\theta_1 - \theta_2)$ °F.	k $\frac{\text{B.t.u.}\cdot\text{in.}}{\text{hr.}\cdot\text{ft.}^2\cdot{}^\circ\text{F.}}$
2037	5.90	3.10
2061	49.5	3.19
2080	98.4	3.23

No error in the slab or in the spherical apparatus has yet been found which adequately explains the disagreement in thermal conductivity results at high temperatures. An investigation of this discrepancy is being continued.

Thermal conductivity results were also compared on the chrome refractory cement between the spherical and slab apparatus, but these results agreed only at extreme temperatures. These measurements were discounted on the spherical apparatus at low temperatures because the chrome cement hemispheres could not be accurately shaped to fit the calorimeter, causing appreciable air spaces in the apparatus. In this high-conductivity material $\left(10 \frac{\text{B.t.u.}\cdot\text{in.}}{\text{hr.}\cdot\text{ft.}^2\cdot{}^\circ\text{F.}} \text{ at } 2000°\text{F.}\right)$, such a condition gives results of little value.

The assembly of the spherical sample in the calorimeter necessitates considerable care, and the process of preparing and placing a sample in the apparatus usually requires about 4 to 5 hours. Thermal equilibrium is attained fairly rapidly, however, and often five specific heat determinations or two thermal conductivity measurements at different temperatures have been made in a day.

The greatest sources of error in specific heat measurements appear to be random and probably occur in determining the heat leakage. The estimated error in this is 1% at maximum temperature. Other random sources of error, such as measurement of time, thermocouple electromotive force, and sample weight, contribute comparatively small errors.

A systematic error of 1% might occur in the power measurement, and an additional error from electrical leakage at extreme temperatures is probably less than 1%. A systematic error may occur also in the blank calorimeter heat capacity, the effect of which will depend on the mass of the material tested. As a result of the system of calculating the temperature increments, especially the initial and final equilibrium checks on the thermocouple calibrations, the error in determining $\Delta\theta$ is less than 0.5%. A conservative estimate of the accuracy would be 3% maximum for samples of low thermal diffusivity and great mass at lower temperatures and 5% minimum for samples of high diffusivity and small mass and at elevated temperatures. Individual determinations often depart from the curve by 3%.

Until a further study is made of the thermal conductivity measurements, no limit of error can be set on these determinations.

Acknowledgment

The idea for the spherical calorimeter described here originated with G. A. Downsbrough, who also began the investigation which resulted in the present equipment. The writer also wishes to express his appreciation for the assistance of the other members of the Physics and McMillan Thermal Conductivity Laboratories. Special thanks are d[illegible] C. B. Bradley for much aid and helpful criticism.

JOHNS-MANVILLE RESEARCH LABORATORY
MANVILLE, NEW JERSEY

Correction*

T. N. McVay and Hewitt Wilson, "Substitution of Topaz, Domestic Kyanite, and Synthetic Mullite-Corundum for India Kyanite," *Jour. Amer. Ceram. Soc.*, **26** [8] 253–66 (1943).

The analyses shown in this report marked "Corhart standard" and "Corhart water quenched" were made of hard material which had been crushed in a crushing plant where all the equipment was steel. These analyses do not represent the true iron oxide content of the cast Corhart block.

* Received September 15, 1943. from Hewitt Wilson, supervising engineer. Electrotechnical Laboratory, Bureau of Mines, Norris, Tenn.

MEASUREMENT OF THE THERMAL CONDUCTIVITY OF FIRE-CLAY REFRACTORIES*

By T. C. Patton† and C. L. Norton, Jr.‡

Abstract

Thermal conductivity determinations have been made on superduty fire-clay, silica, and kaolin refractories, using the Globar-heated, water calorimeter apparatus previously described. The arrangement, which is satisfactory for insulating firebrick, gives considerable error when firebrick samples are tested. Results obtained by different arrangements of the guard samples and heating elements are shown as well as a final arrangement which gives a satisfactory condition of parallel heat flow.

I. Introduction

A Globar-heated, water-flow calorimeter type of apparatus for measuring the thermal conductivity of refractories has been described in detail by Norton,[1] and thermal conductivity values obtained with this tester for several types of insulating firebrick were also given in the same report.

The present paper, a continuation of this work, gives thermal conductivity values for three types of dense firebrick as well as a description of the methods used in obtaining these data. The apparatus used is shown diagrammatically in Fig. 1.

A sample of known thickness is placed in the tester, and a temperature difference between its hot and cold faces is maintained. The heat flows from the hot to the cold face and passes into the water-cooled copper calorimeter. By measuring the temperature rise of the water passing through the calorimeter and the weight of water flowing for a measured time interval, the quantity of heat absorbed by the calorimeter can be determined. The conductivity coefficient, k_f, can be computed from equation (1).

$$q = \frac{k_f \times A \times (t_1 - t_2)}{L} \qquad (1)$$

q = heat transfer per unit time through area A.
A = area of material conducting heat.
t_1 = hot-face temperature of material.
t_2 = cold-face temperature of material.
L = thickness of material.

Changes in the operating technique, the method of side-wall guarding, and the placement of the Globar heating elements will be described here. The need for these changes has resulted from the difference in physical properties that occurs in dense firebrick and insulating firebrick.

II. Operating Procedure

(1) Thermocouples for Sample Brick Measurements

Because the dense, hard structure of firebrick precludes drilling $^1/_{32}$-in. holes through the test brick, the thermocouples could not be threaded through the firebrick as had been done with the insulating firebrick. It was decided, therefore, to use only one hot-face and one cold-face thermocouple. Grooves, $^1/_{32}$ in. wide and $^1/_{32}$ in. deep, were cut in the two 9- by $4^1/_2$-in. faces to embed the couple wires and to locate the junctions at approximately the center points of these two faces. The thermocouples were cemented into the grooves with Alundum cement, with only a thin film covering the thermocouple junction, which gave a smooth refractory surface flush with the brick surface.

The distance between the hot- and cold-face thermocouple junctions was measured with a vernier micrometer, and this measurement was corrected to give center-to-center distance between the couple beads.

Calibrated platinum-platinum 10% rhodium thermocouples (No. 28 wire) were used exclusively to measure the temperature of the sample brick.

(2) Arrangement of Sample Brick in Tester and Heat Flow Measurements

For low-temperature runs, the firebrick samples were placed over the calorimeter and guard-plate area, similar to the placement of the insulating firebrick samples. Two strips of asbestos paper, approximately 0.02 in. thick and 0.5 in. wide, were placed along the $13^1/_2$-in. dimension of the guard plate at the outside edges to prevent actual contact between the sample and the copper surface (Fig. 2).

For high-temperature runs where a high mean temperature of the same sample was required, a layer of insulation was used between the calorimeter and the sample brick. The backing-up insulation was separated from the calorimeter area with the asbestos strips, and the sample brick was also separated from the insulating layer by additional asbestos paper strips (Fig. 2). The main advantage of using a slight separation between these surfaces is that uneven contact pressures caused by uneven surfaces are eliminated.

The procedure for measuring the heat flow and the tolerances for individual readings were the same as those used in testing insulating firebrick.[1]

III. Effect of Backing-Up Insulation

When the sample firebrick were placed on the calorimeter without a layer of backing-up insulation, consistent values were obtained for different thicknesses of the test material up to 2.5 in., indicating that losses

* Presented at the Forty-Fifth Annual Meeting, The American Ceramic Society, Pittsburgh, Pa., April 21, 1943 (Refractories Division). Received May 6, 1943.

† Engineer, Refractories Research Laboratory, Babcock & Wilcox Co., New York, N. Y.

‡ Technical Director, Refractories Division, Babcock & Wilcox Co., New York, N. Y.

[1] C. L. Norton, Jr., "Apparatus for Measuring Thermal Conductivity of Refractories," *Jour. Amer. Ceram. Soc.*, **25** [No. 15, November 1] 451–59 (1942).

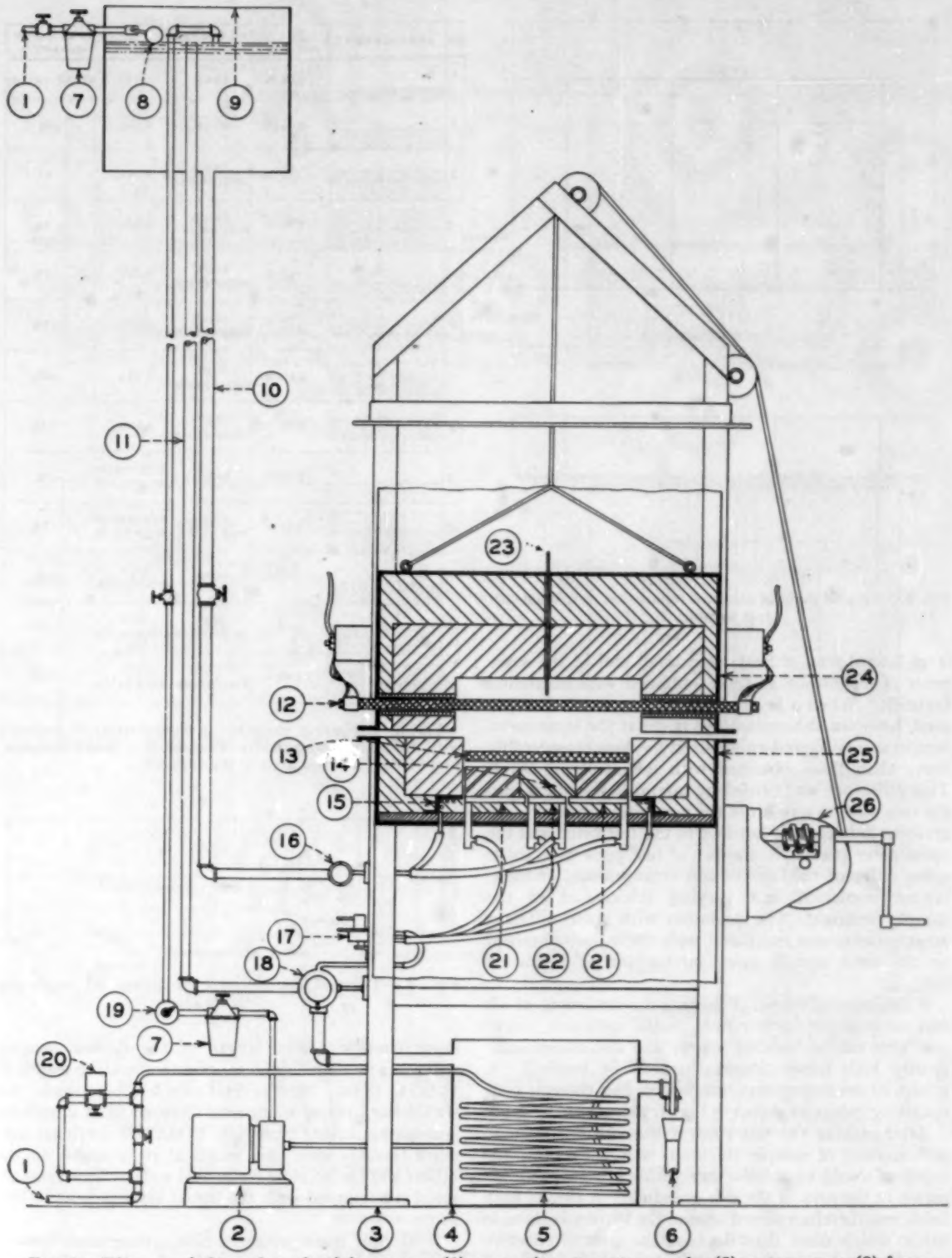

FIG. 1.—Diagram of thermal conductivity tester; (1) connections to water supply, (2) water pump, (3) frame, (4) cooling tank, (5) cooling coil, (6) connection to drain, (7) water filter, (8) float valve, (9) constant-head water supply tank, (10) inlet pipe, (11) overflow pipe, (12) Globar heating elements, (13) silicon carbide slab, (14) test specimen, (15) outer guard, (16) inlet manifold, (17) microregulating valves, (18) outlet manifold, (19) thermostat, (20) magnetic control valve, (21) guard calorimeters, (22) center calorimeter, (23) control thermocouple, (24) heating section, (25) tester section, (26) winch for elevating heater section.

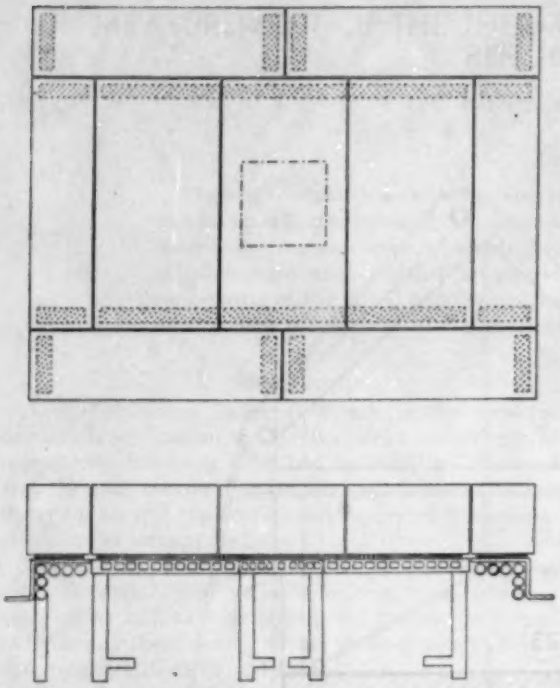

FIG. 2.—Arrangement of asbestos separation strips beneath test samples.

NO.	ARRANGEMENT	THICKNESSES			K VALUE DEVIATION FROM ARRGT. (1)
		TEST BRICK	BACK-UP MAT'L	LATERAL RING	
1		1.20 IN.	NONE	NONE	(BASE VALUE)
2		2.40 IN.	NONE	NONE	<1%
3		1.20 IN.	2.40 IN. FIRE BRICK	NONE	-8%
4		2.40 IN.	2.40 IN. FIRE BRICK	NONE	-9%
5		1.20 IN.	.90 IN. GROUP 28 IFB	NONE	-5%
6		1.20 IN.	1.60 IN. GROUP 28 IFB	NONE	-9%
7		2.40 IN.	.90 IN. GROUP 28 IFB	NONE	-9%
8		2.40 IN	1.60 IN. GROUP 28 IFB	NONE	-14%
9		2.40 IN.	NONE	2.25-4.50 IN. GROUP 20 IFB	<1%
10		2.40 IN.	2.40 IN. FIRE BRICK	2.25-4.50 IN. GROUP 20 IFB	-7%
11		2.40 IN.	NONE	.38 IN. GROUP 28 IFB	+1%
12		2.40	.90 IN. GROUP 28 IFB	.38 IN. GROUP 28 IFB	-12%
13		2.40 IN	2.40 IN. FIRE BRICK	.38 IN. GROUP 28 IFB	-8%

FIG. 3.—Apparent variation in conductivity of firebrick with different arrangements of sample at a mean temperature of 1000 °F. (test area = 9 x 13.5 in.).

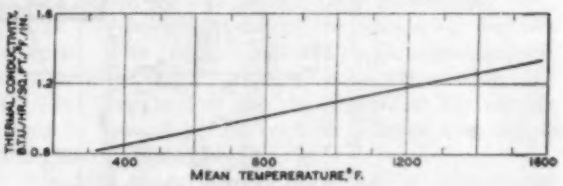

FIG. 4.—Thermal conductivity of group 20 insulating firebrick.

from lateral flow of heat were small and of the same order of magnitude as those obtained with insulating firebrick. When a layer of backing-up insulation was used, however, determinations made at the same mean temperatures showed conductivity values considerably lower than those obtained with no insulating layer. This difference was caused by lateral flow of heat into the side walls as a result of the nonuniform temperature gradient between the hot face of the test brick and the calorimeter plate. A number of test runs were made using different thicknesses and arrangements of backing-up insulation and varying thicknesses of the sample firebrick. The deviation with these different arrangements was compared with the values obtained on the same sample using no backing-up insulation (Fig. 3).

A thickness of 0.5 in. of backing-up insulation, which was selected for further runs, is the minimum thickness that can be handled readily and also allows sufficiently high mean temperatures to be reached. A group 20 insulating firebrick, which has thermal conductivity values as shown in Fig. 4, was selected.

After making the test runs, it was obvious that no combination of sample thickness and backing-up insulation would be satisfactory without an over-all increase in the area of the side guarding. A ring of soap brick was therefore placed around the three 9-in. sample brick, which more than doubled the area of effective sample guarding and necessitated a reduction from 7 in. to $4^1/_2$ in. in the thickness of the furnace side-wall insulation. It was also necessary to reduce the thickness of insulation on the sides of the upper heating chamber to correspond with the increased size of the lower chamber. The length of the Globar heating units was increased from an effective heating length of 14 in. to 18 in. After several runs had been made, the six Globar heating units were changed from a uniform spacing to provide more heat to the side sections; two extra Globars were also added at right angles to the others and placed close to the end walls. This arrangement is compared with the initial arrangement in Fig. 5.

Test runs made with the new arrangement showed agreement between samples placed on the calorimeter and samples backed up with 0.5 in. of insulation. A series of temperature surveys below and above the three test brick was made to compute the amount of lateral heat flow. Using the final arrangement shown

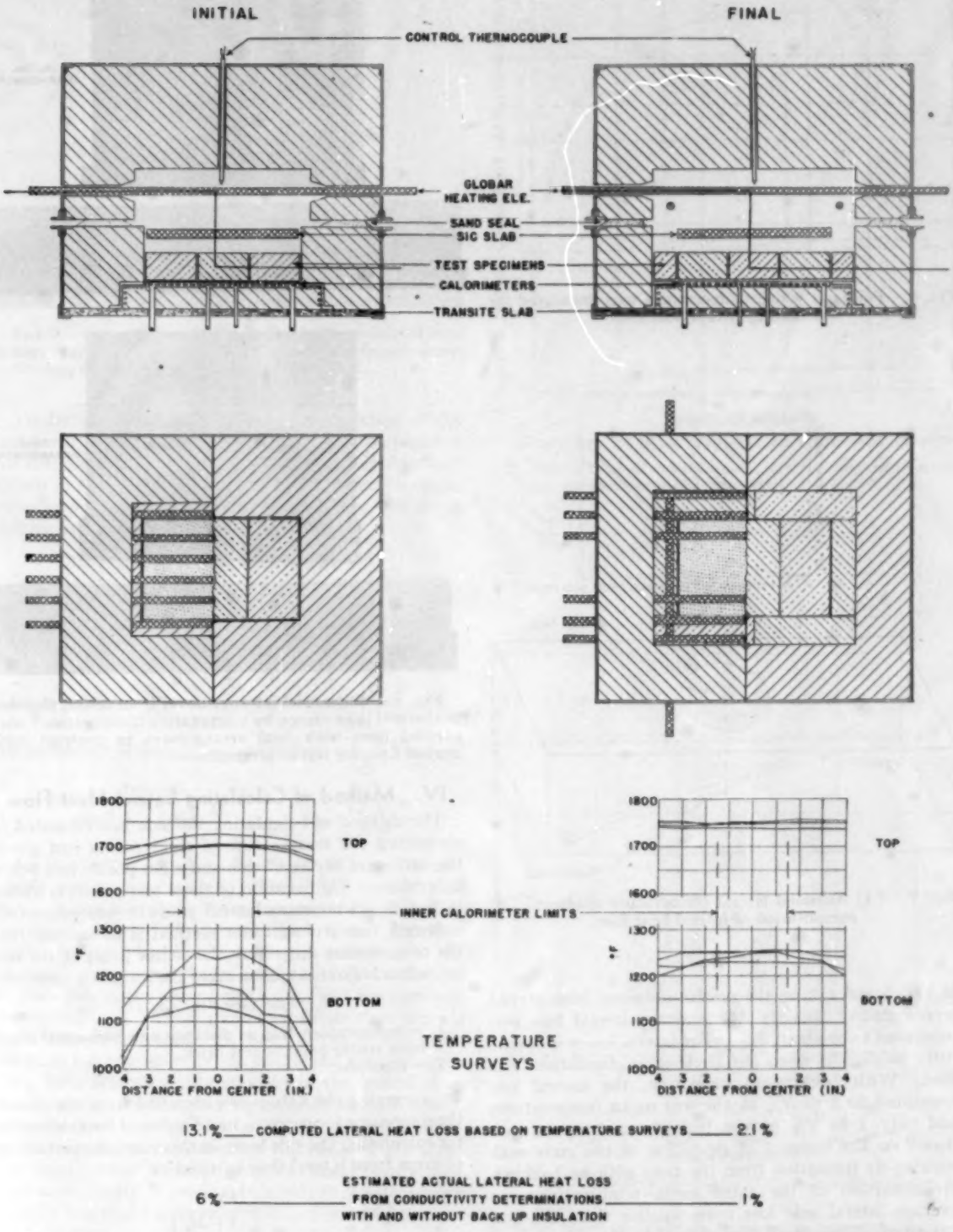

FIG. 5.—Initial and final arrangements of thermal conductivity tester showing heating elements, sample guarding, etc.

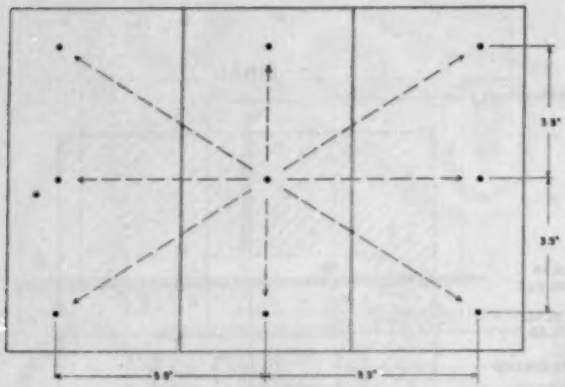

FIG. 6.—Points at which temperatures were measured for calculating lateral heat loss.

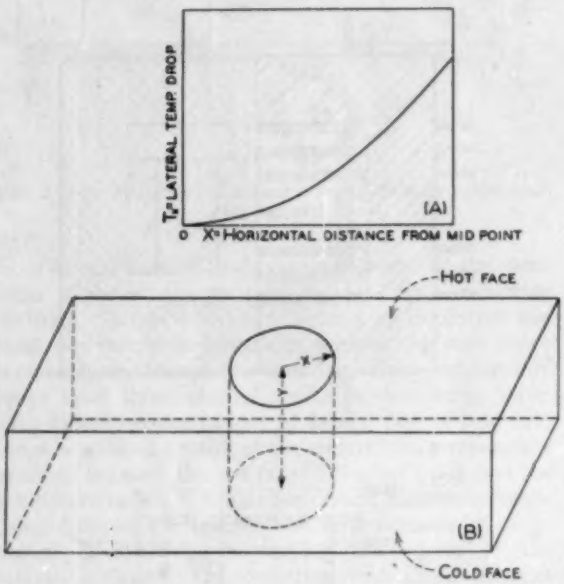

FIG. 7.—(*A*) Assumed lateral temperature gradient; (*B*) computation of lateral heat flow.

in Fig. 5 and taking the results obtained from eleven representative surveys, the average lateral loss was computed to be about 2%. The lateral loss was apparently negligible when no backing-up insulation was used. With backing-up insulation, the lateral loss amounted to 2 to 5% at the low mean temperatures and only 1 to 3% at the high mean temperatures. Based on the amount of deviation of the runs with backing-up insulation from the runs with no backing-up insulation at the same mean temperatures, an average lateral side loss even smaller than 2% was indicated. This small flow of heat to the side showed that a satisfactory condition of straight-line heat flow was obtained and that the arrangement was suitable for testing dense fire-clay brick.

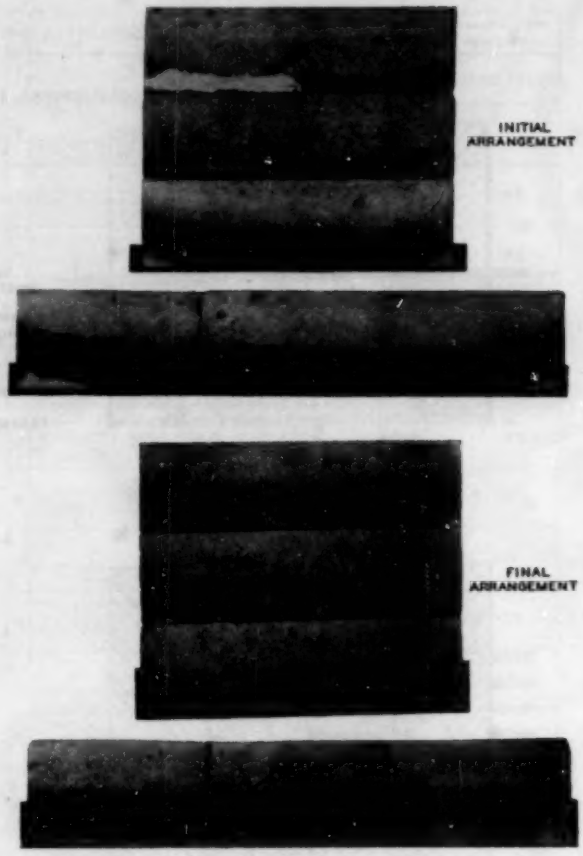

FIG. 8.—Silica brick after removal from tester, showing isothermal lines caused by temperature discoloration; note parallel lines with final arrangement in contrast with curved lines for initial arrangement.

IV. Method of Calculating Lateral Heat Flow

The method of calculating the side loss consisted in measuring the temperature of eight points just above the surface of the test brick and eight points just below its surface. The location of these test points is shown in Fig. 6. A constant lateral gradient was previously assumed, but a more exact method is to assume that the temperature drop from the center point of the test brick in a horizontal plane takes the form of a parabola,

$$t_x = cx^2 \text{ (see Fig. 7 (}A\text{))}$$

t_x = temperature drop at distance x in horizontal plane from center point of test brick.
c = constant.

By averaging the values of c obtained from the sixteen thermocouple locations, a mean value of c was obtained for calculating the side loss; in this case, the percentage of error from lateral flow is equal to

$$\frac{100}{1 + \frac{1}{4c}\left[\frac{\Delta t_y}{y^2}\right]}$$

y = thickness of test sample.
Δt_y = temperature drop through test brick.
c = constant of the parabola.

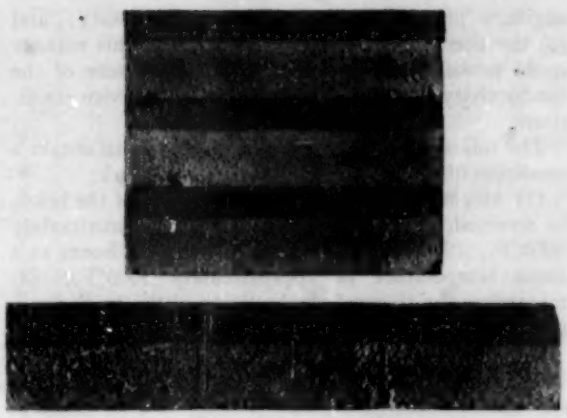

FIG. 9.—Group 20 insulating firebrick after removal from tester; parallel isothermal lines shown by temperature-indicating stain painted on surface before test.

To derive this relation, a cylindrical section of the test brick whose axis is perpendicular to the plane of the calorimeter at the center point of the test brick, as shown in Fig. 7 (*B*), is considered. The length of the cylinder is equal to the thickness, y, of the test brick, and its radius is equal to x.

$$\text{Lateral flow of heat, } Q_l = k \cdot 2\pi x \cdot y \cdot \frac{dt_x}{dx}$$

$$\text{Vertical flow of heat, } Q_v = k \cdot \pi x^2 \cdot \frac{\Delta t_y}{y}$$

k = mean thermal conductivity of test sample.
Δt_y = temperature drop through test sample.

Because $t_x = cx^2$, $\frac{dt_x}{dx} = 2cx$, and $Q_l = 4\pi kx^2yc$,

$$\text{the percentage of error from lateral flow} = \frac{Q_l}{Q_l + Q_v}$$

$$= \frac{4\pi kx^2yc}{4\pi kx^2yc + \pi kx^2 \cdot \frac{\Delta t_y}{y}} = \frac{1}{1 + \frac{1}{4c}\left[\frac{\Delta t_y}{y^2}\right]}$$

An interesting check, independent of the thermocouple survey, was made on the condition of parallel flow. When silica brick are heated, they show discoloration which follows isothermal lines. Figure 8 shows photographs of silica brick run according to the original arrangement shown in Fig. 5 and another set of silica brick run according to the final arrangement shown in Fig. 5. These pictures indicate that there is apparently considerable side flow, in the first case, as shown in the curvature of the isothermal lines, whereas these lines are essentially straight in the second case. A sample of group 20 insulating firebrick was also tested, using the final arrangement in Fig. 5. A temperature-sensitive stain* was painted on the edges of the three test brick; after removal from the tester, isothermal lines were clearly defined and showed that satisfactory straight-line flow had been established (see Fig. 9).

V. Brick Stability

In the course of the investigation, the firebrick samples were observed to undergo permanent changes in thermal conductivity as a result of the heat-treatment to which they were subjected during the tests. Although no attempt is made here to explain the nature of these alterations, this factor of brick instability was

* Nickelous chloride solution.

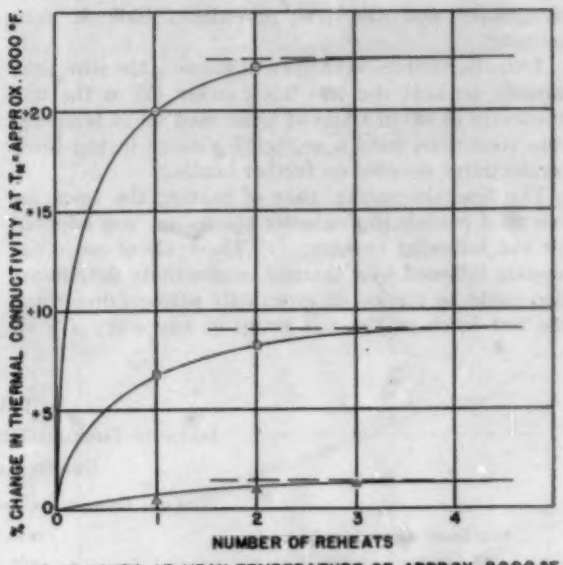

FIG. 10.—Effect of reheating on the stability of thermal conductivity of three types of firebrick.

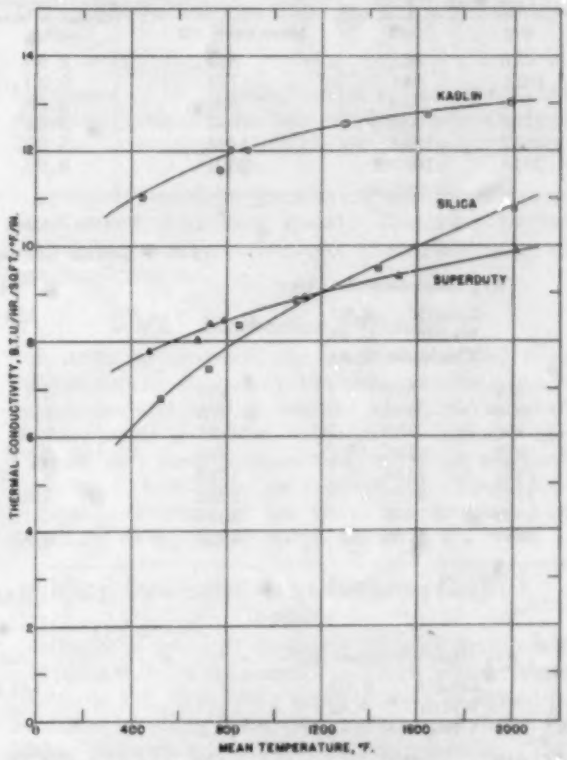

FIG. 11.—Thermal conductivity of three brands of firebrick.

recognized and the test procedures took it into account.

Two alternatives were open in meeting the situation, namely, to heat the test brick either (1) in the test apparatus or (2) in a kiln at some fixed set of temperature conditions until a negligible change in the brick conductivity resulted on further heating.

The first alternative, that of heating the brick for extended periods in the tester apparatus, was adopted for the following reasons: (1) The cycle of an initial heating followed by a thermal conductivity determination could be carried on repeatedly without disturbing the test brick or the test setup in any way; (2) an auxiliary piece of equipment was unnecessary; and (3) the thermal conductivity obtained in this manner could probably be considered a good measure of the conductivity of the brick under average service conditions.

The following heating schedule was used to obtain a condition of brick stability in the present work:

(1) Measuring the thermal conductivity of the brick, as received, at a mean temperature of approximately 1000°F.; (2) heating the brick for 18 ± 2 hours at a mean temperature of approximately 2000°F.; (3) measuring the thermal conductivity of the brick again at a mean temperature of approximately 1000°F.;

TABLE I

DATA ON THERMAL CONDUCTIVITY TEST RUNS

BRAND NAME: STAR

(2.44 in. between hot- and cold-face thermocouples)

Avg. linear dimensions (in.)		Bulk density	Brick (general description)
Length	8.99	105 lb./cu. ft.	Commercial 9-in. straight silica
Width	4.49		
Thickness	2.47		

Face temp. (°F.)			Center calorimeter			
Hot	Cold	Mean temp. (°F.)	Δt rise in water (°F.)	Rate of water flow (cc./min.)	Rate of heat flow (B.t.u./hr./sq. ft.)	Thermal conductivity (B.t.u./hr./sq. ft./°F./in.)
675	362	519	2.80	138	875	6.82
1021	446	734	6.30	130	1748	7.41
982	729	856	2.59	155	857	8.25*
1256	930	1093	3.64	152	1184	8.86*
1657	1214	1436	5.35	152	1736	9.56*
2318	1683	2001	8.65	151	2790	10.72*

BRAND NAME: B & W No. 80

(2.40 in. between hot- and cold-face thermocouples)

Avg. linear dimensions (in.)		Bulk density	Brick (general description)
Length	8.93	138 lb./cu. ft.	Kaolin 9-in. straight
Width	4.48		
Thickness	2.44		

509	332	420	3.14	121	818	11.00
976	568	773	7.36	125	1969	11.61
890	732	811	2.63	141	791	12.02*
972	798	885	2.92	142	884	12.05*
1427	1148	1288	4.92	139	1462	12.60*
1432	1151	1292	4.92	138	1478	12.60*
1838	1453	1645	6.78	142	2049	12.77*
2232	1738	1985	8.85	142	2684	13.04*

BRAND NAME: MEXKO

(2.44 in. between hot- and cold-face thermocouples)

Avg. linear dimensions (in.)		Bulk density	Brick (general description)
Length	9.00	142 lb./cu. ft.	Superduty fire-clay 9-in. straight
Width	4.42		
Thickness	2.48		

618	320	469	2.34	190	950	7.78
763	592	678	1.72	151	565	8.07*
982	481	732	4.32	184	1700	8.29
897	692	795	2.12	154	697	8.30*
1281	974	1128	3.51	150	1126	8.96*
1734	1296	1515	5.24	150	1680	9.38*
2317	1691	2004	7.82	151	2525	9.85*

* Runs made with 0.50 in. of group 20 backing-up insulation.

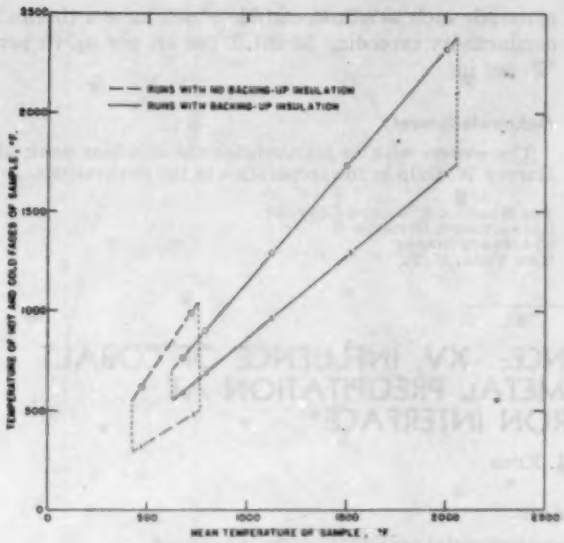
RUNS WITH NO BACKING-UP INSULATION
RUNS WITH BACKING-UP INSULATION
TEMPERATURE OF HOT AND COLD FACES OF SAMPLE, °F.
MEAN TEMPERATURE OF SAMPLE, °F.

FIG. 12.—Temperatures of hot and cold faces of dense firebrick over a range of test temperatures.

(4) heating the brick again for 18 ± 2 hours at a mean temperature of approximately 2000°F.; (5) same as (3); and (6) same as (4).

This cycle was repeated until a negligible change of thermal conductivity was indicated on further reheating. In the case of the three brick tested, two reheatings were sufficient to bring about a condition of brick stability within the temperature range covered by the reheating schedule.

In Fig. 10, the percentage of change in thermal conductivity versus the number of times reheated has been plotted for the three types of brick. Using the method suggested by Austin,[2] the maximum change to be expected on extended heating has been calculated and shown as a dashed line.

These data show that, for strictly comparable results of thermal conductivity measurements on a given type of brick with different testers, it is necessary not only that the brick samples should originate from the same source to insure similar initial firing conditions but that the heat-treatments to which the brick are subjected thereafter in testing should be similar.

VI. Results of Tests

Three types of firebrick were tested. The final arrangement shown in Fig. 5 was used, and the determinations were made after the samples had attained stability by repeated heatings (see Fig. 10). The details of the thermal conductivity runs are given in Table I.

The thermal conductivity values obtained are plotted in Fig. 11. The Star silica and Mexko brands were similar to the samples used in the cooperative tests reported by Nicholls,[3] and it was found that the values for each of these brands fall between the high and low values obtained by the six cooperating laboratories.

In Fig. 12, values for the hot- and cold-face temperatures of a typical dense firebrick have been plotted against mean temperature over a complete range of test temperatures.

[2] J. B. Austin, "Factors Influencing Thermal Conductivity of Nonmetallic Materials," pp. 3–67 in Symposium on Thermal Insulating Materials, American Society for Testing Materials, Philadelphia, 1939. 123 pp.; *Ceram. Abs.*, **20** [4] 97 (1941).

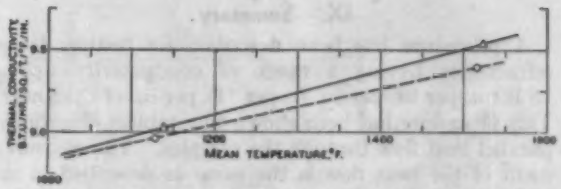

FIG. 13.—Thermal conductivity of same firebrick sample determined by two operators.

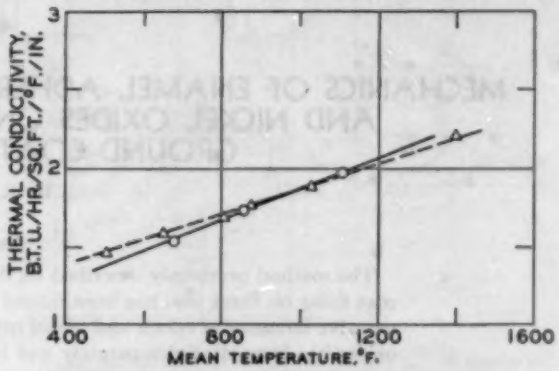

FIG. 14.—Thermal conductivity of group 28 insulating firebrick determined with initial and final tester arrangements.

VII. Duplication of Results

In order to determine the deviation resulting from different operators making the tests, runs were made by one operator and the samples with their attached thermocouples were removed from the furnace; the samples were then replaced and tested by a second operator. These values are given in Fig. 13 and show negligible deviation at low mean temperatures and only 1.5% at high mean temperatures.

VIII. Determinations on Insulating Firebrick Samples

Samples of group 28 insulating firebrick were tested according to both the original and final arrangements (shown in Fig. 5) in order to determine the deviation in values resulting from the changes in location of Globar elements and method of side guarding. The results of this test are shown in Fig. 14 and indicate a negligible deviation. For testing insulating firebrick, it may therefore be concluded that either arrangement is satisfactory and will give strictly comparable results.

[3] P. Nicholls, "Determination of Thermal Conductivity of Refractories," *Bull. Amer. Ceram. Soc.*, **15** [2] 37–51 (1936).

IX. Summary

A procedure has been described for testing dense refractories having a range of conductivity up to 15 B.t.u. per hr. per sq. ft. per °F. per in. of thickness. This procedure has been shown to establish essentially parallel heat flow through the samples. The measurement of the heat flow is the same as described in an earlier paper[1] and has been checked by other independent methods. Further work will be necessary to determine whether this procedure will be satisfactory for materials such as silicon carbide which have a thermal conductivity exceeding 15 B.t.u. per hr. per sq. ft. per °F. per in.

Acknowledgment

The writers wish to acknowledge the excellent work of Harvey W. Culp in the preparation of the illustrations.

The Babcock & Wilcox Company
Refractories Division
85 Liberty Street
New York, N. Y.

MECHANICS OF ENAMEL ADHERENCE: XV, INFLUENCE OF COBALT AND NICKEL OXIDES ON METAL PRECIPITATION AT GROUND COAT-IRON INTERFACE*

By R. M. King

Abstract

The method previously described for determining metal precipitation during ground-coat firing on sheet iron has been refined and used in a quantitative study of the comparative influence of cobalt and nickel oxides on this precipitation. The effect of these oxides has been studied separately and in mixtures, and it has been found that nickel oxide has the more pronounced action. This action is evident even when the ratio of cobalt oxide to nickel oxide is 3 to 1.

I. Introduction

In Part XIV of this series,[1] a method was described for determining the rate at which metal precipitation takes place during firing and cooling at the ground coat-iron interface from ground coats containing varied amounts of cobalt oxide. The present paper gives results of an investigation to determine the influence on metal precipitation of cobalt and nickel oxides, singly and in combination.

Bernard[2] has discussed the influence of cobalt oxide (CoO) on the decomposition temperature of ferrous oxide ("FeO") (see Fig. 1), and the present author offers experimental evidence to show that cobalt oxide has a similar action in ground coats during firing.[1]

Bernard also found that the decomposition of FeO takes place "even with weak concentrations of nickel oxide and at very high temperatures so that the region of stability of the solid solution, NiO-FeO, appears to be extremely limited." A solid solution containing 30% of NiO decomposed completely at 1000°C., and one containing 5% of NiO decomposed completely at 800°C.; the decomposition products in each case are first Fe_3O_4 and metallic nickel and second, Fe_3O_4 and metallic iron. The influence of nickel oxide on metal precipitation during ground-coat firing might therefore be expected to be more pronounced than that of cobalt oxide.

II. Experimental Procedure

The hard and soft ground-coat compositions previously given[1] were also used in this work. Batches of hard and soft frits containing 0.65% of Co_3O_4 and similar batches containing 0.65% of Ni_2O_3 were melted in 30-gm. lots in a small laboratory furnace.* After fritting and drying, they were ground through a 200-mesh sieve. All test samples were blends of two or four frits so that each contained 50% of hard frit and 50% of soft frit, and the Co_3O_4 and Ni_2O_3 totaled 0.65%.

For reasons of application technique, 2% of bentonite was added to the powdered frits. All components of the test sample were mixed thoroughly in the dry state.

The apparatus and procedure previously described,[1] with some refinements, were again employed. These changes resulted in more accurately reproducible values for a given sample.

The test pieces were rivetlike pieces of enameling iron, the heads of which had a diameter of 1/2 in. and a thickness of 1/16 in. The shanks were 1/8 in. in diameter and 9/16 in. long. The heads of the upper pieces were drilled with three 1/16-in. holes placed at the corner of an equilateral triangle and about 1/16 in. from the edge. These holes permitted excess enamel to squeeze out.

Insulating spacers, placed between the test pieces, were 0.204 ± 0.004 in. in diameter and 0.0063 ± 0.0002 in. thick. They were made by dry pressing a body containing 50% each of talc and ball clay and were fired at 1000°C.

---

* Presented at the Forty-Fifth Annual Meeting, The American Ceramic Society, Pittsburgh, Pa., April 21, 1943 (Enamel Division). Received April 20, 1943.

[1] R. M. King, "Mechanics of Enamel Adherence, XIV," *Jour. Amer. Ceram. Soc.*, **26** [2] 41–48 (1943).

[2] Jaques Bernard, "Étude de la Decomposition du Protoxide de Fer et de Ses Solutions Solides," *Ann. Chim.* [Series 11], **12** [1] 5–92 (1939).

* Values based on use of hydrated borax. Values of Co_3O_4 and Ni_2O_3 in previous paper (see page 44 of reference 1) based on use of dehydrated borax; multiply by 0.81 to convert to hydrated basis.

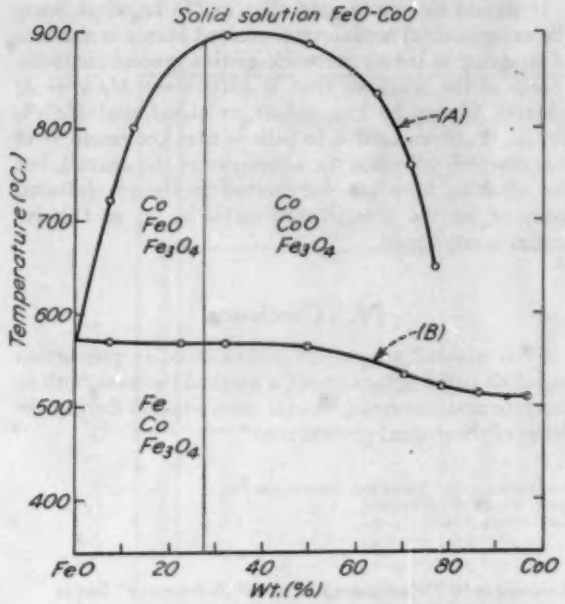

FIG. 1.—Bernard's equilibrium diagram for the solid system FeO–CoO.

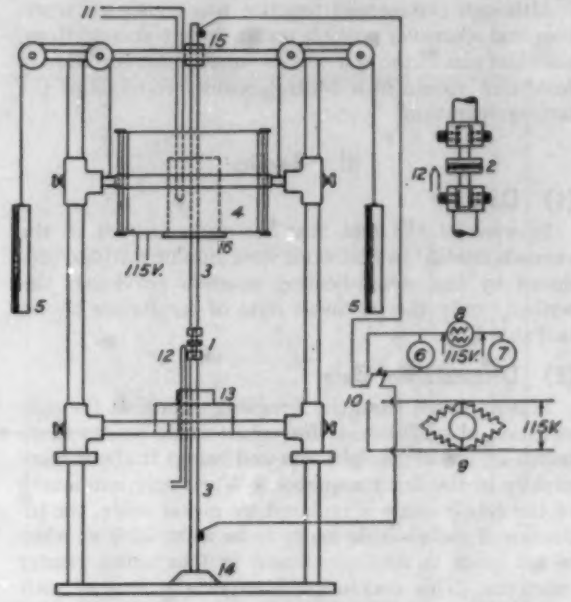

FIG. 2.—Apparatus to determine resistance of enamels: (1) Test-piece assembly; (2) detail of test-piece assembly; (3) rods of heat-resisting alloy; (4) furnace; (5) counterweights for furnace; (6) voltmeter, 1.5 volts a. c.; (7) ammeter, 3.0 amp. a. c.; (8) Variac resistance; (9) Wheatstone bridge; (10) double-pole, double-throw switch; (11) pilot thermocouple; (12) firing thermocouple; (13) block of insulating brick; (14) insulating support (rubber); (15) insulating guide (wood); and (16) asbestos cover pieces.

TABLE I

SIGNIFICANT DATA OF RESISTANCE RESULTS

Co_3O_4 and Ni_2O_3 (%)	R_1*	C†	R_2‡	Sigma (standard deviation)
Enamel melt No. 1§				
0.650 Co_3O_4	10^5	3	5.9	±2.91
0.487 Co_3O_4 / 0.163 Ni_2O_3	10	1	1.45	±0.59
0.325 Co_3O_4 / 0.325 Ni_2O_3	10	1	1.00	±0.26
0.163 Co_3O_4 / 0.487 Ni_2O_3	10^2	1	1.22	±0.51
0.650 Ni_2O_3	10	1	1.07	±0.41
Enamel melt No. 2§				
0.650 Co_3O_4	10^5	5 or 6	234	±118
0.487 Co_3O_4 / 0.163 Ni_2O_3	10^5	1, 2, or 3	95	±109
0.650 Ni_2O_3	10^5	1, 3, or 4	11.35	±7.47

* R_1, order of maximum resistance in ohms during first firing period.

† C, serial number of cooling period during which decrease in resistance began.

‡ R_2, resistance in ohms after complete cooling.

§ C and R_2 for enamel melt No. 1 represent average of six determinations; for enamel melt No. 2, average of three to five determinations.

Assembly was effected by inserting the test pieces and test sample into holes in the ends of the heat-resisting alloy rods and tightening the setscrews until the circuit had a resistance of less than one ohm when the faces of the "rivet" heads were in contact. The upper rod was then raised and held in a detached position by means of a setscrew in a wooden guide in the crossarm of the superstructure (see Fig. 2).

Then 125 mg. of the prepared test sample were placed on the face of the lower test piece and a drop of distilled water was placed thereon with a medicine dropper. The dry enamel was mixed with the water by means of a sharp pointed tool, and the rod just below the test piece was rapped sharply with the same tool to force the wetted sample to flow and thus to bring about uniform distribution of the sample on the face of the test piece.

When the sample had dried to a semiplastic condition, a 0.210-in. core was cut from the center by means of a cork borer. An insulating test piece was then placed in the cavity thus formed. Inasmuch as the weight of the core was 37 ± 2 mg., the weight of the sample actually employed was 88 ± 2 mg.

The upper test rod was then released and lowered into place so that it rested on the sample in alignment with the lower test piece and could have free vertical movement.

After the pilot couple and furnace covers were placed in position, the assembly was ready for firing.

The firing temperature was 1658°F. in all cases and the firing time was 3 minutes and 20 seconds, with a maximum deviation of ±10 seconds for the initial firing, and 2 minutes, with a maximum deviation of ±5 seconds, for all subsequent firing periods. The length of cooling periods between firings was 4 minutes.

Resistance readings were taken at the end of each firing period and at the end of each minute of the cooling period. During the final cooling, additional readings were taken after 10 minutes of cooling and after 24 hours of cooling.

Although commercial practice was simulated wherever and whenever possible under these test conditions, the chief aim of the test was to obtain differentiation of resistance values in a control enamel throughout the testing operation.

III. Results

(1) Data

In view of the fact that resistance curves of the enamels studied in this work were similar to those produced by the cobalt-bearing enamels previously described,[1] only the pertinent data of results are shown in Table I.

(2) Discussion of Data

It is apparent from the foregoing data that the substitution of nickel oxide for cobalt oxide results in an increased metal precipitation and brings it about more rapidly in the firing sequence. When only one fourth of the cobalt oxide is replaced by nickel oxide, the influence of nickel oxide seems to be as striking as when nickel oxide is used alone and in four times greater amounts. This conclusion is especially true of melt No. 1 of the enamel. Results on melt No. 2 are more variable and apparently were caused by unobserved differences in melting procedure. Nickel oxide nevertheless has a marked influence as compared to that of cobalt oxide.

The data obtained with ground coats agrees with that of Bernard[2] inasmuch as the relative influence of cobalt and nickel oxides is the same in the enamels as in the solid solution of the oxides.

Variations in the results from different melts of the same enamel have been mentioned. Although an effort was made to provide identical melting treatments, these variations could not be brought within the variations of the test itself. This effect suggests the possibility of using the procedure described herein for the study of variation in ground-coat melting procedure. Further work along this line is desirable before definite conclusions can be offered.

Data are meager or unobtainable as to desirable relative amounts of cobalt and nickel oxides in commercial ground coats. One statement that the average ratio of cobalt oxide to nickel oxide is about 3 to 1 suggests that the results obtained with this ratio, indicated in the foregoing data, may have commercial significance.

In harmony with this statement is the recent announcement[3] of a proprietary mixture of cobalt and nickel oxides for use in ground-coat frits in which the ratio of 3 to 1 is reported.

It will be noted that the action of cobalt oxide is rather gradual and that of nickel oxide is rather rapid during the series of firings. This fact may be significant in firing in continuous furnaces as compared with firing in box-type furnaces as well as when several firings are required, for example, in the enameling of signs.

[3] "Cobalt-Nickel Oxide Use for Ground-Coat Frits," *Ceram. Ind.*, **40** [4] 114 (1943).

It should be emphasized that in the broadest sense the experimental technique presented herein is a means of studying in cobalt and nickel oxide ground coats the course of the reaction, that is $4MO \longleftrightarrow M_3O_4 + M$ wherein M may be iron, cobalt, or nickel, and M_3O_4 is Fe_3O_4. It is reasonable to believe that the products of this reaction influence the adherence of the enamel, but the adhering force may be exerted by the precipitated oxide or by the precipitated metal as far as this reaction is concerned.

IV. Conclusion

Even a small amount of nickel oxide in proportion to cobalt oxide brings about a marked increase both in the rate and amount of metal precipitation during the firing of sheet-steel ground coat.

Department of Ceramic Engineering
Ohio State University
Columbus, Ohio

References to "Mechanics of Enamel Adherence" Series

The series of papers on "Mechanics of Enamel Adherence" has been in process of publication in the *Journal of The American Ceramic Society* since 1931.

"I, Technique of Preparing Enamel Metal Sections for Microscopic Analysis," by J. O. Lord and W. C. Rueckel, **14** [10] 777–81 (1931).

"II, Effect of Composition and Firing Atmosphere on Adherence of Ground-Coat Enamel," by W. C. Rueckel and R. M. King, **14** [10] 782–88 (1931).

"III, Enamels on Copper, Nature of Their Adherence," by W. K. Carter and R. M. King, **14** [10] 788–94 (1931).

"IV, Some Studies on Adherence of Enamels to Cast Iron," by A. McK. Greaves-Walker and R. M. King, **15** [9] 476–80 (1932).

"V, Study of Enamel-Metal Contact Zones by Chemical Methods," by G. H. Spencer-Strong and R. M. King, **15** [9] 480–83 (1932).

"VI, Petrographic, Metallographic, and X-Ray Study of Enamel-Metal Contact Zones," by Karl Schwartzwalder and R. M. King, **15** [9] 483–86 (1932).

"VII, Further Studies of Enamel-Metal Contact Zones by Microscopic and Metallographic Methods," by G. H. Spencer-Strong, J. O. Lord, and R. M. King, **15** [9] 486–90 (1932).

"VIII, (A) Apparatus for Firing Enamels under Accurate Control of Temperature, Pressure, and Atmosphere, (B) Studies in Firing Enamels under Reduced Pressures," by R. M. King, **16** [5] 232–38 (1933).

"IX, Equilibrium Studies in Some Systems of Enamel Glass and Cobalt, Nickel, and Iron Oxides," by G. H. Spencer-Strong and R. M. King, **17** [7] 208–14 (1934).

"X, The 'Iron Oxide Layer' in Sheet-Steel Ground Coats," by R. M. King, **17** [7] 215–19 (1934).

"XI, Application of Theory of Dendritic Adherence to Development of White Ground Coats for Sheet Steel," by W. L. Housley and R. M. King, **18** [10] 319–20 (1935.)

"XII, Chemical and X-Ray Examination of Metallic Precipitates from Enamels Containing Iron and Cobalt Oxides," by R. M. King, **19** [9] 246–49 (1936).

"XIII, Review of Theoretical Explanations for Formation of Metal Particles in 'Cobalt' Ground Coats and Some Pertinent Experiments," by R. M. King, **20** [2] 53–55 (1937).

"XIV, (1) Role of Cobalt Oxide in Metal and Oxide Precipitation During Ground-Coat Firing Cycle, and (2) Determination of Temperature and Time Intervals of Precipitation," by R. M. King, **26** [2] 41–48 (1943).

OFFICIAL PERSONNEL OF DIVISIONS AND CLASSES, 1943–1944

	Design	Enamel	Glass	Materials and Equipment	Refractories	Structural Clay Products	White Wares
Trustee	C. W. Read	R. L. Fellows	G. W. Morey	J. E. Eagle	J. B. Austin	Frederick Heath, Jr.	F. P. Hall
Chairman	W. A. Weldon	D. G. Bennett	J. F. Greene	E. M. Rupp	C. L. Thompson	L. R. Whitaker	J. R. Beam
Vice-Chairman	Theodore Lenchner	H. D. Carter	K. C. Lyon	J. R. Kauffman	W. R. Kerr	C. P. Austin	
Secretary	Myrtle M. French	D. G. Moore	S. R. Scholes	J. F. Day	S. M. Swain	R. L. Stone	J. W. Whittemore
Division Nominations		F. R. Porter M. J. Bahnsen E. E. Howe	E. W. Tillotson U. E. Bowes R. A. Miller	S. S. Cole J. F. McMahon	R. S. Bradley P. G. Herold	J. H. Isenhour W. C. McGolpin J. G. Seanor	Donald Hagar R. E. Gould
Papers and Program	H. E. Simpson Rexford Newcomb, Jr.	H. D. Carter	K. C. Lyon	V. J. Roehm	E. E. Callinan C. L. Norton, Jr. E. B. Read C. A. Freeman	V. W. Boeker A. C. Jackson H. K. Lynn	C. M. Lambe, Jr. E. P. McNamara
Membership	Theodore Lenchner	J. F. Hunt	R. R. Shively	W. R. Malkin	G. B. Remmey S. F. Walton W. P. Charbonnier A. R. Blackburn	R. R. Robinson A. C. Christopher	John D. Clark
Standards		R. L. Cook W. N. Harrison W. W. Higgins R. M. King F. A. Petersen	F. W. Adams H. P. Hood K. M. Henry	J. S. Breitenstein		E. F. Theobald A. W. Hough	F. P. Hall
Research		J. C. Reimers	H. R. Lillie Alexander Silverman W. R. Lester	R. R. Robinson	D. W. Ross	H. C. Plummer H. G. Schurecht	*Ball clay:* Ralston Russell, Jr. *Steatite:* Glenn Howatt
Classification and Nomenclature	Mrs. J. W. Dixon	G. H. McIntyre	E. P. McNamara	R. G. Janatka	C. M. Dodd	C. F. Wiseman R. E. Grim Morriss Corbman	A. S. Watts J. R. Beam Ralston Russell, Jr. Harry Thiemecke E. K. Koos
Rules		W. A. Deringer	S. R. Scholes	Philip Dressler	S. F. Walton	Howells Frechette	Don Postlewaite
Councillors		J. D. Tetrick Karl Kautz	F. C. Flint R. W. Wampler	V. V. Kelsey		R. A. Shipley C. F. Tefft	
Exhibitions			J. E. Frazier				
Industrial Management			C. J. Uhrmann	C. L. Cruikshank	O. L. Jones	J. C. Peck	A. A. Wells
Bibliography		J. E. Rosenberg					

	Institute of Ceramic Engineers	Ceramic Educational Council
President	H. B. DuBois	R. M. Campbell
Vice-President	R. F. Sherwood	C. M. Dodd
Secretary	Karl Schwartzwalder	E. C. Henry

THE AMERICAN CERAMIC SOCIETY TRUSTEES AND OFFICERS FOR 1943–1944

President: C. E. Bales, Ironton Fire Brick Co., Ironton, Ohio.
Vice-President: E. H. Fritz, Stupakoff Ceramic & Mfg. Co., Latrobe, Pa.
Treasurer: C. Forrest Tefft, The Claycraft Co., Columbus, Ohio
Secretary-Editor: R. C. Purdy, 2525 North High St., Columbus, Ohio
Past-President: L. J. Trostel, General Refractories Co., Baltimore, Md.
Past-President: J. T. Littleton, Corning Glass Works, Corning, N. Y.

TRUSTEES FROM INDUSTRIAL DIVISIONS*

Design: C. W. Read, Shenango Pottery Co., New Castle, Pa. (1946)
Enamel: R. L. Fellows, Chicago Vitreous Enamel Product Co., Cicero, Ill. (1946)
Glass: G. W. Morey, Geophysical Laboratory, Washington, D. C. (1944)
Materials and Equipment: J. E. Eagle, 6305 20th Ave., Green Meadows, Hyattsville, Md. (1945)
Refractories: J. B. Austin, U. S. Steel Corp., Kearny, N. J. (1946)
Structural Clay Products: Frederick Heath, Jr., Owens-Corning Fiberglas Corp., Toledo, Ohio (1945)
White Wares: F. P. Hall, Onondaga Pottery Co., Syracuse, N. Y. (1944)
Institute of Ceramic Engineers: H. G. Wolfram, Porcelain Enamel & Mfg. Co., Baltimore, Md. (1944)
Ceramic Educational Council: J. W. Whittemore, Virginia Polytechnic Institute, Blacksburg, Va. (1944)

* Date of expiration of term of office in parentheses.

DIVISION OFFICERS

Design
Chairman: W. A. Weldon, Locke Insulator Corp., Baltimore, Md.
Secretary: Myrtle M. French, Art Institute of Chicago, Chicago, Ill.

Enamel
Chairman: D. G. Bennett, Mellon Institute, Pittsburgh, Pa.
Secretary: D. G. Moore, National Bureau of Standards, Washington, D. C.

Glass
Chairman: J. F. Greene, Kimble Glass Co., Vineland, N. J.
Secretary: S. R. Scholes, N. Y. State College of Ceramics, Alfred, N. Y.

Materials and Equipment
Chairman: E. M. Rupp, National Engineering Co., 58 Fallis Rd., Columbus, Ohio
Secretary: J. F. Day, Donald Hagar Ceramic Materials, Zanesville, Ohio

Refractories
Chairman: C. L. Thompson, Harbison-Walker Refractories Co., Pittsburgh, Pa.
Secretary: S. M. Swain, North American Refractories Co., Cleveland, Ohio

Structural Clay Products
Chairman: L. R. Whitaker, Carolina Ceramics, Inc., Columbia, S. C.
Secretary: R. L. Stone, Dept. of Ceramic Engineering, Univ. of North Carolina, Raleigh, N. C.

White Wares
Chairman: J. R. Beam, Universal Sanitary Mfg. Co., New Castle, Pa.
Secretary: J. W. Whittemore, Virginia Polytechnic Institute, Blacksburg, Va.

OFFICERS OF THE FELLOWS

Dean: R. B. Sosman, U. S. Steel Corp., Kearny, N. J.
Associate Dean: Howells Frechette, Bureau of Mines, Ottawa, Ontario, Canada.
Secretary-Treasurer: R. M. King, Ohio State University, Columbus, Ohio

INSTITUTE OF CERAMIC ENGINEERS

President: H. B. DuBois, Consolidated Feldspar Corp., Trenton, N. J.
Vice-President: R. F. Sherwood, United Feldspar & Minerals Corp., New York, N. Y.
Secretary: Karl Schwartzwalder, A C Spark Plug Co., Flint, Mich.

CERAMIC EDUCATIONAL COUNCIL

President: R. M. Campbell, N. Y. State College of Ceramics, Alfred, N. Y.
Vice-President: C. M. Dodd, Iowa State College, Ames, Iowa
Secretary: E. C. Henry, Pennsylvania State College, State College, Pa.

LOCAL SECTIONS

Baltimore-Washington
Chairman: D. G. Moore, National Bureau of Standards, Washington, D. C.
Secretary: J. C. Richmond, National Bureau of Standards, Washington, D. C.

Central Ohio
Chairman: H. J. Orlowski, O.S.U. Engr. Expt. Sta., Columbus, Ohio
Secretary: A. C. Jackson, The Claycraft Co., Columbus, Ohio

Chicago
Chairman: Hugo Filippi, 228 N. LaSalle St., Chicago, Ill.
Secretary: J. J. Svec, Industrial Publications, Inc., 59 E. VanBuren St., Chicago, Ill.

Michigan-Northwestern Ohio
Chairman: J. F. Quirk, A C Spark Plug Co., Flint, Mich.
Secretary: W. V. Blake, Macklin Co., Jackson, Mich.

Northern California
President: W. V. Bragdon, California Faience Co., Berkeley, Calif.
Secretary: P. C. Valentine, Del Monte Properties Co., San Francisco, Calif.

Pacific-Northwest
President: Howard Mansur, Washington Brick & Lime Co., Spokane, Wash.
Secretary: J. A. Pask, Univ. of Washington, Seattle, Wash.

Pittsburgh
Chairman: E. E. Marbaker, Mellon Institute, Pittsburgh, Pa.
Secretary: H. E. Simpson, Mellon Institute, Pittsburgh, Pa.

Southern California
Chairman: R. H. Martin, Vernon Kilns, Los Angeles, Calif.
Secretary: W. O. Brandt, Gladding, McBean & Co., Los Angeles, Calif.

St. Louis
Chairman: H. H. Hanna, Pittsburgh Plate Glass Co., Crystal City, Mo.
Secretary: J. H. Ivery, Hydraulic Press Brick Co., St. Louis, Mo.